POLITECNICO DI TORINO

Collegio di Ingegneria Chimica e dei Materiali

Corso di Laurea Magistrale
in Ingegneria Chimica e dei Processi Sostenibili

Tesi di Laurea Magistrale

Heteroleptic Copper (I) Complexes as Photosensitizers in Dye-Sensitized Solar Cells

Relatori

Prof. Marco Vanni
Prof. James Gardner
Prof.ssa Valentina Leandri

Candidato

Angela Raffaella Pia Pizzichetti

Marzo 2019

Abstract

Modern civilization highly depends on energy and finding alternative sources to fossil fuels becomes more and more necessary. The sun is the most abundant energy source available and exploiting it efficiently would result in a great environmental and economic breakthrough. Among the photovoltaic devices, dye-sensitized solar cells (DSCs) emerged for their tremendous commercial potential deriving from a combination of low-cost production and attractive features, such as flexibility and transparency, for indoor and outdoor applications. In the DSCs, a dye anchored to a semiconductor layer (typically TiO_2) is responsible for capturing the sunlight and converting it into electricity. Nevertheless, many commercially available dyes for DSCs are based on a very rare metal, ruthenium, and its replacement with a cheaper, more abundant metal is desirable. A good alternative to ruthenium could be copper, which possesses similar photophysical properties in coordination with diimine ligands, but it is considerably cheaper and relatively earth-abundant. In this work, a particular "on-surface self-assembly" strategy was employed to form, on the surface of TiO_2, heteroleptic copper (I) complexes with a "push-pull" design which facilitates the electron transfer from the copper (I) complex into the conduction band of TiO_2 and enhances the performance of the photovoltaic devices.

This thesis focuses on the investigation of the properties of five new heteroleptic copper (I) complexes bearing the same anchoring ligand but different ancillary ligands. Because of the method employed for their synthesis, a solid-state characterization of the optical and electrochemical properties on TiO_2 was performed employing tools such as UV-Vis spectroscopy, cyclic voltammetry (CV), and differential pulse voltammetry (DPV). As internal benchmark through the entire characterization, the homoleptic copper (I) complex with the anchoring ligand was also studied. Some patterns between the heteroleptic complexes on TiO_2 and their respective homoleptic complexes in solution were found, opening the possibility to predict the behaviour of unknown heteroleptic complexes starting from their corresponding homoleptic. Furthermore, the characterization was necessary to ensure that the complexes were fulfilling the requirements to be employed as dyes. The performances of the heteroleptic, and of the anchoring-ligand homoleptic, copper (I) complexes were then investigated as photosensitizers in DSC devices mainly by measuring the current density-voltage (*J-V*) characteristics at different light intensities and in the dark, the incident photon-to-current efficiency (IPCE), and electron lifetimes. As benchmark for the degree of effectiveness of the device, the state-of-the-art ruthenium (II) complex N719 was also studied. All the copper (I) complexes showed an overall similar behaviour. The *J-V* characteristics showed a power conversion efficiency up to 2,05% for the best performing device, which is 25% of the efficiency of DSCs based on N719. On the other hand, the least performing heteroleptic copper (I) complex studied showed an efficiency of 1,23%. From a general analysis combining all the results obtained, it may be concluded that a reason for the limited photocurrent measured through these devices can be due to incomplete dye coverage of TiO_2. Despite the lower performance compared to the standard dye N719, the simplicity of the system is promising, and its considerable economic advantage could pave the way to the use of DSCs in everyday life applications.

Sammanfattning

Modernt samhälle är mycket beroende på energi och det blir allt mer akut att hitta alternativa källor till fossila bränslen. Solen är den mest riklig energikällan som finns och att utnyttja den effektivt skulle resultera i stora miljö- och ekonomiska genombrott. Färgämne sensibiliserade solceller (”dye-sensitized solar cells”; DSC) utvecklade i 90-talet för sin breda kommersiella potential som härrör från en kombination av låg kostnadsproduktion och attraktiva egenskaper, såsom möjligheter för flexibilitet och transparens. I DSC är ett färgämne förankrat till den ytan av en halvledare (vanligtvis TiO_2). Färgämnet är ansvarigt för att fånga solljuset och överföra elektronerna till halvledaren för att producera el. Många kommersiella färgämnen för DSC är baserade på rutenium, en mycket sällsynt metall. Ersättning av rutenium med en billigare, rikligmetall är önskvärt mot mer hållbara DSC. En bra alternativmetall till rutenium är koppar. Komplexen av koppar(I) har liknande fotofysiska egenskaper till rutenium (II) men koppar är mer vanlig och mindre dyr än rutenium. Heteroleptiska koppar(I) komplexen med en "push-pull" design syntetiserades på ytan av TiO_2 genom "ytan assisterade självmontering". "Push-pull" designen underlättar elektronöverföring från koppar(I)-komplexet till ledningsbandet av TiO_2.

Denna avhandling fokuseras på undersökning av egenskaperna av fem nya heteroleptiska koppar(I) komplex med den samma förankrings ligand men olika distala ligander. På grund av metoden som används i syntesen av heteroleptiska koppar(I) komplex, var karakterisering av komplexen vid optiska och elektrokemiska metoder utfördes på TiO_2. Metoderna för karakterisering var UV-Vis-spektroskopi, cyklisk voltametri (CV) och differentialpuls voltametri (DPV). Som en intern standard genom hela karaktäriseringen studerades även homoleptiska koppar(I) komplex med förankringsliganden. Egenskaperna på heteroleptiska koppar(I) komplexen på TiO_2 ytan kunde förutsägas från mätning av egenskaperna på homoleptiska koppar(I) komplexen. Koppar(I) komplexen är undersöktes som fotosensibiliserare i färg-sensibiliserade solceller. Effektiviteten av solcellerna med koppar(I) komplexen eller rutenium (II) komplex (N719) utvärderades genom att mäta fotokurrentdensitetsspänningen (*J-V*) vid olika ljusintensiteter, incidentfoton-till-ström effektiviteten (”incident photon-to-current efficiency”; IPCE) och laddningsrekombinationen (elektronlivstiden). Koppar(I) komplexen hade övergripande liknande egenskaper i solceller. En kraft omvandlingseffektivitet av 2,05% nås för den bästa solcellen med ett koppar(I) komplex. Medan den bästa effektiviteten med N719 färgämnet var 7,57%. En svaghet i självmonteringen av koppar(I) komplexen på ytan av TiO_2 är den ofullständiga bindningen till ytan men självmonteringen metoden var enkel och kunde skapa många, olika färgämnen i kort tid. Trots den lägre prestandan jämfört med standardfärgen N719 är systemets enkelhet lovande, och dess stora ekonomiska fördel kan bana vägen till användningen av DSC i vardagsläget.

Riassunto breve

La civiltà moderna è fondata sull'uso dell'energia e trovare fonti alternative ai combustibili fossili è diventato sempre più necessario. La radiazione proveniente dal sole è la risorsa energetica più abbondante e disponibile sul nostro pianeta e sfruttarla al massimo comporterebbe una svolta decisiva per l'ambiente e l'economia. Tra i dispositivi fotovoltaici, le celle di Grätzel, conosciute anche come DSC dall'acronimo inglese (dye-sensitized solar cell), sono emerse per il loro enorme potenziale commerciale, dovuto alla combinazione tra basso costo di produzione e interessanti caratteristiche, come la loro flessibilità e trasparenza, che gli conferiscono la possibilità di integrazione negli edifici e l'uso in applicazioni "indoor". Nelle DSC, un foto-sensibilizzatore, detto anche dye, ancorato ad uno strato di un materiale semiconduttore (tipicamente TiO_2), è responsabile della cattura della luce solare e della sua conversione in elettricità. Tra i dye commercialmente disponibili per le DSC vi sono per lo più complessi di coordinazione basati su un metallo molto raro, il rutenio; la sua sostituzione con un metallo più abbondante ed economico è auspicabile per la diffusione di questa tecnologia. Una buona alternativa al rutenio potrebbe essere fornita dal rame, che possiede proprietà foto-fisiche molto simili al primo quando in coordinazione con diimmine; in più è abbastanza economico e relativamente abbondante sulla Terra. Una particolare strategia di "autoassemblaggio sulla superficie" è stata impiegata per formare, sullo strato di TiO_2, complessi eterolettici di rame (I) con un design "push-pull" che facilita il trasferimento di elettroni dal complesso di rame (I) alla banda di conduzione di TiO_2, migliorando così le prestazioni dei dispositivi fotovoltaici.

Questa tesi si concentra sullo studio delle proprietà di cinque nuovi complessi eterolettici di rame (I) che possiedono lo stesso legante di ancoraggio ma diverso legante secondario. A causa del metodo impiegato per la loro sintesi, è stato necessario eseguire la caratterizzazione delle loro proprietà ottiche ed elettrochimiche direttamente sulla superficie del TiO_2, utilizzando strumenti come la spettroscopia UV-Visibile, la voltammetria ciclica (CV) e la voltammetria ad impulsi differenziali (DPV). Come riferimento interno durante l'intera caratterizzazione, è stato studiato anche il complesso di rame (I) omolettico con il legante di ancoraggio. Tra i complessi eterolettici su TiO_2 e i loro rispettivi complessi omolettici in soluzione, è stato individuato un trend con la possibilità di prevedere il comportamento dei primi a partire dal loro corrispondente omolettico. Inoltre, la caratterizzazione ottica ed elettrochimica è necessaria per garantire l'adeguatezza dei complessi come dye. Le prestazioni dei complessi eterolettici e del complesso omolettico con il legante di ancoraggio, sono state quindi studiate come foto-sensibilizzatori nei dispositivi DSC; in particolare è stata misurata la curva di densità di corrente – voltaggio (*J-V*) a diverse intensità di luce e al buio, l'efficienza quantica esterna (EQE o dall'acronimo inglese incident photon-to-current efficiency, IPCE) e infine il tempo di vita dell'elettrone nella banda di conduzione del semiconduttore. Come standard interno, per verificare l'efficacia del dispositivo, è stato anche studiato il ben noto complesso di rutenio (II), N719. Generalmente, tutti i complessi di rame (I) hanno mostrato un comportamento simile. Le curve caratteristiche *J-V* hanno presentato un'efficienza pari fino al 2,05% per il complesso di rame che ha dato le prestazioni migliori (25% dell'efficienza di N719). Da un'analisi generale che combina tutti i risultati ottenuti, si può concludere che una ragione per cui la foto-corrente risulta limitata potrebbe essere data dall'incompleta copertura del TiO_2 da parte del complesso di rame (I) e quindi dallo scarso adsorbimento del dye. Nonostante le prestazioni inferiori rispetto allo standard N719, la semplicità del sistema è promettente e il suo notevole vantaggio economico potrebbe aprire la strada all'utilizzo delle DSC nelle applicazioni della vita quotidiana.

List of Abbreviations

AM	Air Mass
ACN	Acetonitrile
BIPV	Building integrated photovoltaic
bpy	bipyridine
CB	Conduction band
CE	Counter electrode
CV	Cyclic voltammetry
DMSO	Dimethyl sulfoxide
DPV	Differential pulse voltammetry
D-π-A	Donor-πlinker-acceptor
DSC	Dye-sensitized solar cell
E_F	*quasi*-Fermi level
EQE	External quantum efficiency
E_{redox}	Nernst potential or redox potential
Fc	Ferrocene
FF	Fill factor
FTO	Fluorine-doped tin oxide
HOMO	Highest occupied molecular orbital
ILs	Ionic liquids
I_{MP}	Current at maximum power, mA
IPCE	Incident-photon-to-current efficiency
I_{SC}	Short circuit current, mA
J_{SC}	Short circuit current density, $mA \cdot cm^{-2}$
J-V	Current density-voltage

L_{anchor}	Anchoring ligand
$L_{ancillary}$	Ancillary ligand
LUMO	Lowest unoccupied molecular orbital
MLCT	Metal to ligand charge transfer
MPN	3-Methoxy-propionitrile
Mtoe	Million tonnes of oil equivalent
NHE	Normal Hydrogen Electrode
PCE	Photoelectrochemical cells
phen	1,10-Phenanthroline
P_{in}	Intensity of the incident light, W
P_{max}	Maximum power point, W
PV	Photovoltaic
R_{CH}	Characteristic resistance, $\Omega \cdot cm^2$
R_S	Series resistance, $\Omega \cdot cm^2$
R_{SH}	Shunt resistance, $\Omega \cdot cm^2$
SHC	Solar heating and cooling
SS-DSC	Solid state dye-sensitized solar cell
$TBAPF_6$	Tetrabutylammonium hexafluorophosphate
TBP	4-Tert-butylpyridine
TCO	Transparent conducting oxide
UV-Vis	Ultraviolet-visible
V_{MP}	Voltage at maximum power, V
V_{OC}	Open circuit voltage, V
WE	Working electrode
XPS	X-ray photoelectron spectroscopy

τ_e	Electron lifetime, s
η	Overall power conversion efficiency

Table of contents

Sommario

Premessa

Il notevole aumento della popolazione e lo sviluppo dei paesi emergenti hanno portato nell'ultimo secolo ad un drastico aumento del consumo energetico globale. I combustibili fossili sono tutt'ora la fonte primaria di energia, ma vista la loro limitatezza e le conseguenze catastrofiche che la loro combustione sconsiderata sta creando per l'ambiente e il clima, l'interesse pubblico si sta lentamente spostando verso fonti di energia più pulite e rinnovabili. Tra queste ultime, il sole rappresenta la più abbondante, basti pensare che ogni ora fornisce alla Terra più energia di tutto il consumo annuale dell'umanità. L'energia solare può essere sfruttata per la produzione diretta dell'energia elettrica, attraverso il processo fotovoltaico. Nell'ultimo decennio la crescita del fotovoltaico è stata quasi esponenziale e il suo sviluppo può essere riassunto considerando tre principali generazioni. La prima include le celle monocristalline e policristalline al silicio, che attualmente dominano il mercato e coprono circa il 90% dell'intera produzione fotovoltaica. I principali svantaggi dell'uso di queste celle sono la loro rigidità e i costosi processi di produzione dei cristalli di silicio. Inizialmente questa tecnologia era proibitiva su larga scala e questo spiega anche perché il fotovoltaico non si era diffuso tanto quanto altre energie rinnovabili. Negli anni il prezzo dei cristalli di silicio è crollato ma i tempi di ammortamento di un impianto, l'energy payback time (EPBT), sono ancora relativamente lunghi, di circa 2,4 anni. Inoltre, essi hanno un'elevata dipendenza dalla temperatura e dall'inclinazione rispetto al sole. La seconda generazione del fotovoltaico si basa sulla riduzione dei costi mediante l'impiego della tecnologia a "film sottile"; ne fanno parte i pannelli a silicio amorfo, le celle al cadmio-tellurio e le celle al rame-indio-gallio-selenio. Queste celle sono più flessibili, meno suscettibili a rottura ma, presentando meno materiale, la loro efficienza risulta più bassa e pertanto il costo del sistema risulta maggiore. La terza generazione comprende nuove tecnologie a film sottile con materiali emergenti. Questa generazione è per la maggior parte ancora a livello sperimentale e molte ricerche si concentrano nei laboratori dove nuovi materiali diversi vengono testati e sviluppati ingegneristicamente in diversi sistemi. Le diverse generazioni del fotovoltaico possono anche essere categorizzate sulla base del materiale attivo utilizzato nella cella solare come raffigurato in Figura 2.4. Secondo questa catalogazione, la terza generazione è rappresentata proprio dai nuovi materiali emergenti e ne fanno parte le celle basate sui quantum dots, le perovskiti, le celle organiche e le celle di Gräztel (o dall'acronimo inglese "dye-sensitized solar cell", DSC).

Dye-sensitized solar cell

Tra le celle solari emergenti le dye-sensitized solar cell hanno fin dall'inizio catturato l'attenzione di molti ricercatori e la loro crescita è stata dettata dalla scoperta di O'Regan e Gräztel pubblicata nel loro articolo in *Nature* nel 1991. Si tratta di una tecnologia ispirata al processo naturale della fotosintesi, che ha il potenziale di avere un forte impatto commerciale grazie al suo basso costo di produzione, bassi tempi di ammortamento (meno di 1 anno) e alta variabilità di design. Queste celle possiedono un alto grado di adattabilità e potere estetico: possono essere trasparenti o di vari colori, di diverse forme, stampate su materiali rigidi come il vetro o flessibili come le plastiche. Queste peculiari caratteristiche conferiscono l'opportunità

a queste celle di essere competitive sul mercato data la possibilità di integrazione negli edifici ("building integrated photovoltaic", BIPV) e, viste le loro buone prestazioni sotto luce diffusa, per il loro uso nelle applicazioni "indoor".

La Figura 2.6 mostra lo schema di una convenzionale cella liquida di Gräztel: da sinistra verso destra vi è raffigurato l'elettrodo di lavoro (anodo) con un sottile strato di semiconduttore, tipicamente TiO_2, dove il composto foto-attivo (dye), il cuore centrale del sistema, è ancorato, un elettrolita liquido e infine un contro elettrodo (catodo) su cui è presente un film di catalizzatore.

Il principio di funzionamento base della DSC è rappresento in Figura 2.9. Il foto-sensibilizzatore è dapprima eccitato grazie all'energia della luce visibile e l'elettrone salta dall'orbitale molecolare occupato a più alta energia (HOMO) all'orbitale molecolare non occupato a più bassa energia (LUMO). A seguire, l'elettrone è iniettato nella banda di conduzione del semiconduttore, TiO_2, dove raggiunge l'elettrodo di lavoro e passando attraverso un carico esterno, raggiunge il contro elettrodo, generando una corrente. La forma ossidata della coppia redox viene ridotta sul catalizzatore del contro elettrodo e a sua volta riduce la forma ossidata del dye rigenerandolo e completando il ciclo. Il massimo foto-voltaggio all'interno della cella (che corrisponde al voltaggio a circuito aperto, V_{OC}) è dato dalla differenza tra il livello di Fermi (E_F) del semiconduttore e il potenziale di Nernst (E_{redox}) della coppia redox dell'elettrolita.

L'elettrodo di lavoro usato è un substrato di vetro ricoperto da uno strato trasparente di ossido conduttore, comunemente ossido di stagno drogato con fluoro (FTO). Su questo strato conduttivo si prepara un film di biossido di titanio, stabile e non tossico, che possiede tra le sue varie forme cristalline la struttura *anatasio*, preferita alla struttura termodinamicamente più stabile *rutilo*. Questa preferenza è dovuta al fatto che la struttura *anatasio* possiede una differenza di energia tra il massimo della banda di valenza e il minimo della banda di conduzione (band gap) più alta, incrementando la performance della cella stessa.

L'elettrolita gioca un ruolo fondamentale e contiene tre principali componenti: la coppia redox, co-additivi e il solvente. I requisiti fondamentali della coppia redox sono un alto coefficiente di diffusione per facilitarne il trasporto all'interno della cella, minimo assorbimento della luce visibile, alto potenziale redox, bassa ma sufficiente forza spingente per rigenerare il dye ossidato, buona stabilità e proprietà non corrosive verso i contatti metallici. Tra le coppie redox, la più impiegata è la coppia ioduro/triioduro, I^-/I_3^-, ma altre, ampiamente studiate di recente, sono le bipiridine di cobalto, $[Co(bpy)]^{3+/2+}$. Nei diversi studi, noti in letteratura, la presenza di co-additivi come i sali di litio e la 4-tert-butilpiridina (TBP) risulta di notevole importanza per aumentare la performance del dispositivo. Infine, il sovente dell'elettrolita deve possedere un'ampia finestra elettrochimica, una elevata costante dielettrica, una bassa viscosità per facilitare la diffusione e una bassa pressione di vapore per aumentare la stabilità.

Il contro elettrodo è preparato con un substrato di vetro conduttore sul quale è depositato un sottile film di catalizzatore. Per la coppia redox ioduro/triioduro tipicamente il catalizzatore utilizzato è il platino, mentre per le coppie di cobalto possono essere impiegati carbonio poroso o poli(3,4-etilendiossitiofene) (PEDOT).

Il foto-sensibilizzatore, il dye, ricopre il compito fondamentale di sfruttare l'energia delle radiazioni del sole. Le caratteristiche essenziali che un dye deve possedere sono: un largo spettro di assorbimento nella regione del visibile o vicino all'infrarosso, dove si evidenzia una maggiore quantità di energia solare disponibile, un potenziale dello stato eccitato più negativo del potenziale della banda di conduzione (CB) del semiconduttore e uno stato fondamentale con un potenziale più positivo rispetto al potenziale della coppia redox. Attualmente una miriade di dye diversi sono stati testati. Tra i complessi di coordinazione, caratterizzati da uno ione metallico centrale coordinato con leganti quali bipiridine e fenantroline, spiccano quelli di rutenio (II). L'assorbimento della luce visibile è dovuto ad un processo di trasferimento di

carica da metallo a legante (MLCT), in cui l'elettrone è eccitato dall'orbitale *d* del metallo all'orbitale antilegame π^* dei leganti. I complessi di rutenio (II) hanno raggiunto un'efficienza superiore al 10% e hanno mostrato ottime proprietà fotovoltaiche. Mostrano, infatti, un ampio spettro di assorbimento, buona stabilità e livelli energetici adeguati. Un altro dye, che ha raggiunto il valore record di efficienza del 13%, è un complesso sistema basato su una struttura porfirinica coordinata con lo zinco. La sua struttura possiede un meccanismo "donatore-πlinker-accettore" (D-π-A), il quale incorpora un sistema "push-pull" dove il trasferimento elettronico è agevolato dal gruppo donatore al gruppo accettore per la loro conformazione strutturale. Questo sistema è atto ad aumentare l'assorbimento luminoso e a facilitare l'iniezione dell'elettrone nella banda di conduzione del semiconduttore. Anche i dye organici hanno dato buone prestazioni e la loro complessa struttura sintetizzata combina alti valori di coefficienti di estinzione molare con questo sistema "push-pull". Tuttavia, nella ricerca di nuovi dye spesso si utilizza come riferimento il complesso di rutenio (II) conosciuto con il nome N719, per la semplicità del sistema e per la sua buona risposta.

L'obiettivo è quello di trovare un sistema paragonabile a quello del rutenio, basato quindi su un complesso di coordinazione, ma impiegando un metallo che sia più economico e più abbondante sulla Terra.

I complessi di rame (I)

I complessi di rame (I) sono stati introdotti per la prima volta come foto-sensibilizzatori da Sauvage *et al.* in celle fotoelettrochimiche nel 1983. L'interesse per questi complessi è dato dalle simili proprietà foto-fisiche del rutenio quando in coordinazione con le diimmine, il loro considerevole vantaggio economico e la loro relativa abbondanza sulla Terra. Recentemente Constable e colleghi hanno riportato vari lavori sull'uso di complessi di rame (I) come dye nelle DSC. Il loro principale svantaggio è che possiedono in generale un coefficiente di estinzione molare più basso rispetto a quello del rutenio. A livello foto-fisico, entrambi assorbono nel range tra 400 e 550 nm con un trasferimento di carica dal metallo al legante. La principale differenza tra i due metalli è che quando il complesso di rame viene eccitato e la densità di elettroni si muove dal rame (I) sui leganti, questo risulta formalmente in rame (II)*. Pertanto, mentre i complessi di rutenio (II) non subiscono alcun cambiamento di geometria, i complessi di rame (I) passano da una geometria tetraedrica (tipica del rame (I)) ad una geometria planare (tipica del rame (II)), che lascia spazio a maggiori interazioni con le molecole di solvente diminuendone la stabilità dello stato eccitato e cambiando le proprietà ottiche ed elettrochimiche del complesso stesso. La Figura 2.13b mostra come la presenza di specifici sostituenti nei leganti può limitare questa distorsione minimizzando la planarizzazione e assicurando le caratteristiche del complesso. Queste posizioni, anche definite per il loro effetto, "posizioni di blocco", sono ad esempio le posizioni 2,9 nella 1,10-fenantrolina e 6,6' per la 2,2'-bipiridina. Inoltre, per aumentare la prestazione del complesso, si è voluto introdurre lo stesso sistema "push-pull" che richiama quello precedentemente descritto. Per incorporare tale meccanismo sono stati utilizzati complessi eterolettici di rame (I) con due diversi leganti. Come mostrato in Figura 2.14 sono presenti un legante di ancoraggio, attaccato sullo strato dell'elettrodo di FTO/TiO_2 e accettore di elettroni, l'atomo di rame, che ha la funzione di collegare e donare elettroni e un legante secondario, scelto per aumentare la densità elettronica sull'atomo del metallo.

La prima sfida per generare i complessi eterolettici di rame (I) è data dalla inaffidabile formazione del complesso desiderato in soluzione. A causa della labilità del sistema che rapidamente scambia leganti, i complessi eterolettici tenderebbero in soluzione all'equilibrio dando miscele dei rispettivi omolettici e solo parziale presenza dell'eterolettico desiderato.

Sono note in letteratura diverse strategie per prevenire la disgregazione del complesso. La strada che si è seguita in questo lavoro è quella proposta da Constable *et al.* ed è basata su un "auto-assemblaggio sulla superficie" come mostrato in Figura 2.15. Questo particolare processo consiste dapprima nell'immergere il substrato di TiO_2 in un primo bagno del solo legante di ancoraggio, capace di unirsi al semiconduttore grazie alla presenza di gruppi reattivi quali gli acidi carbossilici. Una volta ottenuto il substrato funzionalizzato, questo è immerso in un secondo bagno con il complesso omolettico del legante secondario. Durante questo secondo bagno, attraverso un meccanismo di scambio, sulla superficie del biossido di titanio si forma quindi il complesso eterolettico desiderato. Adoperando questo metodo di auto-assemblaggio, il carattere distintivo di questi complessi eterolettici, oggetto di studio in questa tesi, è il bisogno di doverli studiare sulla superficie di TiO_2, rendendo la caratterizzazione più complessa.

I leganti di interesse

Scegliendo leganti differenti si raggiungono diversi assorbimenti di luce. Inoltre, per limitare la planarizzazione del complesso, sono stati selezionati leganti possedenti le preaccennate "posizioni di blocco".

Come legante di ancoraggio, è stato scelto l'acido 6,6'dimetil-2,2'bipiridin-4,4'dibenzoico, L1, mostrato in Figura 3.2 e sintetizzato da un collaboratore dell'Università di Uppsala. In letteratura, infatti, l'intero complesso con questo legante era già stato testato ed aveva prodotto una tra le migliori efficienze nei complessi di rame (I), raggiungendo un valore pari al 3%. Nelle "posizioni di blocco" i sostituenti possono essere gruppi metilici o gruppi fenilici, tuttavia studi precedenti hanno dimostrato che la presenza dei gruppi fenilici da un lato aumentano l'assorbimento nel rosso, dall'altro diminuiscono di gran lunga la conversione in corrente elettrica nel funzionamento della cella, soprattutto se presenti nel legante di ancoraggio; pertanto L1 è stato scelto con sostituenti metilici.

Per quanto riguarda i leganti secondari, come anticipato, essi devono essere donatori di elettroni per essere efficienti nella loro funzione all'interno del sistema "push-pull". La loro scelta è stata dettata per coprire un ampio range di proprietà diverse, derivanti dal diverso impedimento sterico delle "posizioni di blocco", dalle diverse proprietà redox e dalla diversa rigidità del cuore della struttura. In generale si auspicava anche un elevato grado di coniugazione dato che la delocalizzazione degli elettroni nella sovrapposizione degli orbitali *p* dei doppi legami comporta un aumento dell'assorbimento della luce. I leganti selezionati L2, L4, L5, L6 e L7 sono mostrati in Figura 3.3. Ad eccezione del legante L5 che è stato scelto per le peculiari caratteristiche note dalla letteratura e sintetizzato da collaboratori del KTH, tutti gli altri leganti sono commercialmente disponibili e acquistati dalla Sigma Aldrich. Ad eccezione di L6 che è una 2,2' biquinolina, tutti gli altri possiedono come struttura base una fenantrolina. Per quanto riguarda la formazione dei complessi omolettici a partire dai leganti, questa è stata realizzata sempre dai collaboratori del KTH.

Caratterizzazione dei foto-sensibilizzatori

I substrati per la caratterizzazione ottica ed elettrochimica sono preparati su vetro conduttore. Lo strato di semiconduttore, TiO_2, è stato preparato tramite la tecnica del "doctor blading" che prevede l'uso di una bacchetta di vetro cilindrica per spalmare equamente la pasta di TiO_2 sul vetro tenuto fermo da nastro adesivo. Questa tecnica, nonostante potesse comportare maggiore disomogeneità dello strato, è stata preferita rispetto allo "spin coating" poiché permetteva substrati di semiconduttore più spessi (di circa 7-8 μm). È seguito dal processo di

sinterizzazione per ottenere la desiderata superficie porosa di nanoparticelle. Infine, i substrati sono stati immersi nelle soluzioni di interesse per effettuare il metodo di "auto-assemblaggio sulla superficie".

Per la caratterizzazione ottica dei dye è stata impiegata la spettroscopia ultravioletti-visibile (UV-Vis). L'assorbimento dei fotoni in questi range comporta transizioni elettroniche nella molecola e gli elettroni sono eccitati dall'HOMO al LUMO, dove solo i fotoni con energia pari o maggiore della transizione possono essere assorbiti, ricordando che l'energia dei fotoni è inversamente proporzionale alla lunghezza d'onda (Equazione 4.1). L'assorbimento nel visibile è stato studiato sia per i complessi omolettici di rame (I) in soluzione sia per i complessi eterolettici di rame (I) su TiO_2 e il loro confronto è mostrato in Figura 4.6. Siccome l'interesse è nel range del visibile gli spettri riportano lunghezze d'onda tra 750 e 400 nm. Come riportato in letteratura, tipici assorbimenti dei complessi di rame mostrano una transizione energetica primaria e un'ampia spalla che si estende nella porzione del rosso dello spettro. La prima dipende dal grado di delocalizzazione degli elettroni sui leganti, la spalla è invece collegata al grado di distorsione dei complessi. Quando la spalla è quasi assente come nel caso del complesso omolettico con L5, $[Cu(L5)_2]^+$, il complesso mantiene maggiormente la configurazione tetraedrica del rame (I). Quando è visibile una spalla più pronunciata, questo è indice di una distorsione più facile nella conformazione planare. Nel caso di $[Cu(L7)_2]^+$, l'ampia spalla però non può essere razionalizzata così facilmente dato che è tipica dei sostituenti 2,9-dianisili. Per quanto riguarda $[Cu(L1)_2]^+$, è stato raffigurato tramite una linea-punto in quanto misurato in metanolo a differenza degli altri complessi omolettici che sono stati misurati in acetonitrile. Una prima differenza che risalta all'occhio è il maggior allargamento degli spettri quando misurati sul film di TiO_2 anziché in soluzione. Questo confronto può essere direttamente fatto con $[Cu(L1)_2]^+$, che è presente in entrambe le caratterizzazioni. Inoltre, il valore di lunghezza d'onda di massimo assorbimento, λ_{max}, risulta leggermente spostato verso il blu quando il complesso è adsorbito sul biossido di titanio. Quest'ultimo può essere spiegato dalla presenza di differenti ambienti chimici ed elettronici che giocano un ruolo importante nella posizione della banda di assorbimento.

Tra i complessi omolettici, dal rosso verso il blu dello spettro, è stato osservato il seguente ordine: $[Cu(L6)_2]^+$, $[Cu(L1)_2]^+$, $[Cu(L4)_2]^+$, $[Cu(L2)_2]^+$, $[Cu(L5)_2]^+$ e ultimo $[Cu(L7)_2]^+$. Un assorbimento spostato nel rosso è più desiderabile in quanto, come già detto, è lì che lo spettro solare è più ricco. L'ordine è in accordo con il grado di coniugazione presente nella molecola ad eccezione di $[Cu(L7)_2]^+$ che possiede un ampia spalla che come precedentemente menzionato è tipica dei suoi sostituenti.

I complessi su TiO_2 seguono un trend simile: $[Cu(L1)(L6)]^+$, $[Cu(L1)_2]^+$, $[Cu(L1)(L4)]^+$, $[Cu(L1)(L5)]^+ \approx [Cu(L1)(L2)]^+$, ma i loro valori di assorbanza mostravano valori abbastanza bassi, tra 0,2 e 0,4, suggerendo un basso grado di adsorbimento del complesso sulla superficie. Tracciando un grafico dei λ_{max} dei complessi omolettici in soluzione sull'asse delle ascisse e i complessi auto-assemblati sulla superficie di TiO_2 con il legante di ancoraggio sull'asse delle ordinate (Figura 4.8), è stato individuato un andamento lineare che tiene in considerazione sia l'influenza del substrato sia l'assemblaggio con L1. Questo andamento è interessante in quanto può essere usato come strumento per prevedere il comportamento di nuovi complessi eterolettici a partire dai corrispettivi omolettici in soluzione. Per esempio è stato utilizzato per individuare il valore di λ_{max} di $[Cu(L1)(L7)]^+$, siccome la presenza dell'ampia spalla ne impediva una localizzazione diretta dallo spettro.

Attraverso la legge di Lambert-Beer, $A = \varepsilon\, c\, l$, è stato calcolato il coefficiente di estinzione molare riferito al valore di lunghezza d'onda di massimo assorbimento, $\varepsilon_{\lambda max}$. Questo valore è indicativo di quanto fortemente una sostanza assorbe la luce ad una specifica lunghezza d'onda, pertanto è altamente desiderabile avere elevati valori di ε per avere un buon rendimento nella cella. La Tabella 4.1 mostra i valori di λ_{max} e $\varepsilon_{\lambda max}$ dei complessi omolettici

in soluzione. Eccetto $[Cu(L1)_2]^+$ e il complesso di rutenio (II) N719, i valori si riferiscono a soluzioni di acetonitrile, mentre per i due citati i valori si riferiscono a soluzioni di metanolo, data la loro insolubilità nel primo. L'N719 è stato inserito per avere un riferimento utile per l'impiego dei complessi di rame (I) all'interno del sistema delle DSC. I valori di ε dei complessi $[Cu(L7)_2]^+$, $[Cu(L6)_2]^+$ e $[Cu(L2)_2]^+$ sono molto più bassi in confronto a quelli del rutenio. Il complesso $[Cu(L4)_2]^+$ ha invece valori comparabili mentre il complesso $[Cu(L1)_2]^+$, il cui valore è stato riportato dal lavoro di Biagini *et al.,* è addirittura più alto. Il calcolo dei valori dei coefficienti di estinzione molare per i complessi eterolettici, data la peculiarità del loro assemblaggio, non è stato realizzato in quanto avrebbe portato ad elevati errori nel risultato finale.

Per il calcolo della distanza HOMO-LUMO, si è provato a misurare anche lo spettro di emissione, che rileva l'energia dei fotoni emessa dalle molecole durante la loro transizione dallo stato eccitato allo stato fondamentale. La distanza HOMO-LUMO la si può accuratamente calcolare come intersezione tra lo spettro di assorbimento e lo spettro di emissione. Tuttavia, non è stato possibile identificare alcun chiaro spettro di emissione dalle misure effettuate nonostante i diversi tentativi fatti, probabilmente ciò è dovuto a meccanismi di smorzamento (quenching) che hanno coperto i picchi di interesse. Una stima approssimativa può anche essere fatta dal solo spettro di assorbimento, ad esempio prendendo il valore di lunghezza d'onda relativo all'inizio dell'insorgenza dell'assorbanza (onset). Così facendo in Tabella 4.2 è stata riportata la distanza HOMO-LUMO dei complessi eterolettici.

Per la caratterizzazione elettrochimica, è stata misurata la voltammetria ciclica (CV) sui complessi omolettici in soluzione e la voltammetria ad impulsi differenziali (DPV) sui complessi adsorbiti su TiO_2 in modo da determinarne i potenziali di ossido-riduzione. Nella voltammetria ciclica, il potenziale viene modificato linearmente avanti e indietro tra due estremi e si misura la corrente anodica e catodica, da cui si determina $E_{1/2}$ dal valore intermedio tra il picco anodico e il picco catodico. Nella voltammetria ad impulsi differenziali, il potenziale si porta da un valore iniziale ad un valore finale applicando piccoli impulsi e le reazioni possono essere analizzate con maggior sensibilità.

La Figura 4.9 mostra la voltammetria ciclica dei complessi omolettici con i soli leganti secondari, misurati in acetonitrile (ACN) con 0,1 M di tetrabutilammonio esafluorofosfato ($TBAPF_6$) come elettrolita di supporto, misurati *versus* $Ag/AgNO_3$ e riportati *versus* ferrocene. Le curve esibiscono un chiaro punto di ossidazione e riduzione legato al passaggio da Cu(I) a Cu(II). All'interno della serie, dal più al meno ossidabile, troviamo: $[Cu(L7)_2]^+$, $[Cu(L4)_2]^+$, $[Cu(L2)_2]^+$, $[Cu(L6)_2]^+$ e $[Cu(L5)_2]^+$. I potenziali redox riflettono due aspetti principali dei complessi: l'efficacia delle "posizioni di blocco", che sposta a valori più elevati il potenziale, e l'effetto donatore di elettroni, che sposta il potenziale a valori più bassi. Questo spiega perché il complesso $[Cu(L5)_2]^+$ è quello più difficile da ossidare, infatti possiede i gruppi sec-butil nelle "posizioni di blocco" che sono i più ingombranti nella serie. È seguito da $[Cu(L6)_2]^+$ che possiede gruppi fenili, stericamente esigenti in quelle posizioni, invece i complessi $[Cu(L7)_2]^+$ e $[Cu(L4)_2]^+$ sono i più facili da ossidare per il maggior effetto elettron-donatore dovuto alla presenza dei sostituenti. Infine, $[Cu(L2)_2]^+$ ha potenziale leggermente più alto rispetto a $[Cu(L4)_2]^+$ dato che la loro struttura è simile, ma il primo non possiede i gruppi fenili elettron-donatori nelle posizioni 4,4' del corpo principale.

Uno studio particolare per il complesso del legame di ancoraggio, $[Cu(L1)_2]^+$, è stato condotto data la sua totale insolubilità in acetonitrile. Siccome non si era in possesso direttamente del complesso ma solo di quantità limitata del legante, per il calcolo della voltammetria ciclica è stata utilizzata una soluzione di 1,5 mM di Cu(I) e 3 mM di L1 in dimetilsolfossido (DMSO) con 0,1 $TBAPF_6$. Così facendo, altri meccanismi possono aver influenzato il risultato della CV, come una monosostituzione sul rame (I) del solvente con il legante o una coordinazione tra i gruppi carbossilici e il rame stesso. La Figura 4.10 mostra la

CV, a sinistra, del solo Cu(I) e, a destra, del mix L1 e Cu(I). La voltammetria del complesso risulta poco chiara, ma è ragionevole pensare che i picchi di ossidazione e riduzione sono quelli segnati nella figura tramite due tratti neri e che il potenziale redox cade intorno allo 0,12 V *vs* Fc^+/Fc in DMSO (0,1 $TBAPF_6$).

Per un paragone tra i complessi omolettici ed eterolettici, la DPV si è preferita dato l'elevato spessore del substrato di TiO_2 impiegato. In Figura 4.11 è mostrato un confronto tra i complessi omolettici in soluzione e i complessi auto-assemblati su TiO_2. $[Cu(L1)_2]^+$ anche in questo caso è usato come indicatore interno ma con particolari accortezze. Quando in soluzione, come già detto, è infatti misurato in DMSO, ma assemblato sulla superficie è stato misurato in ACN. Data la dipendenza della chimica redox dal solvente e tenendo in considerazione uno studio su un complesso di rame pubblicato da Meyer *et al.*, circa 0,13 V sono stati aggiunti al valore del potenziale redox del complesso per passare dalla soluzione in DMSO a quella di ACN. Questa aggiunta è giustificata dalla differente interazione tra i complessi di rame con solventi più o meno coordinanti.

Come fatto per la lunghezza d'onda di massimo assorbimento, è stato rappresentato in Figura 4.12 un grafico, tracciando, sull'asse delle x, i potenziali di ossidazione dei complessi omolettici in soluzione (con l'aggiunta su $[Cu(L1)_2]^+$) e, sull'asse delle y, i complessi auto-assemblati sulla superficie di TiO_2 con L1. Tuttavia, un pattern come quello osservato per λ_{max} non è stato individuato. Speculando sui risultati, possono essere suggeriti due comportamenti direttamente influenzati dai principali aspetti che si riflettono sui potenziali redox. Un primo comportamento, seguito dai leganti L4, L6 e L7, sembra dominato dall'effetto elettron-donatore di questi ultimi, che influenza maggiormente il potenziale all'interno del complesso eterolettico, i quali differiscono infatti solo di qualche decina di mV dal loro valore omolettico. Un secondo comportamento, seguito da L2 e L5, è dominato dall'effetto delle "posizioni di blocco", che nel caso omolettico sono più efficienti che in quello eterolettico, che risulta spostato a potenziali più bassi di 60-110 mV. Date le varie assunzioni fatte per $[Cu(L1)_2]^+$ si è preferito tenerlo fuori da entrambi i comportamenti. Tuttavia, questi trend ipotizzati necessitano di ulteriori conferme, studiando altri leganti secondari con caratteristiche diverse.

Nota la distanza HOMO-LUMO e considerando che il livello di HOMO corrisponde al potenziale di ossidazione *vs* l'elettrodo normale a idrogeno (NHE), in Figura 4.13 è raffigurato il diagramma dei livelli energetici dei complessi eterolettici auto-assemblati sulla superficie del TiO_2. Tutti i complessi soddisfano i requisiti necessari per un'efficace iniezione dell'elettrone sulla banda di conduzione del semiconduttore e una sufficiente forza spingente per la rigenerazione del dye tramite la coppia redox, che nel caso in figura è ioduro/triioduro, I^-/I_3^-. Pertanto, possono essere tutti impiegati come dye nella successiva caratterizzazione.

Caratterizzazione dei dye all'interno delle DSC

Per valutare le prestazioni dei complessi auto-assemblati su TiO_2 è stata dapprima misurata la curva di densità di corrente – voltaggio (*J-V*), la quale rappresenta la relazione tra la corrente generata dalla luce attraverso il dispositivo elettronico e il voltaggio applicato tra i due terminali del circuito (Figura 5.1). La struttura base della cella solare è un diodo, in presenza di luce i fotoni sono assorbiti e gli elettroni si muovono dall'anodo al catodo generando una corrente di polarizzazione inversa, chiamata foto-corrente. L'efficienza totale è il parametro di base utilizzato per confrontare le prestazioni delle celle solari ed è descritto dall'Equazione 5.1, dove I_{SC} è la corrente di cortocircuito, la V_{OC} è il voltaggio a circuito aperto, FF corrisponde al "fill factor" o fattore di riempimento, e P_{in} è l'intensità della luce incidente. Il valore di I_{SC} si ottiene quando nessun voltaggio esterno è applicato e poiché dipende dall'area ci si riferisce più comunemente alla densità di corrente di cortocircuito, J_{SC}. La V_{OC} è una misura del lavoro che

può essere fatto dalla foto-corrente: in pratica corrisponde al punto in cui la corrente indotta da un voltaggio applicato compensa totalmente la foto-corrente fino a far risultare una corrente totale nulla. Il "fill factor", spesso dato in percentuale, è dato dal prodotto di corrente e voltaggio al punto di massima potenza diviso il prodotto tra I_{SC} e V_{OC}. Un altro utile parametro per definire la cella è la resistenza caratteristica definita come $R_{CH} = V_{MP}/J_{MP}$, ma che in caso di buoni valori di FF, può essere approssimata con $R_{CH} \approx V_{OC}/J_{SC}$. All'interno del circuito, come mostrato dalla Figura 5.4, le resistenze in serie e le resistenze di shunt sono i principali agenti che influenzano il "fill factor". Le resistenze in serie, R_S, modificano la curva *J-V* nella zona vicino alla V_{OC} e sono resistenze ai contatti e al passaggio di elettroni all'interno del dispositivo. Le resistenze di shunt, R_{SH}, provengono da percorsi alternativi che la corrente generata dalla luce può seguire, sono dovuti a errori di fabbricazione e alla presenza di scarichi della corrente. Queste ultime influenzano la pendenza della curva *J-V* vicino al punto della J_{SC}.

I parametri sopra descritti sono influenzati da fattori ambientali come la temperatura, l'intensità della luce, le condizioni del cielo, la posizione del sole e l'orientamento della Terra. Pertanto, per un confronto oggettivo tra le diverse celle solari, sono state definite condizioni standard che includono la distribuzione dello spettro solare, intensità e orientamento della radiazione, e la temperatura. Queste condizioni sono espresse come "AM 1,5 G", dove AM è la cosiddetta massa d'aria, 1,5 corrisponde al reciproco del cosθ, dove θ è l'angolo di elevazione solare, angolo di Zenit, pari a 48°; infine G si riferisce all'irraggiamento globale quindi somma di quello diretto, diffuso e riflesso. In queste condizioni l'illuminazione si definisce di "1 sole" pari a 1000 Wm^{-2}. In generale, il flusso generato di elettroni è direttamente proporzionale all'intensità luminosa, mentre il foto-voltaggio aumenta in maniera logaritmica con l'intensità della luce. Effetti che si evidenziano a più basse intensità luminose sono l'aumento dell'influenza delle resistenze di shunt e del peso degli "stati intrappolati" nel quale gli elettroni sono bloccati senza avere l'energia sufficiente per l'iniezione e che quindi il risultato è una perdita di efficienza.

La corrente di buio è definita in assenza di intensità luminosa, quando si applica una polarizzazione diretta e si raggiunge un certo valore soglia, una barriera di iniezione, dove gli elettroni iniziano a muoversi dal catodo verso l'anodo e a generare una corrente molto grande. La corrente di buio può dare informazioni sulla ricombinazione tra gli elettroni iniettati e la coppia redox ossidata, dato che al buio nessun dye è nello stato eccitato. Inoltre, può dare informazioni riguardo la dimensione e la quantità di dye che copre le nanoparticelle di TiO_2, siccome esso lavora da barriera in questo processo di ricombinazione.

L'efficienza quantica esterna (EQE o dall'acronimo inglese incident photon-to-current efficiency, IPCE) è una misura della capacità della cella di convertire in elettricità una radiazione incidente ad una data lunghezza d'onda. È data dal rapporto tra la densità di corrente di cortocircuito e il flusso di fotoni monocromatico incidente. L'IPCE è utile per stimare i processi che possono limitare le prestazioni del dispositivo. Dall'integrazione dello spettro IPCE, la densità di corrente ottenuta dovrebbe essere pari a quella misurata dalla curva caratteristica *J-V*, tuttavia spesso quest'ultima risulta più grande. Ciò è principalmente dovuto alla dimensione diversa della maschera con cui si effettuano le misure e l'uso di una sorgente di luce differente anche se entrambe calibrate nelle condizioni standard. L'Equazione 5.4 descrive i fattori che influenzano l'IPCE: l'efficienza di raccolta della luce (dall'acronimo inglese "light harvesting efficiency", LHE), l'efficienza di iniezione (ϕ_{inj}), l'efficienza di rigenerazione del dye ossidato (ϕ_{reg}) e infine l'efficienza della raccolta delle cariche (η_{cc}).
Infine, l'ultima misura effettuata per la caratterizzazione dei dispositivi, è il tempo di vita dell'elettrone (τ_e) nella banda di conduzione del semiconduttore, il quale determina la dinamica del processo di ricombinazione delle cariche. Tempi di vita più elevati sono desiderabili per ottenere maggiori prestazioni dalla cella. Il tempo di vita dell'elettrone è inversamente proporzionale alla densità elettronica nel TiO_2 e quindi anch'esso ha un andamento logaritmico

con il voltaggio: all'aumentare di esso diminuisce il tempo di vita dell'elettrone. In condizioni di carico infinito, o a circuito aperto, viene calcolata la risposta dei tempi di salita e discesa della V_{OC} a seguito dell'applicazione di un segnale di voltaggio ad onda quadra. La stima del tempo di vita può dare una maggiore comprensione e un maggior controllo su questi processi di ricombinazione.

Per la fabbricazione dei dispositivi fotovoltaici di interesse, sono stati preparati sperimentalmente:

- Un elettrodo di lavoro con un film di TiO_2 trasparente ed un film di TiO_2 antiriflettente preparato tramite serigrafia ("screen printing"). Segue una prima sinterizzazione e poi l'immersione in una soluzione di $TiCl_4$ per la formazione di un "blocking layer". Infine, una seconda fase di sinterizzazione prima di proseguire con il processo di "auto-assemblaggio sulla superficie" del complesso desiderato.
- Un contro elettrodo preparato con vetri conduttori preforati con un buco, su cui è applicato un sottile strato di platino come catalizzatore.
- L'elettrolita, la cui composizione è stata determinata a seguito di un primo processo di ottimizzazione, che viene inserito tramite la formazione di vuoto all'interno dei due elettrodi precedentemente sigillati tra di loro con una cornice di Surlyn, resina ionomerica trasparente.

I primi studi dei dispositivi con i complessi di rame (I) si sono focalizzati sull'ottimizzazione del sistema, per comodità solo sul complesso ($[Cu(L1)(L4)]^+$). In particolare, si è definita dapprima la coppia redox, poi lo spessore e infine il solvente e la concentrazione dell'elettrolita.

Sia la coppia di cobalto, ($[Co(bpy)]^{3+/2+}$), che la coppia ioduro/triioduro (I^-/I_3^-) sono state provate nel sistema in esame, con un evidente vantaggio dell'uso della seconda, in accordo con la maggior parte della letteratura che utilizza questa coppia redox per altri complessi di rame(I).

Lo spessore del substrato di TiO_2 è stato ottimizzato per trovare il giusto equilibrio tra l'uso di substrati più sottili, che comportano una minor presenza di dye sulla superficie, e substrati più spessi, che aumentano il grado dei processi di ricombinazione dato che gli elettroni devono fare un percorso più lungo e turbolento prima di raggiungere l'elettrodo di lavoro. Il valore di spessore ottimale trovato si trova tra i 12-14 μm;

I primi solventi e le composizioni dell'elettrolita testati sono stati suggeriti dalla letteratura, in particolare dai lavori di Constable *et al.* e Biagini *et al.* Come solvente i primi utilizzavano 3-metossipropionitrile, mentre i secondi una miscela di acetonitrile e valeronitrile in proporzioni 85/15 in volume. Quest'ultimo è mostrato in Tabella 5.2 e ha esibito notevoli miglioramenti nell'efficienza della cella, pertanto è stato poi impiegato nell'intera caratterizzazione. Aumenti delle quantità dei co-additivi, quali il sale di litio e la tert-butilpiridina (TBP), sono stati testati in quanto noti per aumentare le prestazioni finali delle celle, ma hanno portato ad un maggior desorbimento del complesso di rame (I) dal substrato, causato dal probabile incremento dell'interazione tra il rame e l'elettrolita e quindi creando una minor stabilità nel tempo, come mostrato in Figura 5.13. L'ottimizzazione dell'elettrolita è fondamentale in quanto controlla il trasporto delle cariche e il completamento del ciclo all'interno della cella. La dimensione della coppia e la viscosità del solvente sono i principali fattori che influenzano questo trasporto. Tramite l'impiego dell'elettrolita proposto da Biagini *et al.* l'uso della coppia ioduro/triioduro in acetonitrile/valeronitrile non comporta limitazioni di questo tipo.

In generale tutti i complessi di rame (I) hanno mostrato un comportamento simile. Le curve caratteristiche *J-V* sono mostrate in Figura 5.16, misurate in condizioni standard e al buio. Come punto di riferimento per verificare l'efficacia del dispositivo, è stato anche studiato il complesso ben noto di rutenio (II), N719. Per il complesso di rame che ha dato le prestazioni migliori, $[Cu(L1)(L4)]^+$, l'efficienza ha raggiunto il 2,05%. A seguire $[Cu(L1)(L7)]^+$ con

l'1,73%, $[Cu(L1)(L5)]^+$ con l'1,71%, $[Cu(L1)(L2)]^+$, $[Cu(L1)(L6)]^+$ e $[Cu(L1)_2]^+$ con rispettivamente l'1,43%, 1,23% e 1,17%; mentre per il dispositivo basato su N719, l'efficienza ha raggiunto il valore di 7,57%. I valori di efficienza sono stati misurati come media di più celle sigillate contemporaneamente per ridurre la quantità di errori casuali e si è giunti ad un massimo di circa il 25% della performance di riferimento del complesso di rutenio. Tra i parametri delle varie celle, mostrati in Tabella 5.6, la principale differenza che risalta tra i complessi di rame (I) e il complesso di rutenio (II) è nella corrente, che poi si rispecchia anche nella efficienza. Tuttavia, i complessi di rame (I) presentano dei buoni "fill factor", FF, che non fanno pensare a problemi di ricombinazione, ad elevate resistenze in serie o che siano affetti da particolari resistenze allo shunt. I valori delle varie resistenze sono stati calcolati e mostrati in Tabella 5.9 anche in paragone con N719. Si può notare che i complessi $[Cu(L1)(L5)]^+$ e $[Cu(L1)(L6)]^+$ sono maggiormente affetti da resistenze in serie, che si rispecchiano poi in valori di FF leggermente più bassi rispetto agli altri. Questo comportamento necessita di ulteriori prove prima di giungere ad una conclusione certa; d'altronde si è osservato che la differenza in questi due complessi si riscontra anche nei loro potenziali di ossidazione nella serie, i quali sono più alti di L1. Per quanto riguarda il complesso $[Cu(L1)_2]^+$, nonostante fosse lo stesso complesso usato da Biagini *et al.*, nella caratterizzazione effettuata in questo studio, ha dato valori che sono circa un terzo rispetto a quelli riportati nella letteratura. Questo potrebbe sempre essere dovuto all'uso della soluzione creata tramite la miscela tra il legante e il rame (I), che potrebbe aver influenzato l'effettiva presenza del complesso stesso.

Tramite la diretta osservazione dei substrati, in Figura 5.18, è evidente come i colori dei complessi di rame risultano molto meno intensi rispetto al colore di N719 e ciò lascia pensare ad una scarsa copertura del dye sulla superficie delle nanoparticelle di TiO_2. Ancora più interessante è il cambiamento di colore dei complessi subito dopo l'iniezione dell'elettrolita all'interno della cella, questo comportamento porta a speculazioni già accennate sulle interazioni tra il rame e le piridine dei co-additivi ma soprattutto sulle interazioni tra il rame e le molecole di ioduro nell'elettrolita.

Osservando le curve ottenute dalle misure dell'IPCE, Figura 5.20, la forma dello spettro dà maggiori informazioni su LHE, "light harvesting efficiency", e fornisce dati sulla raccolta delle cariche. Questo risultato, unito agli alti valori di FF, può essere considerato come un'ulteriore prova della limitata copertura da parte del dye sul biossido di titanio. Inoltre, si è notato che tutte le curve hanno il valore di lunghezza d'onda del picco massimo, $IPCE_{max}$, che cade nello stesso intervallo per tutte, tra 470-490 nm a prescindere dal valore di lunghezza d'onda di massimo assorbimento, λ_{max}. Ciò è ancora più evidente nel caso del complesso $[Cu(L1)(L6)]^+$ che subisce lo spostamento maggiore. Questo fatto supporta l'ipotesi di una possibile interazione tra il rame e l'elettrolita.

I diversi comportamenti dei principali parametri delle celle studiate sono stati misurati anche a varie intensità luminose e sono mostrati in Figura 5.19. I valori di efficienza rimangono costanti o subiscono un leggero miglioramento a metà dell'intensità luminosa standard. Tuttavia, ad un decimo di essa l'efficienza risulta molto più bassa a causa della limitata attivazione del meccanismo di trasferimento elettronico e alla probabile presenza di numerosi "stati intrappolati" che diventano molto più influenti. Tendenzialmente i fattori di riempimento tendono a migliorare ad intensità luminosa più bassa, la densità di corrente diminuisce linearmente ed il voltaggio, a circuito aperto, segue un andamento logaritmico.

Le misure dei tempi di vita degli elettroni dei complessi di rame (I) sono mostrate in Figura 5.21, dove sono tracciate in scala semi-logaritmica contro il voltaggio; in questo modo è individuato un andamento lineare tra il diminuire dei tempi di vita e l'aumentare del voltaggio. Per confrontare con buona approssimazione i tempi di vita dei diversi complessi tra di loro, si prende un valore fissato di potenziale. Così facendo, siccome E_{redox} è sempre uguale, dato l'uso della stessa coppia redox in tutta la caratterizzazione, si prende lo stesso valore dell'energia di

Fermi e, assumendo simili coperture e quantità di cariche per tutti i complessi, si può fare un confronto più obiettivo. I valori riscontrati sono molto simili tra loro, dell'ordine del 10^{-2} s, e hanno relativamente mantenuto la sequenza delle prestazioni dei dispositivi, per esempio $[Cu(L1)(L4)]^+$ ha esibito la miglior efficienza e il valore più alto di tempo di vita degli elettroni.

Infine, è stata studiata la stabilità delle celle nel tempo; in particolare, sono mostrati in Figura 5.22, i valori di efficienza e i fattori di riempimento. Tutti i dispositivi nei primi giorni di vita mostrano un andamento crescente. Un aumento dell'efficienza nel tempo è un andamento già identificato in passato per i complessi di rutenio (II) e altri complessi di rame (I) ed è stato spiegato come una riorganizzazione della molecola di dye sulle nanoparticelle di TiO_2. Tuttavia, i complessi $[Cu(L1)(L5)]^+$ e $[Cu(L1)(L6)]^+$, dopo i primi giorni anziché raggiungere un plateau stabile come gli altri complessi, diminuiscono nel tempo e questo loro comportamento è rafforzato anche dall'andamento dei "fill factor" che diminuiscono anziché rimanere pressoché costanti come negli altri casi. Per quanto riguarda i valori di J_{SC} essi seguono lo stesso andamento delle efficienze, mentre i valori di V_{OC} non cambiano significativamente nel tempo, ad eccezione del particolare comportamento di $[Cu(L1)(L5)]^+$ che parte da valori di 630 mV, subito dopo l'inserimento dell'elettrolita, e poi si stabilizza a valori intorno ai 570 mV simili agli altri complessi.

Un importante test sulla stabilità a lungo termine è stato eseguito su $[Cu(L1)(L4)]^+$ i cui parametri sono stati calcolati circa due mesi dopo la chiusura della cella ottenendo risultati paragonabili a quelli calcolati dopo pochi giorni.

Conclusioni e prospettive future

Le proprietà di nuovi complessi eterolettici di rame (I) sono state investigate tramite la spettroscopia UV-Vis, la voltammetria ciclica e la voltammetria ad impulsi differenziali, i quali hanno fornito esaustive informazioni sui loro comportamenti ottici ed elettrochimici. Tramite queste misure sono stati trovati i loro livelli energetici e controllata la loro adeguatezza nel loro utilizzo come foto-sensibilizzatori. È stato trovato un trend lineare delle lunghezze d'onda di massimo assorbimento tra i complessi omolettici ed i complessi eterolettici con lo stesso legante di ancoraggio. Un trend che tiene in considerazione sia la presenza dello stesso legante in tutti gli eterolettici sia il loro adsorbimento sul biossido di titanio e che permette future predizioni sul comportamento di complessi eterolettici ignoti. Per quanto riguarda i potenziali di ossidazione le cose sono invece più complicate e non è stato identificato un trend ben definito.

Le prestazioni dei complessi di rame (I) caratterizzati e auto-assemblati su TiO_2 sono state investigate all'interno dei dispositivi DSC. Da un'analisi generale che combina tutti i risultati ottenuti, si può concludere che una ragione per cui la foto-corrente risulta limitata potrebbe essere la non completa copertura delle nanoparticelle di TiO_2 da parte dei complessi di rame(I) e quindi scarso adsorbimento del dye. Inoltre, si potrebbero ipotizzare forti interazioni tra l'atomo di rame e l'elettrolita. Nonostante le prestazioni inferiori rispetto allo standard N719, la semplicità del sistema è promettente e il suo notevole vantaggio economico potrebbe aprire la strada all'utilizzo delle DSC nelle applicazioni della vita quotidiana.

Un sistema molto interattivo, così come le DSC, è naturale che susciti molte curiosità che richiedono una ulteriore esplorazione. In particolare, dai risultati di questo studio, alcuni aspetti sono da approfondire e da comprendere fino in fondo.

Vi è innanzitutto bisogno di testare altri leganti secondari in modo da verificare e affinare i trend riguardanti la prevedibilità delle proprietà ottiche ed elettrochimiche dei complessi eterolettici a partire da quelli omolettici.

Un altro punto di ricerca interessante sarebbe quello di analizzare più da vicino l'influenza dei gruppi carbossilici presenti nel legante di ancoraggio e la loro sospetta coordinazione con l'atomo di rame.

Per quanto riguarda l'applicazione dei complessi eterolettici di rame (I) nei dispositivi DSC, un importante obiettivo sarebbe quello di verificare l'efficacia del sistema di "auto-assemblaggio sulla superficie" e trovare un modo per sintetizzare più complesso eterolettico sul TiO_2. È già in corso un passo successivo su questa ricerca che riguarda studi di spettroscopia fotoelettronica a raggi X (XPS) atti a definire con maggior precisione la quantità di legante di ancoraggio e quella di legante secondario sulla superficie.

Inoltre, sempre sul funzionamento all'interno del dispositivo, sarebbe interessante approfondire le interazioni che avvengono tra il rame e l'elettrolita, in particolare con la coppia ioduro/triioduro e il co-additivo 4-tert-butilpiridina.

Infine, poiché uno dei principali svantaggi pratici delle celle solari liquide DSC è la natura volatile del solvente dell'elettrolita, un progetto futuro potrebbe concentrarsi sull'uso di questi complessi eterolettici di rame (I) come foto-sensibilizzatori in DSC allo stato solido (SS-DSC).

1 Introduction

"I'd put my money on the sun and solar energy, what a source of power. I hope we don't have to wait until oil and coal run out, before we tackle that."

Thomas Edison, 1931

The dramatic increase of the world population and the development of the emerging countries led to a tremendous enhancement of global energy consumption during the past century. According to the "Renewables 2018 global status report",[1] fossil fuels nowadays still provide substantially most of the primary energy supply, up to 79,6% of the total, while renewable energies reach only the 10,4%. Public concern towards more clean and sustainable sources has been heightened by the limited amount left of fossil fuels and by the disastrous consequence of the greenhouse effect caused by their careless combustion.

Among the renewable energies, the sun represents the most abundant source of energy, it offers about 10'000 times more than the global population energy need. The Sun supplies to the Earth $3{,}8 \cdot 10^{24}$ J every year. Covering only 0,1% of the Earth's surface with solar cells with an efficiency of 10% would be enough to satisfy the energy need of the entire humanity.[2] So far, the science of solar cells has been dominated by silicon photovoltaic cells, which reached efficiencies up to 26,7% in the laboratory[3] and 17% for the commercial ones.[4] However, they are mechanically rigid and their main drawbacks include their toxicity, low abundance of the materials, and temperature-dependent efficiency.[5]

Dye-sensitized solar cells (DSCs) are emerging photovoltaic devices which offer the prospect of cheap fabrication together with other attractive features, such as mechanical flexibility. This emerging technology has received much more attention after the breakthrough of Grätzel and O'Regan published in their *Nature* paper in 1991.[6] The technology offers incomparable selling points such as higher variability in their design, high flexibility, short energy payback time (<1 year), enhanced performances under diffuse light and higher temperatures, compared to the competitors.[5] At the moment, the record efficiency for DSCs has reached 13% efficiency, as reported by Mathew and co-worker[7] with a synthesized porphyrin-based complex with zinc, and a donor-πlinker-acceptor, D-π-A, design. Other organic dyes also report quite a high efficiency, but the dye mostly used as a benchmark is the ruthenium (II) complex known as N719, whose response was widely studied and reported in the literature.[8,9] Despite all the attempts of further optimization, it reached a plateau around 12% efficiency.[9]

The current dyes employed in DSCs are based on either expensive rare materials like ruthenium or compounds which require hard work of synthesis. The challenge is then to replace the use of these dyes and especially ruthenium, since it is one of the rarest elements and most expensive metals, with more abundant and cheap metals. Finding new materials is essential to move towards more efficient devices and environmentally friendly solution. In the literature, ruthenium (II) complexes were compared with possible alternatives from earth-abundant metals of the first row of the d-block. So far, the most suitable alternative seems copper, significantly cheaper than ruthenium and with similar photophysical properties.[10]

Copper (I) complexes with structural ligands with "blocking" substituents, i.e. substituents in the 2,9 positions of the 1,10-phenanthroline and 6,6' positions of the 2,2'-

bipyridine, influence positively the properties of copper (I) as photosensitizers in DSCs. These positions indeed effectively minimize the flattening of the pseudo-tetrahedral coordination into a square planar geometry, limiting solvent or electrolyte access to the copper centre.[11] To further improve the performance of DSCs containing copper (I) complexes as dyes, a "push-pull" design, which facilitates the electron transfer across the dye system, was incorporated. Thus, two different ligands were employed: an "electron acceptor" able to anchor to the FTO/TiO_2 electrode, (L_{anchor}), and an "electron donor" ancillary ligand ($L_{ancillary}$). To generate the heteroleptic Cu(I) diimine complexes, "on-surface self-assembly" method exploited by Constable and co-workers[9] was employed to avoid the ligand exchange mechanism occurring in solution.

Nevertheless, this method restrains the study of the heteroleptic complexes only on the surface on TiO_2, making the characterization of the complexes more challenging, thus only few studies based on this technique were done in the past.[9,12]

1.1 The aim of the Thesis

Making dye-sensitized solar cell devices more available in the everyday life by using cheap and sustainable metals with decent efficiency, could lead to a breakthrough and open the door to a greener future in agreement with the economic demands.

In this thesis, five different heteroleptic copper (I) complexes that could be used as photosensitizers were explored. An anchor ligand (L1) able to bind the surface of TiO_2 through the carboxylic acid moieties was first selected. The other ancillary ligands (L2, L4-L7) were chosen to give a variability of the optical and electrochemical investigation. To study these complexes, $[Cu(L1)(L_X)]^+$, their "self-assembly" on TiO_2 was first made, and, as internal comparison of the properties, a self-assembled $[Cu(L1)_2]^+$ on TiO_2 was also studied. This thesis aims to explore their optical and electrochemical properties in order to determine a pattern starting from their corresponding homoleptic copper (I) complexes, $[Cu(L_X)_2]^+$. The ability to make predictions of their behaviours ahead their synthesis could be a significant tool for further researches about other anchor and ancillary ligands. Furthermore, such characterization is necessary to verify if they are suitable dyes for DSCs applications. Finally, this thesis aims to investigate these simple, and mostly commercially available ligands in their operation within the cell, to study their interesting behaviour in the intriguing system of the DSC and to verify their effective competency with the other competitors in the market.

1.2 The structure of the Thesis

The "Background" of the thesis aims to give a small overview of the world energy consumption, the need to move towards renewable sources and, in particular, why focusing on the solar energy, immense source to exploit. Among the emerging photovoltaic cells, the great potential of the dye-sensitized solar cells (DSCs) is discussed with their low-cost and simple manufacturing, the state-of-the-art and practical application for this technology. The current dyes employed are either expensive and rare materials like ruthenium or synthetically complex, based on low yield reaction and intense work of purification. Heteroleptic copper (I) complexes, which integrates a "push-pull" system, are cheaper and more available alternative with the potential to let this technology to catch on.

The "Ligand of interest" chapter provides a glance of the ligands that will be used through the entire study, how they have been chosen and what are their main features. It is described

one anchoring ligand, for direct adsorption on TiO_2 surface and five different ligands employed as ancillary, with an electron donator feature.

In the chapter "Characterization of the dyes", a description of the main techniques needed to characterize the heteroleptic copper complexes on TiO_2, both optically and electrochemically, was given. The homoleptic copper (I) complex of the anchoring ligand was also characterized on TiO_2 as internal benchmark. A correlation of the properties between the heteroleptic copper (I) complexes on TiO_2 and their respective homoleptic in solution was found. Furthermore, the characterization was necessary to prove that the complexes were satisfying the requirements to be employed as dyes.

"Characterization of the device" lists and explains the main measurements required to characterize a solar cell device. The efficiency of the device lies at the heart of the current density-voltage (*J-V*) characteristics. The importance of the incident photon-to-current efficiency (IPCE) curve drove the attention to some interaction dye-electrolyte within the cell. A closer inspection of the recombination process occurring in the cell by considering the electron lifetime, and a detailed description of the laboratory fabrication process employed are also given in this chapter. At first, an optimization of the electrolyte composition and thickness of the substrate was done, followed by the characterization of all the heteroleptic copper (I) complexes which were then compared with the homoleptic copper (I) complex of the anchoring ligand and the state-of-the-art ruthenium (II) complex N719, used as a benchmark.

"Conclusions" remark how interesting are these heteroleptic copper (I) complexes which alone lead to high curiosity and even more in their application in such intriguing system as the DSCs. The use of copper (I) complexes as alternative dyes, affordable by all in the every-day life. The possibility of spreading this technology with a higher degree of installations that fulfill the economic market demand in terms of low-cost application and solution for energy supply.

"Future outlooks" focus on the on-going research about the investigation of more commercially available ligands (anchor and ancillary) to coordinate in this self-assembling on TiO_2 with copper (I) and the desire of further investigation of the effectiveness of the ligand exchange mechanism through X-ray photoelectron spectroscopy (XPS) technology is reported as well. The main goal would be to find a way to revolutionize the copper (I)-based system and push the equilibrium towards the formation of the complexes on TiO_2.

2 Background

2.1 World Energy Consumption

The industrial revolution, which took place from the 18th to 19th century, transformed the world from a predominantly agrarian, rural society into a new energy-based society, reaching a point of no return in the amount of energy needed every day. This revolution was driven by the discovery of sources of energy which we mostly still rely nowadays on, such as natural gas and petroleum. Energy demand kept growing during the years mostly due to population growth, technological development, and economic expansion. World population counts today about 7,5 billion of inhabitants, almost double the value of 50 years ago. Concomitantly, primary energy consumption grew by nearly a factor of 3 during the same years, in million tonnes of oil equivalent (Mtoe) it went from 4'910 to 13'511.[13] This growth is also directly correlated to the development of the emerging countries and their entrance in the market economy.

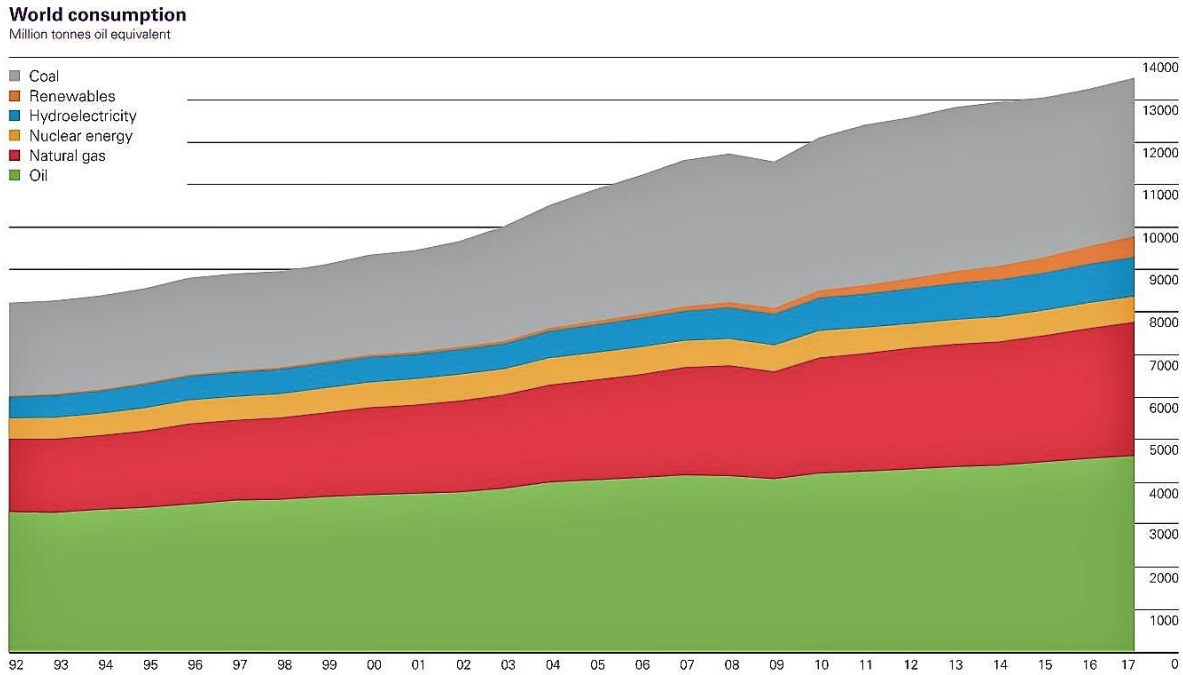

Figure 2.1: World primary energy consumption.[13]

These data are expected to grow even more during the next years because the fast developing of the today-societies will require more and more energy to satisfy their needs and supply for a constantly growing population. According to the United Nation, the Earth population is expected to reach 9,7 billion inhabitants by 2050.[14]

Based on the "Renewables 2018 global status report", of the energies employed, 79,6% are supplied by fossil fuels, 10,4% by renewable energies, 7,8% by traditional biomass and finally 2,2% by nuclear energy. Even if renewable energies reached the 10% level, fossil fuels still provide substantially mostly of the global primary energy supply. By thinking that the latter are destined to finish, much bigger steps should be taken towards renewable energies. Even

though according to BP's Statistical Review of World Energy, their power grew by 17% in 2018,[13] this value should grow much faster to overcome the simultaneous increase of energy consumption. Furthermore, the replacement of fossil fuels is made more preeminent due to environmental issues. The large emission of CO_2 that followed the industrial revolution, combined with a high degree of deforestation, broke the equilibrium of the greenhouse gases and led to the phenomenon, object of many discussions, of the global warming. As a result, the rise in temperature led, among many others, the Arctic ice to melt, the sea level to rise and many more catastrophic meteorological events to occur.

2.2 Towards renewable energies

Climate change is one of the greatest challenges our generation has to face. The replacement of fossil fuels by renewable energies has the potential to mitigate and to limit the effects of climate change.[15] The energy required by our growing technology-society needs more than ever to develop the use of unlimited clean energy sources. Considering that electricity is the energy where the renewables are employed the most, the global scenario for its production at the end of 2017 is shown in **Figure 2.2**. Renewable electricity was counting 26,5%, which included, first of all, hydropower with 16,5%, followed by wind power with 5,6% and bio-power with 2,2%, while solar photovoltaic (PV) was counting only 1,9% and lastly, ocean, concentrated solar power (CSP), and geothermal power with 0,4%.[1]

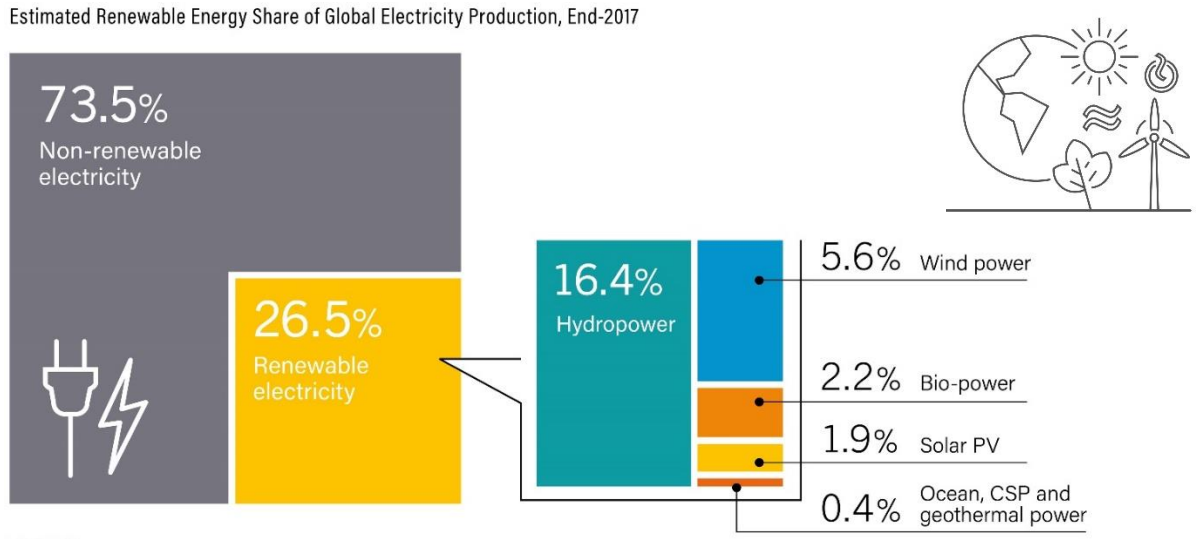

Figure 2.2: Estimated renewable energy of global electricity production at the end of 2017.[1]

Hydropower takes the energy of water flows for example from rivers, falls or dams. Its capacity to store energy through pumped-storage plant makes the technology more valuable than intermittent sources. Despite this benefit, the use of dams and pumped-storage plants can have catastrophic impacts, we have only to bear in mind the Banqiao dam failure in 1975, Henan, China.[16] Wind power exploits airflow with turbines to produce electricity through mechanical generators. It can be harvested everywhere since wind is everywhere, but its production can fluctuate a lot also in the short-time scale. Bio-energy is the energy produced from biological material that can produce heat via direct combustions. Even though it provides a good alternative to fossil fuels, it has been criticized since partly led to deforestation or for taking land and water resources needed for food production. Geothermal energy exploits the heat coming by convection from the Earth's core-mantle. The main drawback is that it is only

located on specific sites. Solar energy is the most exploitable resource just considering that every hour the sun provides more energy to the earth than the human annual consumption.[17] Nevertheless, since solar power required expensive technology, other renewable sources widespread much more.[18]

2.3 Development of Photovoltaic

Solar energy can be harvested by different technologies such as photovoltaic (PV), which works by the direct conversion of light to electricity, and solar heating and cooling (SHC), which collects thermal energy and uses it to provide hot or cool water to domestic or building spaces.[19]

The dream to capture the sunlight and turn it into a valuable and desired electric power gained the attention of researchers and engineers, ever since the French scientist Edmond Becquerel discovered the photoelectric effect.[2] PV devices have been studied and developed hugely in the past decade (see **Figure 2.3**).

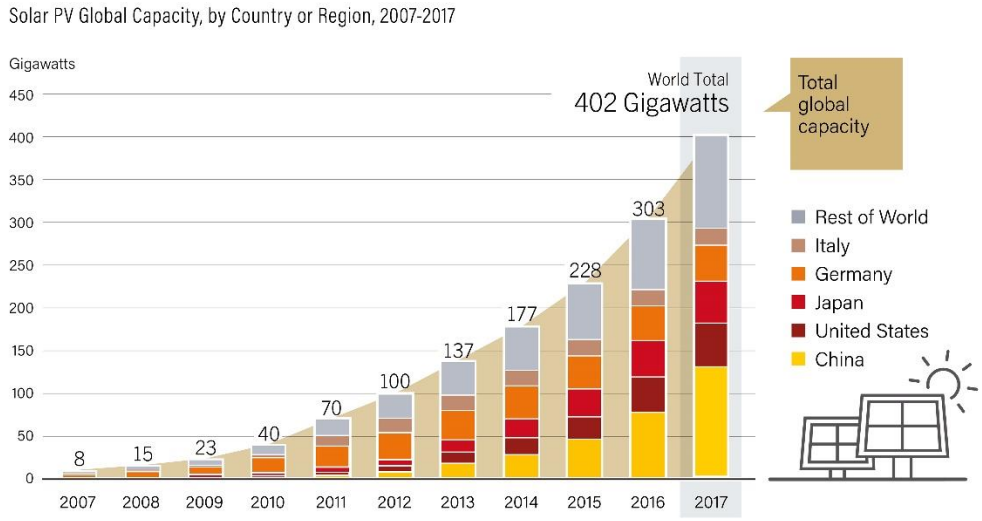

Figure 2.3: Global growth of cumulative PV capacity in gigawatts (GW) with regional shares.[1]

Worldwide the growth of photovoltaics has almost been exponential. In 2017, the photovoltaic capacity increased by 99 GW with a 34% growth of new installations. Handful of utilities have started combining battery banks with PV, to help to mitigate the problems associated with sun presence dependence.[20]

The development of the photovoltaic technology can be summarized in three main stages. The first generation of PV cells includes p-n junction solar cells, based on monocrystalline and polycrystalline silicon wafers (c-Si), which are the main materials currently used by the photovoltaic industry and covers up to 90% of the current PV market.[21] However, they are mechanically rigid and they require a complicated production which limits their use in domestic applications. Indeed, to grow the silicon crystal an expensive "Czochralski process" is required due to intense extraction, purification, and energy demanding processes.[22] Initially, this technology was prohibitively expensive and therefore it could not be used in large scale, but over the years the price of Chinese crystalline silicon dropped down.[23] Furthermore at present, a monocrystalline silicon-cell has recorded an efficiency of 26,7% and a polycrystalline silicon cell reached the maximum at around 22,3%.[3] Those values refer to efficiencies of cells made in research laboratories, but the commercially available ones have an efficiency of 17%.[4] The drawbacks of these solar cells include also their toxicity and temperature-dependent

efficiency.[5] The International Energy Agency (IEA) reported a total energy payback time (EPBT) of mono-crystalline silicon-based PV panels operated in Europe of 2,4 years today.[24] The second generation of PV cells is also known as the stage of thin-film solar cells such as amorphous silicon (a-Si), copper indium gallium diselenide (CIGS) and Cadmium Tellurium (CdTe) devices.[25] The name arises from the use of films of material ranging from fractions of a nanometre to few micrometres in thickness instead of the typical rigid 100-200 µm silicon wafers. A key advantage of this technology is the lower use of raw materials and easier manufacturing procedures. They are easier to handle and more flexible, less susceptible to damage, but their main disadvantage is the lower average efficiency in comparison of c-Si cells, which increases the overall system cost.[21] The third generation of solar cells is the generation of the emerging thin-films. These technologies are still mostly based on laboratory researches, which are working on making the solar cells more efficient over a wider band of solar energy, including the visible transparency, less expensive and available for more and different applications. High level of research in the materials and development in device engineering, are nowadays spent on this generation of solar cells.[21] Even if they are still not fabricated on large scale, some companies are becoming interested in their development.

Photovoltaic can also be categorized based on the active materials employed for the solar cells as shown in **Figure 2.4**. The third generation in this sense is included in the emerging or novel materials and refers to dye-sensitized solar cells, colloidal quantum dot, perovskite, and organic cells.

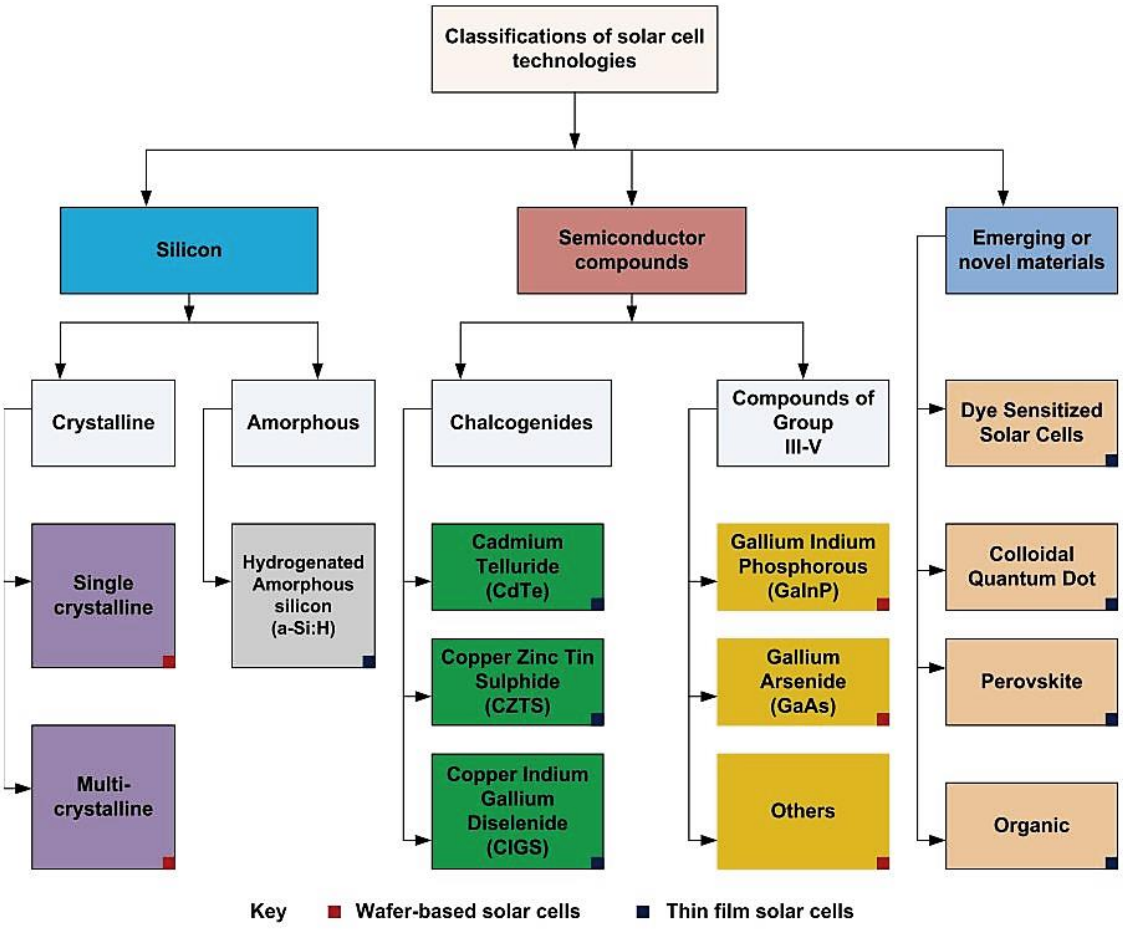

Figure 2.4: Classification of solar cells based on the primary active material.[21] Down to the right, each technology is also categorized into wafer-based or thin-film technologies.

Any solar cell based on a single p-n junction has a theoretical thermodynamic limit (the Shockley-Queisser limit) on their power conversion efficiency of 33,7%.[26] This maximum occurs at the semiconductor band gap of 1,34 eV. The limit arises from the energy loss, which is due to the relaxation of the photons when their energies are higher than the band gap of the semiconductor and considering that the photons with energy lower than this band gap do not contribute. The silicon solar cell has a band gap of 1,1 eV, resulting in maximum theoretical efficiency of about 32%.[26] The potential to overcome the Shockley-Queisser limit can be achieved with tandem cells, hot carriers effect, and multiple carrier ejection. In the first case, multiple cells with different bandgaps are used so that each cell converts a restricted range of photon energies close to its bandgap.[27]

The highest efficiency, reached so far, was achieved by the Fraunhofer Institute for Solar Energy System ISE together with Soitec and CEA-Leti groups. It is a multi-junction solar cell that converts 46% of light into electrical energy.[28] **Figure 2.5** shows the state-of-the-art of all the photovoltaics technology updated until now.

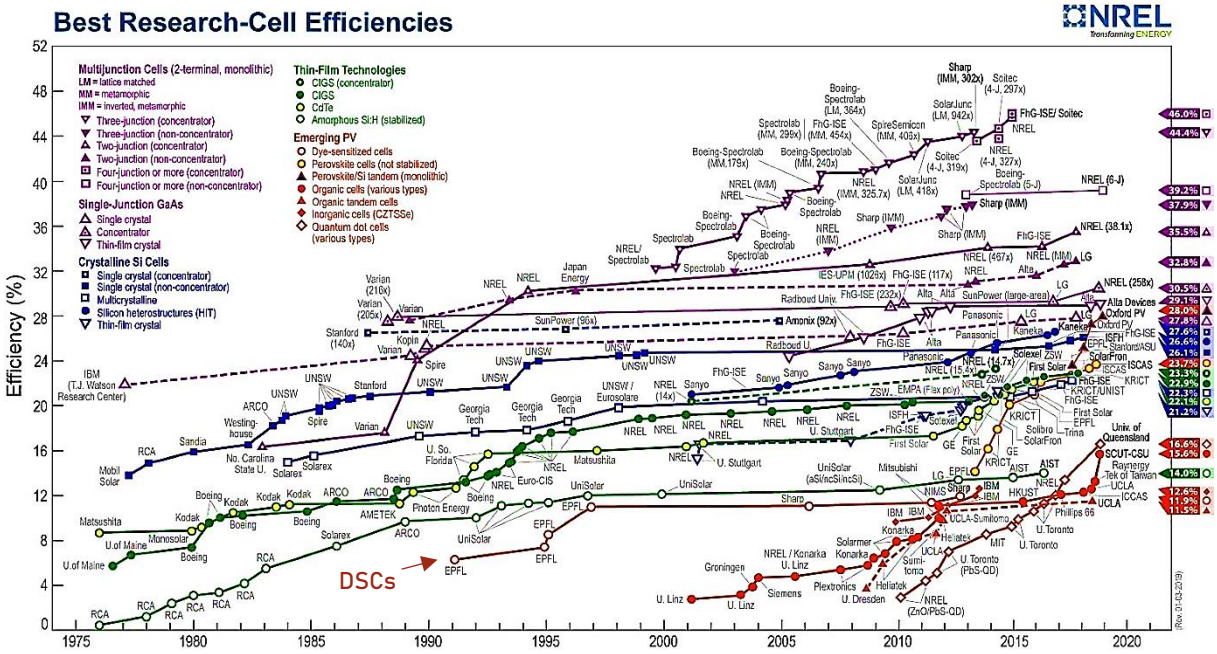

Figure 2.5: Record efficiencies for different types of solar cells reported by the National Renewable Energy Laboratory (NREL).[29]

2.4 Dye-Sensitized Solar Cells

Of all the emerging solar cells, dye-sensitized solar cells (DSCs) have gained, since the beginning, thriving interest.[21] The development of DSCs was popularized by the breakthrough of O'Regan and Grätzel published in their *Nature* paper in 1991.[6] DSCs differ from the other devices since the function of light absorption and charge carrier transport occur in separate materials. Its technology is inspired by the natural process of photosynthesis. Photosensitization is the electrochemical process occurring during photosynthesis in green plants. The photons of visible light are absorbed in the chloroplasts of the plant, where cause the chlorophyll pigment to promote an electron to a higher molecular energy level. This energy will then be stored in the form of chemical bonds.[30]

2.4.1 DSCs design

A conventional liquid-based DSC configuration is shown in **Figure 2.6**. The most commonly used substrate for the working electrode (anode) and the counter electron (cathode) is glass coated with transparent conducting oxide (TCO) layer, commonly fluorine-doped tin oxide (FTO). The photoactive compound, the central core of this system, is a coloured molecule which generates a separation of charges upon light irradiation. To support the dye and collect the electrons there is a thin layer of semi-transparent semiconductor. The electrolyte containing a redox mediator fills the space between the sandwich-assembled electrodes and interacts with the catalyst-coated counter electrode. This arrangement enables the production of cheap solar cells and allows the construction of semi-transparent cells in any-colour.

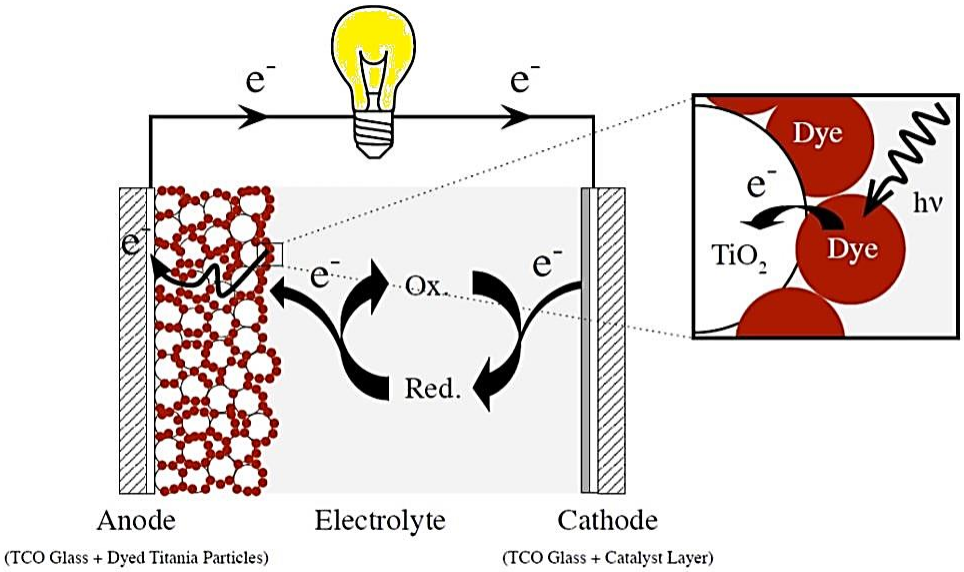

Figure 2.6: Scheme of a conventional DSC device.[31]

At present, several mesoporous films, redox mediator and numerous dyes have been investigated. Among the metal oxide systems that have been tested, TiO_2 has the highest efficiency and stability. Titanium (IV) oxide is stable and nontoxic, and it has several crystal polymorphs. *Rutile* is the thermodynamically most stable crystalline form, though *anatase* is the preferred phase for DSCs since anatase crystals have larger bandgap and higher conduction band (CB) compared to rutile, where the bandgap is the energy difference between the top of the valence band and the bottom of the conduction band. It is important to control the film thickness of TiO_2, the particle size and the porosity of the layer to obtain the best performance.[5]

The electrolyte contains three main components: the redox couple, co-additives and the solvent. **S**everal redox couples have been investigated in the state-of-the-art of the DSCs, to reduce the driving force needed for dye regeneration and to increase the photovoltage of the device. The redox potential follows the Nernst equation and is related to the activities of the redox couple. The mass transport of the ions of the couple between the photoanode and the counter electrode is also important, both in the medium of the electrolyte and between pore spaces in the semiconductor. The redox couple investigated include transition-metal complexes and organic redox couples. The requirements of a good redox couple are high diffusion coefficient to facilitate mass transport, fast electron transfer kinetics at the counter electrode, minimal absorption of the visible light, high redox potential to optimize the photo-voltage and low but sufficient driving force for regeneration of the oxidized dye molecules, good stability and not corrosive towards metal contacts. The traditional redox couple mainly used since the

beginning of DSC development is iodide/triiodide, I^-/I_3^-. This redox couple has suitable characteristics and, compared to the others, minimizes recombination losses but has a large driving force to regenerate the dye that limits the voltage output and conversion efficiency. This is probably due to a complex regeneration mechanism of the dye which involves the formation of intermediates such as $I_2^- \cdot$ radical.[32] More recently, bipyridine-cobalt (II/III) redox couple, $Co(bpy)_3^{2+/3+}$, attracted the attention of researchers and efficiencies comparable with I^-/I_3^- were achieved.[33] The presence of specific co-additives, such as Li salts and tertbutyl pyridine (TBP), result in an enhancement in the device performance.[5,34] Their main effects are attributed to the modification of the redox couple potential, and a shift of the conduction band of the semiconductor.[5] Regarding the solvent of the electrolyte, important properties are a wide electrochemical window, high dielectric constant for a good solubility of the redox couple and the co-additives, low viscosity to ease diffusion and low vapour pressure for high stability. No single solvent can satisfy all the requirements, thus a mix of solvents in different proportions are generally used. Some examples are acetonitrile (ACN), valeronitrile, methoxypropionitrile (MPN) and ionic liquids (ILs).[5]

The counter electrode (CE) is prepared by depositing a thin layer of catalyst onto the conducting FTO glass substrate. The main catalyst used for the iodide/triiodide redox couple is platinum (Pt), but other catalysts have been investigated for other redox couples such as a low-cost porous carbon and poly(3,4-ethylenedioxythiophene) (PEDOT), mostly for the reduction of Co (III).[35]

The dye is an essential part of DSCs. The sunlight spectrum covers a wide range of wavelengths that go from the ultraviolet and visible to the infrared. As shown in **Figure 2.7**, the spectrum is rich in the visible and near-infrared regions but poor in the ultraviolet region. Since in the semiconductor the bandgap is large, only UV light would be sufficiently strong for its photoexcitation. To overcome this problem, dyes that can absorb in the visible region of the solar emission spectrum cover the surface of the semiconductor. The irradiation has a direct component and a diffuse component which arises by the scattering of the sunlight in the atmosphere. The standard solar spectrum used for efficiency measurements of solar cells is "Air Mass (AM) 1.5 Global".

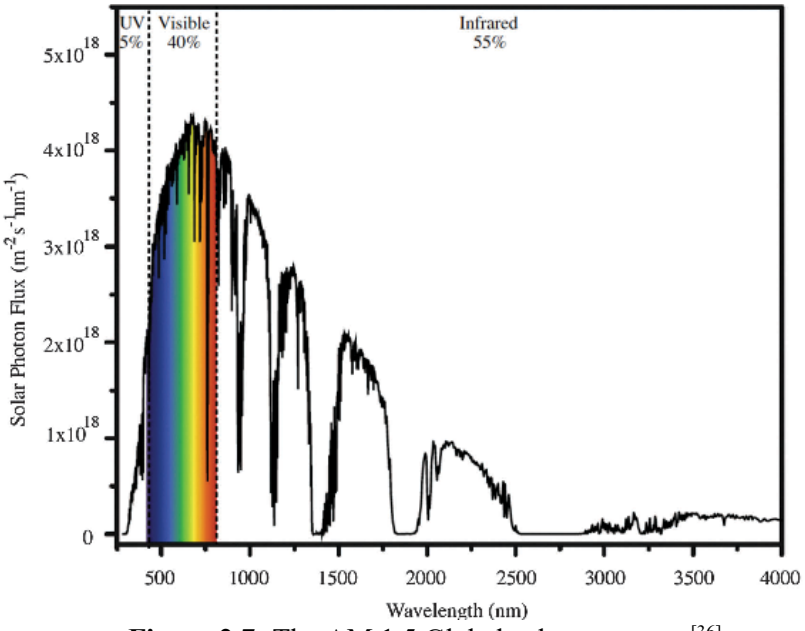

Figure 2.7: The AM 1.5 Global solar spectrum.[36]

Thousands of different dyes, such as metal-coordination complexes and organic compounds were investigated in the past decades. Essential characteristics for a

photosensitizing dye are a broad absorption spectrum in the visible and near-infrared region, an excited-state potential more negative than the conduction band edge potential of the semiconductor, a ground-state potential more positive than the redox potential of the redox couple to favour the regeneration, a low tendency to form aggregates on the semiconductor surface and good photo, electrochemical, and thermal stability. Moreover, the dye needs to have anchoring groups, such as COOH or H_2PO_3, to strongly bind onto the semiconductor surface.

Coordination complexes dyes, among which stands out ruthenium complexes, have a central metal ion, which plays a fundamental role in the overall properties of the complex, coordinated with ligands, typical bipyridines or phenanthrolines. These ligands also link the dye onto the semiconductor through anchoring groups. Visible light absorption is due to metal to ligand charge transfer (MLCT) process, excitation of an electron from the metal d-orbitals to the antibonding π^* orbital of a coordinated ligand.[9] Ruthenium (II) complexes have reached over 10% efficiency and have shown the best photovoltaic properties. They show broad absorption spectrum, good stability, and suitable excited and ground-state energy level.

The dye that which currently detain the record efficiency value of 13% is a porphyrin-based complex coordinated with zinc system, reported by Mathew and co-worker[7] and shown in **Figure 2.8a**. It possesses a donor-πlinker-acceptor structure, D-π-A, that creates a "push-pull" system which enhances light harvesting and electron transfer from the donor group to the acceptor group, which is attached to the semiconductor and ease the direct injection of the electron into the conduction band. Organic dyes also showed good performances, they have high molar extinction coefficients and are synthesized to incorporate the "push-pull" mechanism which enhances light harvesting and electron injection.

The benchmark used for DSCs efficiency is the ruthenium (II) complex known as N719 whose molecular structure is shown in **Figure 2.8b**. Its wide spectral response and high absorbed-photon-to-current efficiency makes this the state-of-the-art dye. The record efficiency for N719, despite all the attempts of further optimization, reached a plateau around 12%.[9]

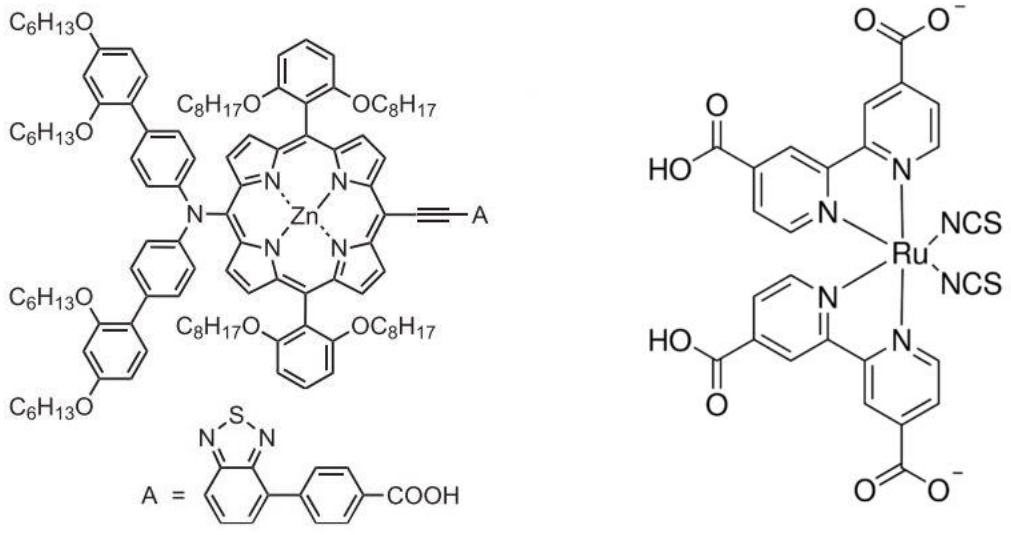

(a) (b)

Figure 2.8: Porphyrin-based zinc system which gave the highest efficiency of 13% (a).[7] Ruthenium (II) N719, the benchmark dye (b).

The challenge is to replace the use of ruthenium since it is one of the rarest elements and most expensive metals, with more abundant and cheap metals. Finding new materials is essential to move toward more efficient devices and environmentally friendly solutions. The

current literature compares all the possible alternative between the Earth-abundant metals from the first row of the d-block.[10]

2.4.2 The working principle of a DSC

The schematic desired electron transfer processes in a DSC are illustrated in **Figure 2.9** by the black arrows numbered from 1 to 5.

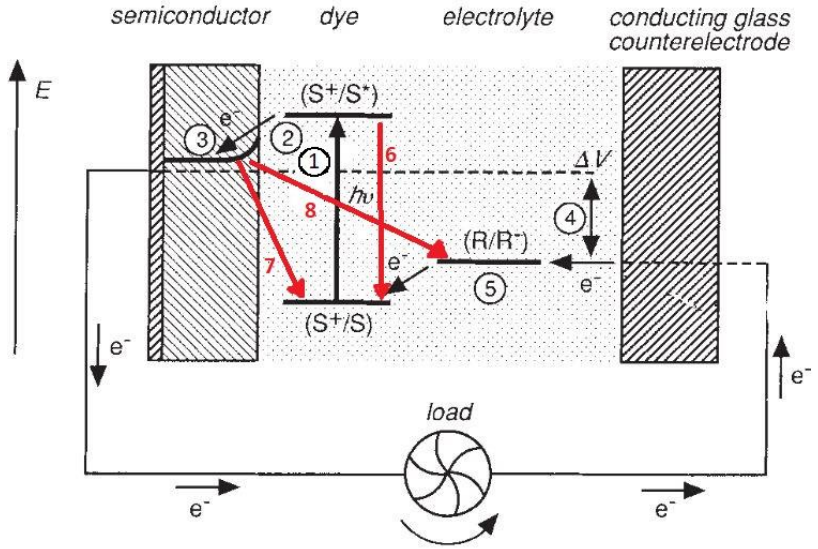

Figure 2.9: Schematic representation of the working principle of a DSC.[6]

The electron of the dye is first excited from the highest occupied molecular orbital (HOMO, S^+/S) into the lowest unoccupied molecular orbital (LUMO, S^+/S^*) by absorbing visible light. Following, the electron is injected into the conduction band of the semiconductor (usually TiO_2). The electron injected in the semiconductor reaches the working electrode and, passing through the load, it reaches the counter electrode where the oxidized form of the redox mediator is reduced. This reduced form finally regenerates the oxidized dye completing in this way the cycle. The use of mesoporous semiconductor electrode increased enormously the internal surface area where the dye can attach thus the fraction of the incident photons that is absorbed and excite the electrons of the dye.

The maximum photovoltage, ΔV, which is correlated to the open-circuit voltage (V_{OC}), corresponds to the difference between the *quasi*-Fermi level (E_F) of the semiconductor of the working electrode and the Nernst potential (E_{redox}) of the redox couple in the electrolyte.[5,6,9] Besides the desired pathway, unwanted reactions may lead to efficiency losses. **Figure 2.9** shows, with red arrows, the main undesired reactions numbered from 6 to 8. Reaction 6 is the direct recombination from the excited state to the ground-state of the dye. Reactions 7 and 8 represent the recombination of injected electrons in the semiconductors with the oxidized dyes and the oxidized form of the redox couple present in the electrolyte, respectively. To avoid this last recombination process, a compact blocking layer of compact metal oxide (usually still of TiO_2) is deposited on the anode.[5]

2.4.3 Applications of DSCs

DSCs have the potential to make an impact on economics thanks to its low production cost compared to the conventional PV, high design opportunities and short energy payback time. DSCs can have a significant impact on building integration or consumer products thanks to their adaptability and aesthetics, for example, they can be transparent or have a different variety of colours.[37] The use of natural dyes such as chlorophyll extracted from spinach and pigments from berries, even if achieved very low performance (of the magnitude of cents % efficiency), demonstrate their simplicity.[38] Transparency, colour, shape, layout, and other DSC's features can be easily varied by changing the printing parameters and paste/dye formulations used in the printer process. Also, technologies to manufacture large-area devices are present nowadays and easy to employ.[39]

The cell can be made with two plates of glass or flexible roll-to-roll plastic sheets coated with the transparent conducting layer. The flexible factor enables them to fit very different applications. Currently, in the market, companies like G24 (UK), Samsung Elec (Korea), Sony Corporation (Japan) and Exeger (Sweden) are mostly focusing on the electronic products for "on-the-go" solar power for mobile devices. **Figure 2.10** shows one of the products presented by G24, innovative bags incorporating DSC technology to use as phone chargers.

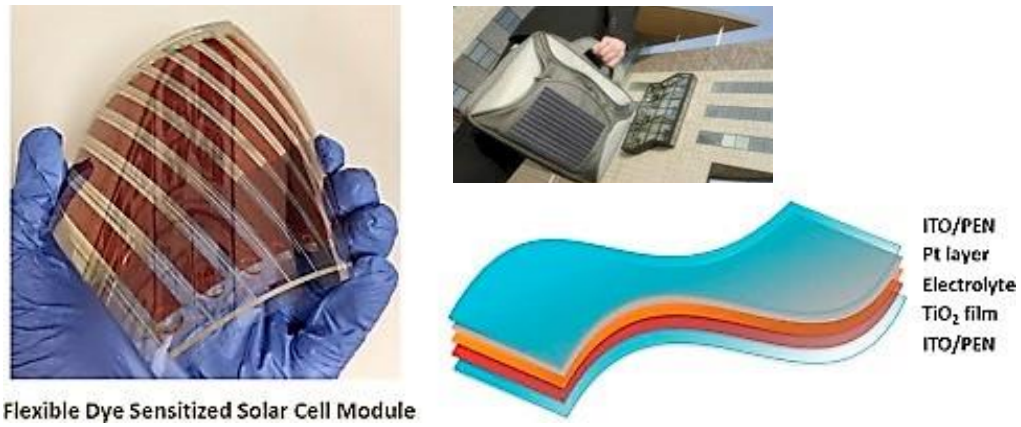

Figure 2.10: Flexible dye-sensitized solar cell printed with the roll-to-roll technology.[40]

Because of the wide range in colours and the good performance under diffuse light, other uses consist of indoor applications. Sony Corporation (Japan) has presented some prototype LED lamps which use panels of DSCs to power (**Figure 2.11a**). AISIN SEIKI Co., Ltd and TOYOTA Central R&D Labs., Inc. in Japan developed some leaf-shaped transparent DSCs with four colours, based on ruthenium (II) complexes (shown in **Figure 2.11b**).

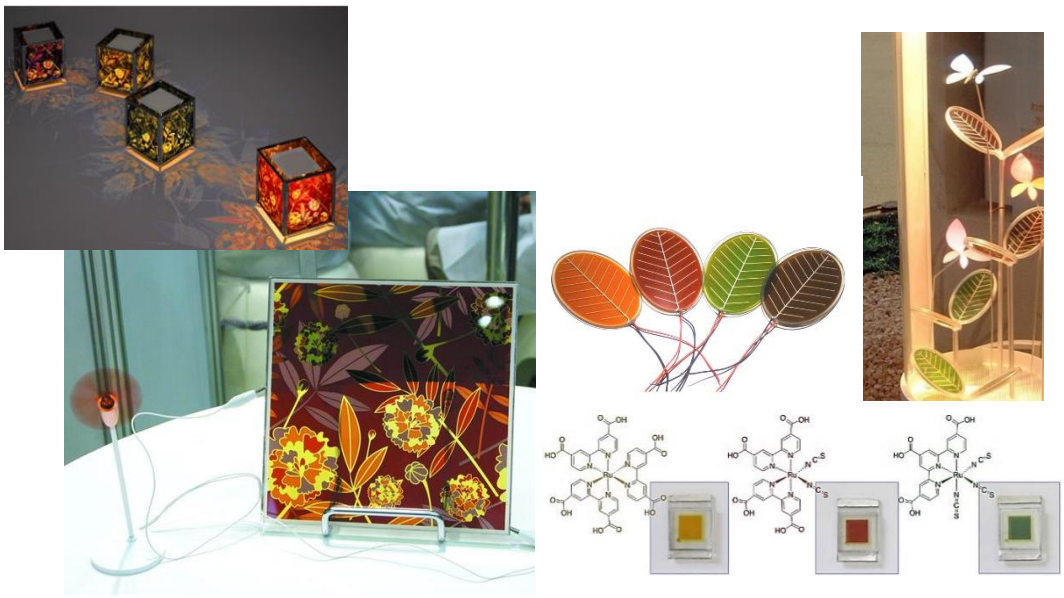

(a) (b)

Figure 2.11: Sony Corporation prototype LED lamps which use DSCs panels to power (a).[41] Leaf-shaped transparent DSCs with four colours, based on ruthenium (II) complexes (b).[42]

Furthermore, the possibility to make them transparent, enables the incorporation in glass windows for building integrated photovoltaic (BIPV). This has enormous potential because of its affordable cost and large areas employed. One of the most known examples of building integration is given by the Swiss Tech Convention Center covered with panels of organic dye-sensitized solar cells.

2.5 Copper (I) complexes as Dyes in DSCs

Copper (I) complexes were first introduced as dyes in photoelectrochemical cells (PCE) by Sauvage and co-workers in 1983.[43] Copper (I) diimine complexes present similar photophysical properties to ruthenium (II) diimine complexes; thus, they have the potential to replace the latter with the advantage that copper is relatively earth-abundant metal and comparatively cheaper, necessary requirements to base a technology on industrial scale.

By comparing the prices in the market of copper and ruthenium, the importance of replacing ruthenium-based dyes with copper-based dyes is evident. **Figure 2.12** shows 5 years of market prices for copper, to the left, and ruthenium, to the right. The system of unit mass underlined even more the huge discrepancy in price and availability between these two metals, which is approximately of three orders of magnitude. Indeed, the price of ruthenium is shown in Euro/grams while copper prices are shown in Euro/tonne. Furthermore, the graphs show that while the price of copper is stable in the years, the price of ruthenium highly suffer from an increment in recent years and its evolution is heavily floating.

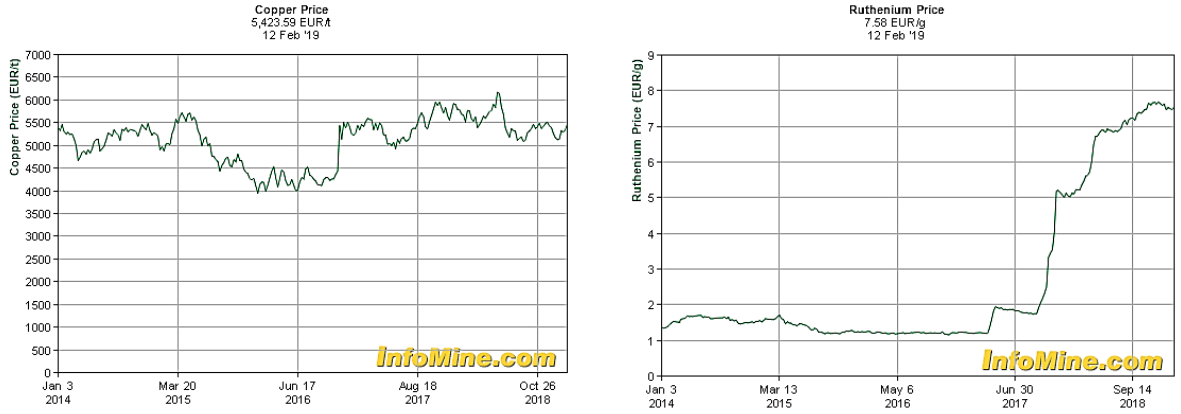

(a) (b)

Figure 2.12: Comparison of market prices for copper (a)[44] and ruthenium (b)[45].

Recently, more work on copper complexes for DSCs applications has been reported by Constable and co-workers.[9] The main problem of these complexes is their molar extinction coefficients which are usually lower than those of the ruthenium complexes. Photo-physically they both have a metal-to-ligand charge transfer (MLCT) excited-state and absorption range between 400 and 550 nm. Excitation in that range moves the electron density from the Cu(I) centre to the ligands which results formally in Cu(II)* centre (see **Figure 2.13a**). The formation of the MLCT have different characteristics: in ruthenium complexes, there is little change in the geometry between the ground-state and the excited-state, while the copper complexes undergo a significant geometrical rearrangement during the MLCT process. Copper (I) complexes have a tetrahedral configuration while their excited-state undergo a Jahn-Teller distortion. Adopting the copper (II) geometry, a square-planar configuration which leaves room for interaction with the solvent molecules, lowering the stability and the energy gap between the ground-state and the MLCT-state, shortening the excited-state lifetime, and changing the properties of the complex. As shown in **Figure 2.13b**, ligands with specific substituents can limit the distortion from the tetrahedral geometry and assure the necessary characteristics of the complex to be employed as photosensitizer.[11]

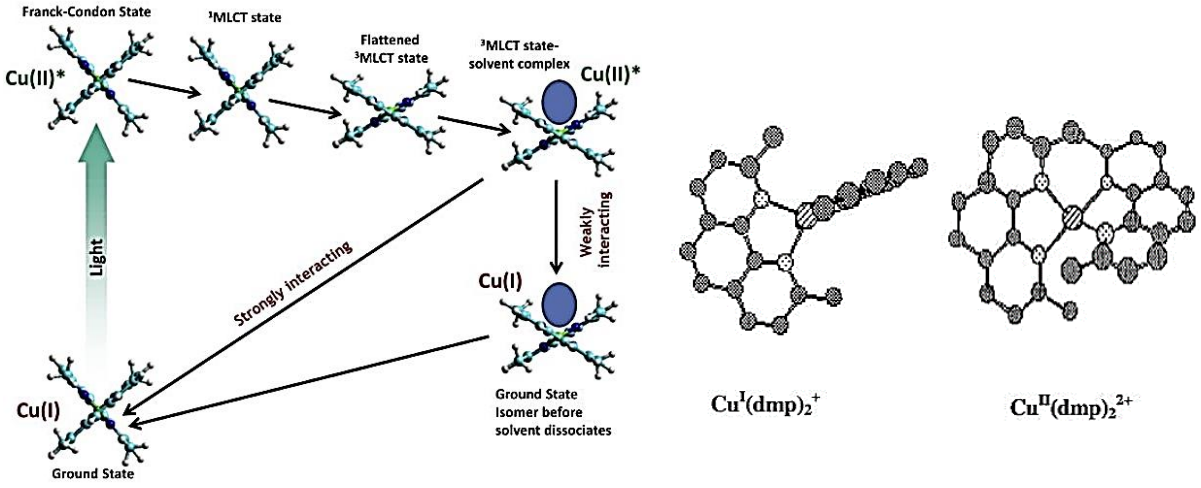

(a) (b)

Figure 2.13: The excited-state dynamics of a copper diimine complex (a).[11] The effect of the "blocking" positions (b).[46]

For example, positions such as 2,9 of the 1,10-phenanthroline and 6,6' of the 2,2' bipyridine, positively influence the excited-state properties of copper (I). These "blocking" positions indeed effectively minimize the flattening of the pseudo-tetrahedral coordination into a square planar geometry, limiting solvent or electrolyte access to the copper centre. To be a good photosensitizer, copper complexes need specific optical and electrochemical characteristics, avoid as far as possible ligand scrambling, and have an excited-state highly energetic to promote electron transfer.

To further improve the performance of DSCs containing copper (I) complex dyes, a "push-pull" system, which recalls the design used for the organic dyes and the porphyrin-based zinc system, can be incorporated. This "push-pull" system will indeed facilitate the electron transfer across the dye by using heteroleptic complexes with two different ligands: the anchoring ligand, (L_{anchor}), which is electron acceptor and able to attach to the FTO/TiO_2 electrode, the copper centre, linker and electron donator, and the ancillary ligand ($L_{ancillary}$) which is chosen to increase the electron density on the metal centre. Ideally, the HOMO is located on the copper core and the LUMO is located on the acceptor group.

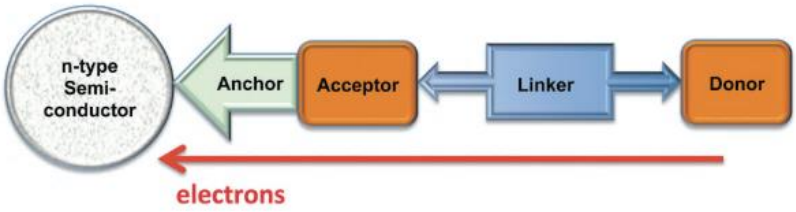

Figure 2.14: Schematic representation of the "push-pull" system. In a copper (I) complex, the *donor* is the ancillary ligand, the *linker* is copper (I) and the *acceptor-anchor* is the anchoring ligand.[9]

The first challenge was to generate heteroleptic Cu(I) diimine complexes. Indeed, competition with the formation of the homoleptic compounds prevents the reliable formation of the desired heteroleptic complex in solution. Due to the Cu(I) complexes lability and the rapid ligands exchange occurring, heteroleptic complexes in solution tend to equilibrate giving statistical mixtures.

$$2[Cu(L_{anchor})(L_{ancillary})]^+ \leftrightarrow [Cu(L_{anchor})_2]^+ + [Cu(L_{ancillary})_2]^+$$

The first known route to prevent ligand scrambling was the HETPHEN approach which uses particularly steric substituents that do not allow the formation of the corresponding homoleptic complex, thus pushing the equilibrium in favour of the heteroleptic species.[11] It requires highly sterically demanding substituents but allows the heteroleptic complex to be adsorbed on the TiO_2 surface via one single dye-bath step.

Constable *et al.*[9] developed several routes to stabilize heteroleptic dyes by using an "on-surface self-assembly" approach. First, soaking the TiO_2 substrate in a solution of L_{anchor} and establishing the proper anchoring through the carboxylic acid moieties onto the surface of the semiconductor. **Figure 2.15** shows the main two routes that shall ensure the heteroleptic complex to be formed. The first route is soaking the functionalized surface in a solution of a homoleptic copper(I) complex formed with the ancillary ligand $[Cu(L_{ancillary})_2]^+$, which leads to the formation of the desired heteroleptic complex through a ligand exchange mechanism. The second route consists of soaking the functionalized surface in two separated baths, the first one with $[Cu(NCMe)_4]^+$ and the second one with only $L_{ancillary}$.

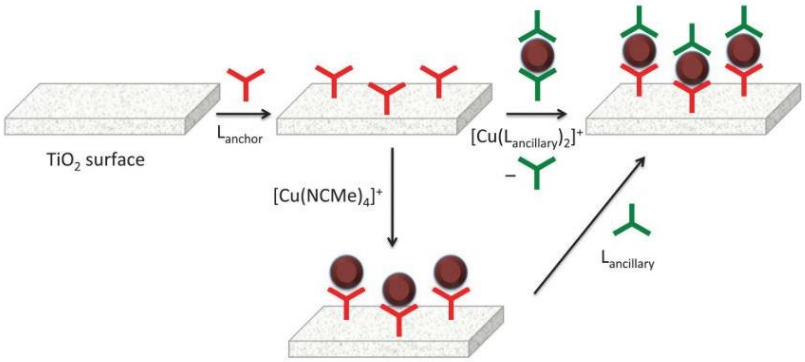

Figure 2.15: On-surface assembly approach to heteroleptic copper (I) dyes.[9]

The distinctive character of using the method exploited by Constable and co-workers is the possibility of studying the heteroleptic complexes only on the surface on TiO_2, which makes the characterization of the complexes more challenging. Nevertheless, to use simple and mostly commercialized ligands the use of the "on-surface self-assembly" method is necessary.

To date, there are literature reports based on homoleptic copper (I) employed in DSCs but only a few reports based on heteroleptic copper (I) complexes.[9]

3 Ligands of interest

The photosensitizer plays a key role in DSCs. Improving solar light harvesting is one of the most important steps of the photovoltaic process and it directly impacts the efficiency of the device, since more photons would be available to be converted into electricity. Its absorption spectrum should resemble as closely as possible the solar spectrum to obtain the maximum allowable light harvesting. By choosing different ligands, different light harvesting can be reached. Transition metal complexes are coloured due to the splitting of the d orbitals when the ligands approach and bond to the central metal ion.[47] Depending on the ligands, the difference in energy between the new levels affect the amount of energy, thus the colour of light that will be absorbed. To avoid the flattening of the tetrahedral configuration to a square-planar geometry, ligands with sterically hindered "blocking positions" were chosen.

3.1 Anchoring ligand

Within the homoleptic copper (I) complexes known from the literature, one of the best power efficiency was reached by Biagini and co-workers,[48] who reached 3% (unmasked) with the complex shown in **Figure 3.1**. This complex has ligands with methyl substituents in the 6,6' positions of a 2,2' bipyridine core, to sterically protect the copper centre and pose a strain toward oxidation of the Cu(I) complex into the corresponding Cu(II). Through the carboxylic acid groups, the ligand is able to anchor the TiO_2 surface.

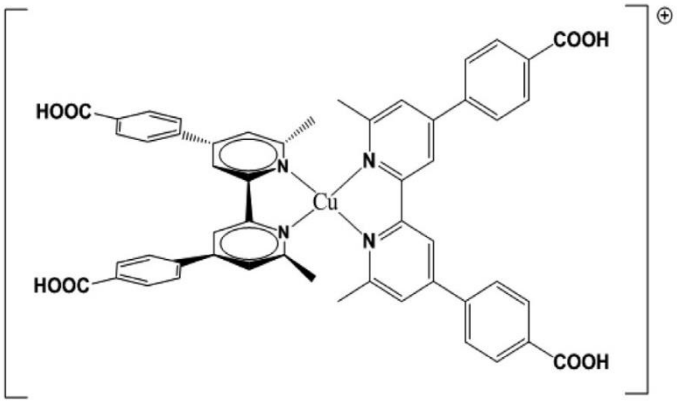

Figure 3.1: The homoleptic Cu(I) complex showing the best performance as dye in DSCs.[48]

In the literature, it is found that, in most of the cases, the 6,6' substituents on the 2,2'-bipyridine are either alkyl or aryl groups.[11] Constable and co-workers[9] studied the influence of those alkyl or aryl groups in the "blocking" positions in both anchoring and ancillary ligands with the same peripheral units. The dyes were prepared with the same "on-surface assembly" technique previously described. Enhanced absorption of the Cu(I) complex towards longer wavelengths was observed when phenyl substituents were present in both cases as ancillary and as anchoring. Nevertheless, when anchoring ligands with phenyl groups were used as photosensitizers in DSCs, the conversion of absorbed light into electrical current was

substantially lower than the conversion measured by employing dyes containing methyl substituents in the anchoring ligand. By following these results, an anchor ligand bearing the methyl groups in the aforementioned positions was selected for this work. In particular, the ligand used is the one that, in its homoleptic Cu(I) complex form, gave one of the highest efficiency in the literature.[48]

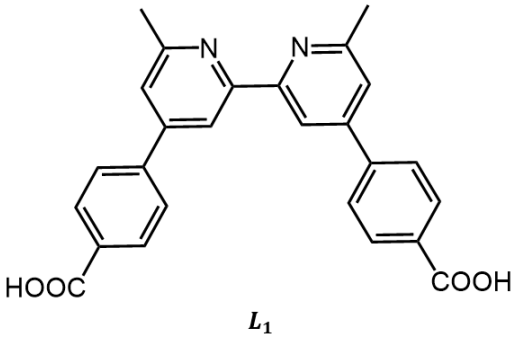

L_1

Figure 3.2: L_{anchor}; 6,6'-dimethyl-2,2'-bipyridine-4,4'-dibenzoic acid (L1).

The ligand was synthesized by Dr. Bo Xu and co-workers in a joint collaboration between KTH - Royal Institute of Technology, and Uppsala University.

3.2 Ancillary ligands

As previously mentioned, the ancillary ligands aim to be suitable donors to enhance electron transfer and minimize recombination. The ancillary ligands were chosen in order to cover a relatively wide range of proprieties deriving from different steric hindrance and redox properties influenced by the nature and the positions of the substituents, and the rigidity of the molecular core. A high degree of conjugation was also desired since the delocalization of the electrons in the overlap of the p orbitals of the double bonds increases light harvesting.

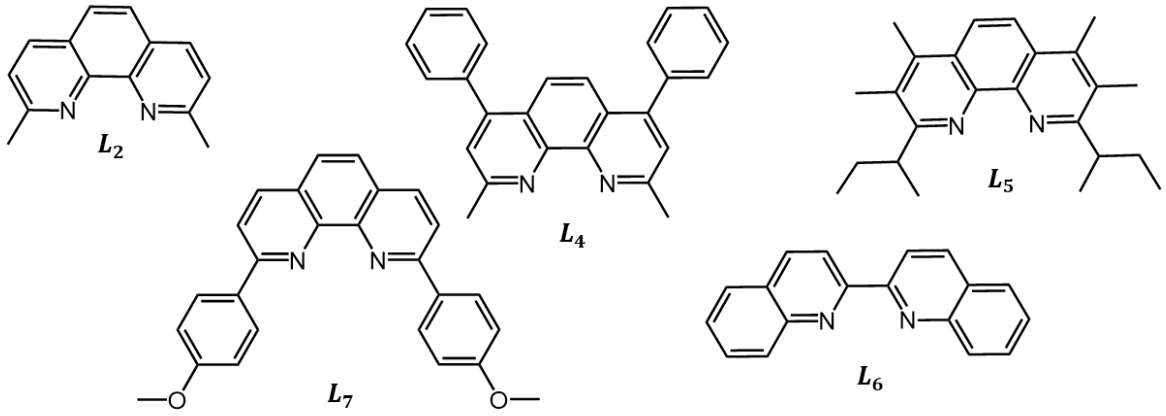

Figure 3.3: Ancillary ligands employed in this work.

With the exception of ligand L5, which was previously synthesized by Dr. Valentina Leandri and co-workers in the same research group at KTH, all the other ancillary ligands were commercially available.

L5 (2,9-di(*sec*-butyl)-3,4,7,8-tetramethyl-1,10-phenanthroline, dsbtmp) was designed by Castellano *et al.*[49] and chosen for its long excited-state lifetimes, of the order of μs. Thanks to the combination of *sec*-butyl groups as 2,9 substituents and the four methyl groups in the 3,4,7, and 8 positions of the phenanthroline core, the Cu(I) metal centre results well insulated from solvent interactions causing only a light geometrical distortion in the excited-state, robust MLCT and high thermodynamic and photochemical stability in solution.

The other ligands commercially available, are known as 2,9-dimethyl-1,10-phenanthroline or Neocuproine (L2), 2,9-dimethyl-4,7-diphenyl-1,10-phenanthroline or Bathocuproine (L4), 2,2′-Biquinoline (L6) and 2,9-dianisyl-1,10-phenanthroline (L7). They were all purchased by Sigma Aldrich. Regarding the formation of the homoleptic complexes starting from these ligands, this was carried out by the same co-workers at KTH who synthesized ligand L5.

L2 has been largely studied in different other works[50–52] for its simple but rigid structure due to the phenanthroline and the presence of the methyl groups in the 2,9 positions. L4 was investigated since it highly resembles L2 and the possible variations deriving from the addition of the phenyl groups can be studied. Ligand L6 is quite different from the others, since possessing a different core structure. It has a much more flexible structure and the external phenyl rings assume the role of “blocking” positions comparable with the methyl groups. Finally, L7, with its anisyl substituents, introduces bulkier substituents in the phenanthroline 2,9 positions.

4 Characterization of the dyes

4.1 Steady-State Spectroscopy

4.1.1 Ultraviolet – Visible (UV-Vis) Spectroscopy

Visible spectroscopy investigates the spectral absorption of the dyes which directly affects the perceived colour of the chemicals involved. Absorption of photons in the ultraviolet (UV) and in the visible (Vis) causes the molecules to undergo electronic transitions: the electron is excited from a lower energy (HOMO) to a higher energy molecular orbital (LUMO). Only photons with equal or higher energy than this transition will be absorbed. The energy of the photons is inversely proportional to the wavelength and their relationship is described in Equation 4.1.

$$E = \frac{h \cdot c}{\lambda} \qquad 4.1$$

Where h is the Planck constant equal to $6{,}626 \cdot 10^{-34}$ J·s, c is the speed of light equal to $2{,}99 \cdot 10^{8}$ m/s and λ is the wavelength.

A UV-Vis spectrometer consists of a light source, a deuterium arc lamp for the UV range and a tungsten filament for the visible range, a diffraction grating, monochromator or prism, splits the incoming light into its component wavelength, which is then measured by a detector. The detector converts the light into current and plots the absorbance against wavelength.

The wavelength that corresponds to the highest absorption is referred to λ_{max}. The resulting spectrum is an absorbance graph versus wavelength. Absorbance (A) at a specific wavelength is related to transmittance (T) as shown in Equation 4.2.

$$A = -log_{10}(T) = -log_{10}\left(\frac{I}{I_0}\right) \qquad 4.2$$

Where I is the intensity of light passing through the sample and I_0 is the initial intensity.

In this case, UV-Vis Spectroscopy study is needed to know the maximum wavelength of sun absorption (visible range) and which ligands bring the highest harvesting. Indeed, the more is the energy that can be absorbed from the sun, the more the electrons excited that can be injected into the semiconductor band. It can also be used to calculate the molar extinction of the substance in solution. According to the Beer-Lambert Law, $A = \varepsilon c l$, the molar extinction coefficient of a particular complex (ε) at a specific wavelength can be calculated by knowing the concentration (c), the absorbance at that wavelength (A), and given the optical path length (l).[47]

The equipment used for the absorption of the visible light measurements was a double-beam Varian Cary 300 Bio UV/Vis Spectrophotometer. The UV-Vis scan rate was 600 nm/min, the data interval 1,000 nm and the average time was 0,100 s. For the solid-state absorption, a first background of the TiO_2 layer on glass was measured before and subtracted from the samples.

4.1.2 Emission spectroscopy

Emission spectroscopy is a spectroscopic technique, which measures the energy (in nm) of photons emitted by the molecules during their transition from the excited-state to the ground-state. According to the electronic structure each molecule or, in this case, each complex emits a characteristic set of discrete wavelengths. In order to test the photoluminescence of the heteroleptic complexes on the surface of TiO_2, attempts of recording optical emission were done with a Cary Eclipse Fluorescence Spectrophotometer.

4.1.3 Determination HOMO – LUMO gap

The energy or wavelength of the electronic transitions depends as mentioned on the HOMO – LUMO gap. In **Figure 4.1**, S_0 and S_1 stand for the *singlet* ground-state and the *first singlet* excited-state. Emission is red shifted, also called Stokes shift, because of the non-emissive relaxations processes occurring before fluorescence.

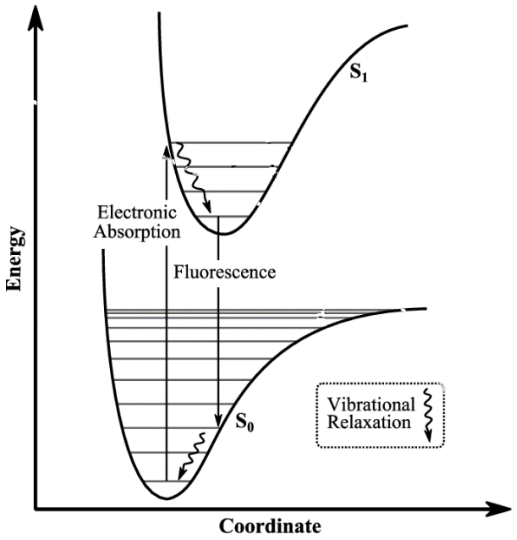

Figure 4.1: Electronic transition.[53]

The HOMO–LUMO gap can be accurately calculated as the intersection of the absorption spectrum with the emission spectrum. A rough estimation could also be made by the absorption spectra only. HOMO–LUMO gap can be calculated based on the absorption edges.[54] Other ways based on the same theory are using the "onset" of the absorption spectra or the energy related to 10% of the normalized absorption.[55]

4.2 Electrochemistry

Electrochemistry is a powerful tool to investigate the tendency of compounds to undergo chemical changes such as oxidation or reduction.[56] Cyclic voltammetry (CV) of the homoleptic copper complexes in solution and differential pulse voltammetry (DPV) of the dyes adsorbed on the TiO_2 surface were performed to determine the redox potentials of the different complexes.

4.2.1 Theoretical Background

In a typical measurement, a three-electrode setup is used: a working electrode, a counter electrode, and a reference electrode, all immersed in a solution with a supporting electrolyte.

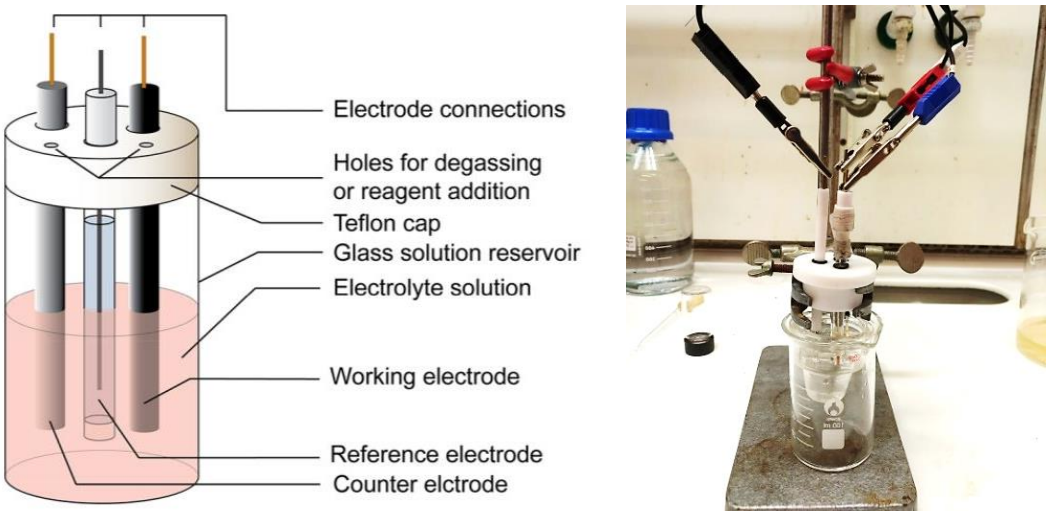

Figure 4.2: Electrochemistry basic set up. To the left a schematic representation of the electrochemical cell.[56] To the right, a picture of the set-up during the study work.

Through an external power source, such as a potentiostat, voltage is applied to the electrodes to drive the process. The potential is relative to the reference electrode and it is scanned at the working electrode while the current flows towards the counter electrode. At the working electrode, an electron transfer occurs and the supporting electrolyte in the solution diffuses to balance the charge and complete the electrical circuit.

In cyclic voltammetry, as shown in **Figure 4.3**, the potential is linearly scanned backward and forward between two extremes, with a triangular waveform. When the potential of the working electrode is more positive than the redox couple present in solution, this couple oxidized and produce an anodic current. Cathodic current is produced on the return scan when the working electrode potential is more negative than the reduction potential of the redox couple and its reduction occurs.

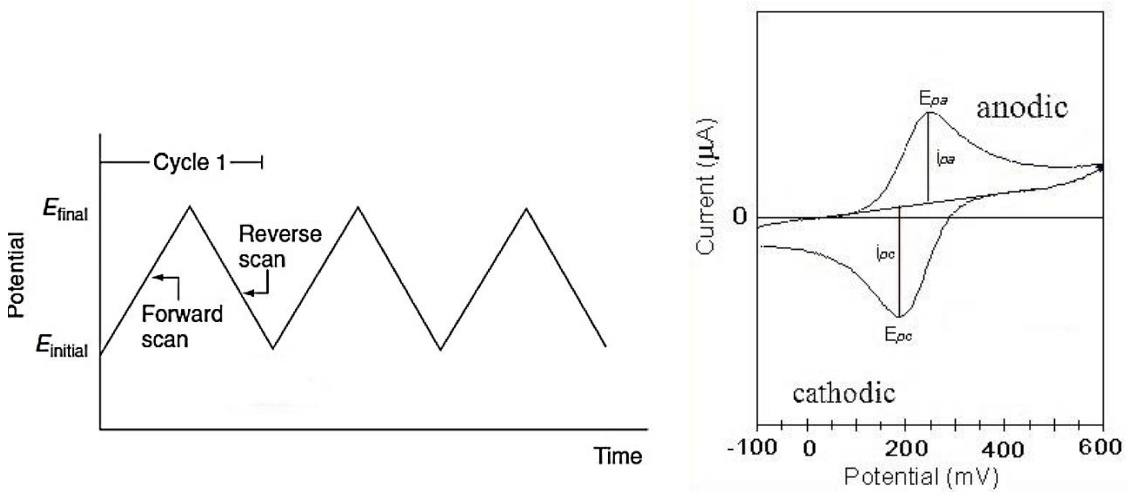

Figure 4.3: Cyclic voltammetry potential as a function of time (a). The expected response of a reversible redox couple during a single potential cycle, (IUPAC convention) (b).[57]

In the CV, the formal redox potential is experimentally determined as $E_{1/2}$, i.e. the potential obtained from the average potential of the anodic peak (E_{pa}) where the oxidation takes place, and of the cathodic peak (E_{pc}) where the reduction takes place. In a fully reversible electrochemical reaction, the peak to peak separation is lower than 57 mV, but it can be higher due to uncompensated solution resistance and non-linear diffusion.[56] When the electron transfer at the working electrode is slower than the mass transport (charge-transfer controlled), the process is electrochemical irreversible.

By measuring DPV, the potential is incremented from an initial to a final value by applying potential pulses and only the current generated by the oxidation and the reduction of the redox couple at the electrode, faradaic current, is extracted, thus electrode reactions can be analyzed more precisely and higher sensitivity is achieved.[58]

Electrochemical measurements were performed using an Ivium Technologies vertex potentiostat. In this work, a glassy carbon as working electrode, a platinum net as counter electrode and a $Ag/AgNO_3$, reference electrode were used. The supporting electrolyte solution mostly employed was 0,1 M tetrabutylammonium hexafluorophosphate ($TBAPF_6$) in acetonitrile, although, due to lack of solubility in that solvent, a solution of 0,1 M $TBAPF_6$ in dimethyl sulfoxide was used for the CV and DPV of $[Cu(L1)_2]^+$ in solution. DMSO was chosen for these measurements for its wider electrochemical window (EW) compared to MeOH.

Three cycles for CV measurements were recorded with a scan rate of 50 mV/s and sensitivity of 10^{-5} A/V. DPV measurements were using potential pulses of 50 mV for 0,1s in periods of 0,5s and with the same sensitivity.

The reference electrode was finally calibrated against the ferrocene/ferrocenium redox couple. Using the potential of the oxidation of ferrocene as an internal standard is an important advantage since variables such as type of reference electrode and reference electrode degradation are eliminated and higher reproducibility of the measures is reached.[59] By knowing that the potential of ferrocene in ACN *vs* NHE (Normal Hydrogen Electrode) is 0,63, the redox potential *vs* Ferrocene was then converted to V *vs* NHE.[56]

4.3 Self-assembly of the heteroleptic copper (I) complexes

All the substrates were prepared on coke-glass with a ~300 nm layer of fluorine-doped tin oxide (SnO_2:F from Pilkington glass; FTO). The glass was cut by using a diamond-tipped glass cutter and then cleaned with acetone and dried with air. Cleaned substrates were covered with TiO_2 by operating doctor blading technique directly from paste GreatCell Solar (18NR-T). This technique concerns the use of cylindrical glass rod to coat the surface evenly with paste while the substrate is held still with some tape. Doctor blading was preferred to spin coating since thicker TiO_2 layers were needed. It also has some advantages such as less paste wasting, though the thickness and the homogeneity of all the substrate highly depend on the ability of the operator.

After doctor blading the substrates were left in the oven for the sintering process: 25 min to reach 350 °C, where it stays for 15 min, and 15 min to reach 500°C; half an hour at that temperature is then needed to complete the sintering and form the desired porous surface of nanoparticles.

The conducting glasses with an active layer of TiO_2 undergo a "on-surface assembly" process (shown in **Figure 4.4**), in which they were first soaked in a 1 mM solution of the anchoring ligand, L1, in MeOH overnight. Then, the functionalized surfaces were soaked in a 1 mM solution of the homoleptic complex $[Cu(L_{ancillary})_2]^+$ in acetonitrile (ACN) for 1 day, resulting in ligand exchange and the formation of the desired heteroleptic complex.

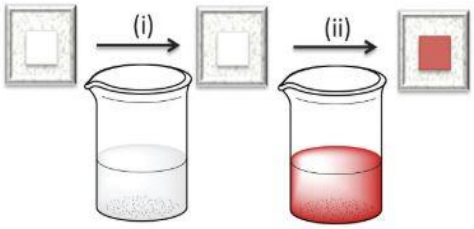

Figure 4.4: First step: soaking an FTO/TiO_2 electrode in a colourless solution of 1 mM of L1 in MeOH (i). Second step: the functionalized electrode is rinsed with MeOH and soaked in a coloured solution of 1 mM $[Cu(L_{ancillary})_2]^+$ in ACN (ii).[9]

The amount of the ligand and the complexes in solution was optimized by starting with the values reported in the literature[12,51,60,61] and finding the best compromise in terms of minor waste and highest adsorption efficiency.

The samples from the aforementioned self-assembly process are shown in **Figure 4.5**.

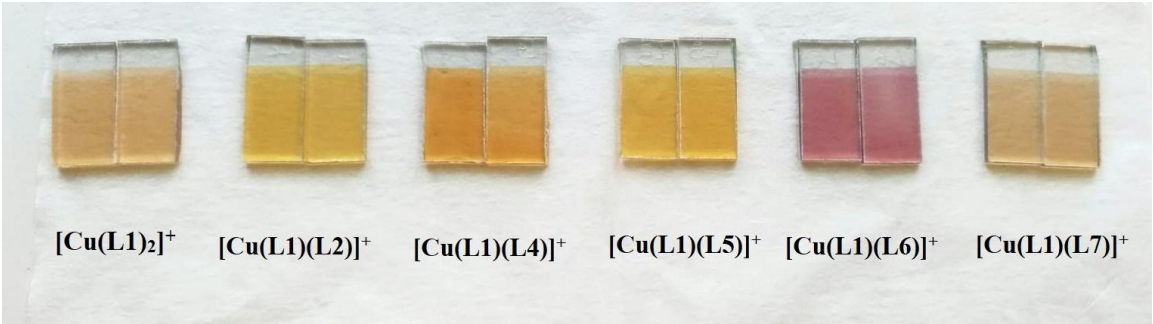

Figure 4.5: Doctor-bladed TiO_2 layer on FTO substrates with the self-assemble copper (I) complexes within the study

The thickness of the TiO_2 layer of the samples was measured with a profilometer, Veeco Dektak 150, and was around 7-8 µm.

4.4 Optical characterization

4.4.1 Results

The UV-Vis measurements were conducted on all the homoleptic complexes in solution and all the prepared substrates of the self-assembled complexes on TiO_2. The absorption spectra were measured from 750 to 400 nm since we were interested in the absorption of the visible light only. The recorded spectra are shown in **Figure 4.6**.

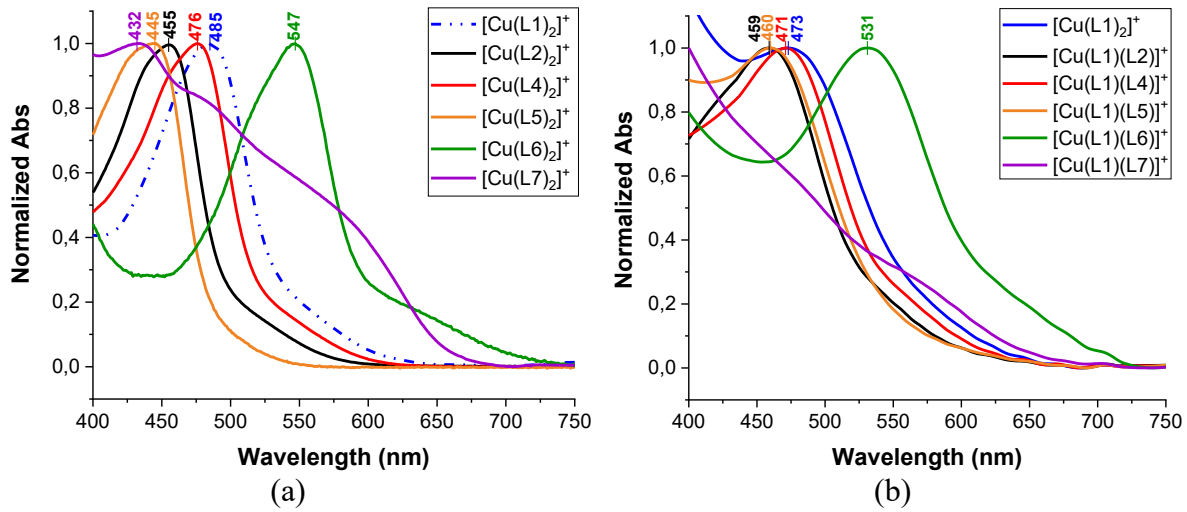

Figure 4.6: Normalized absorption spectra of the homoleptic Cu(I) complexes, dash-dotted line in MeOH and solid line in ACN solution (a). Normalized absorption spectra of the self-assembled Cu(I) complexes adsorbed on the TiO_2 surface (b).

As reported in the literature,[11] a typical absorption spectrum of a Cu(I) complex shows a primary energy transition usually located at around 450 nm, and a broad shoulder which extends towards the red portion of the spectrum. These features depend on the degree of the electronic delocalization and on the substituent 2,9 positions in the phenanthrolines, at the 6,6' positions of the bipyridine, and at the lateral phenyl group in the biquinoline ligand.

In general, the structure of the different ligands, influence the position of the maximum absorption wavelength (λ_{max}) and its shoulder towards longer wavelengths, which has been correlated to the degree of the distortion of the copper complexes.[11] When the shoulder is almost absent in the absorption spectrum, for instance $[Cu(L5)_2]^+$, the complex retain the pseudo-tetrahedral conformation even in the excited-state. A more visible shoulder feature indicates easier transformation into a flattened conformation due to lower frequency vibrational motions. Complex $[Cu(L7)_2]^+$ shows a really broad shoulder, which is typical of systems with 2,9 dianisyl substituents thus, it cannot be easily rationalized.[62]

Complex $[Cu(L1)_2]^+$ in **Figure 4.6a**, was represented dash-dotted since it was measured in MeOH, due to its insolubility in acetonitrile. However, the different solvent used to measure the visible absorption spectrum should not substantially influence λ_{max} since light absorption is not influenced by the processes that occur after charge transfer such as interaction with the

solvent that follows a flattening of the complex structure, and considering that the viscosities and the dielectric constants for methanol and acetonitrile are quite similar.[46]

Excluding $[Cu(L7)_2]^+$, a pattern from the narrower to the broader shoulder, i.e. from the lowest to the highest geometrical distortion, can be identified from the homoleptic complex series: $[Cu(L5)_2]^+$, $[Cu(L4)_2]^+$, $[Cu(L1)_2]^+$, $[Cu(L2)_2]^+$, and $[Cu(L6)_2]^+$. This trend could be explained by the importance also of the 4,7-diphenyl substituents in the phenanthrolines or 4,4' substituents in the bipyridine for the change in structure conformation.

Heteroleptic copper complexes were measured directly in solid-state from the samples with TiO_2 film. A first evident feature is a broadening in the spectra when measured on the semiconductor surface. This can be directly observed by the comparison of the homoleptic complex $[Cu(L1)_2]^+$ in solution and on the TiO_2 surface. Moreover, the maximum absorption spectra, λ_{max}, appears to be slightly shifted to the blue, lower wavelength, when absorbed on TiO_2 rather than in solution. This latter aspect can be due to the different experienced chemical and electronic environments which can play a relevant role in the absorption band positions. For instance, a complex adsorbed on TiO_2 can be assumed not surrounded by solvent molecules, while in solution different solvation conditions and ligand exchange can occur. Finally, it should be considered that the carboxylic moieties of the anchoring ligand, L1, when on TiO_2, are bonded to Ti atom instead of a proton, being therefore chemically different.

Within the homoleptic complexes, when moving from the red to the blue part of the visible spectrum, the following order was observed: $[Cu(L6)_2]^+$, $[Cu(L1)_2]^+$, $[Cu(L4)_2]^+$, $[Cu(L2)_2]^+$, $[Cu(L5)_2]^+$ and lastly $[Cu(L7)_2]^+$. A shift towards the red end of the spectrum is highly desirable since it increases light harvesting efficiency at lower energies where the solar spectrum is rich.[12]

The complexes on TiO_2 follow similar trend of the complexes in solution, from lower energy to higher energy: $[Cu(L1)(L6)]^+$, $[Cu(L1)_2]^+$, $[Cu(L1)(L4)]^+$, $[Cu(L1)(L5)]^+ \approx [Cu(L1)(L2)]^+$. However, on TiO_2, the absorption values were quite low, in the range of 0,2-0,4, suggesting low adsorption of the complex on the surface.

Finally, through the Beer-Lambert law, the molar extinction coefficient, ε, was calculated in acetonitrile solutions for the complexes that did not have any reported value of such parameter in the literature. **Figure 4.7** shows the determination of the molar extinction coefficient for complex $[Cu(L4)_2]^+$. By varying the concentration of the solution so that the absorption range was between 0,2-0,8, taking the slope of the line, $A = \varepsilon\, c\, l$, referred to the maximum absorption wavelength, $\varepsilon_{\lambda max}$ was extrapolated where the optical path length was considered equal to 1 cm as the width of the cuvette.

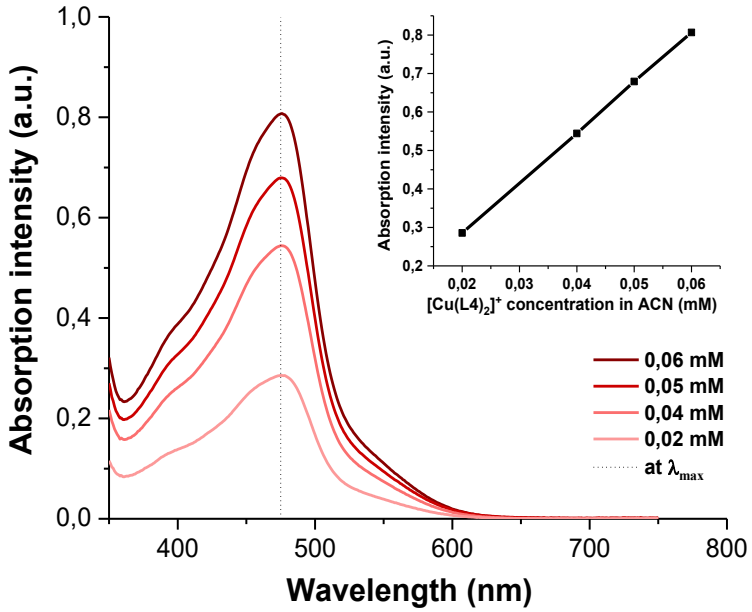

Figure 4.7: Determination of the molar extinction coefficient through the Beer-Lambert law for complex $[Cu(L4)_2]^+$.

The molar extinction coefficient is indicative of how strongly a substance absorbs light at a specific wavelength. Higher ε values can considerably improve the photocurrent and enhance efficiency of the solar cells by improving light harvesting. Biagini and co-workers[48] observed that a high extinction coefficient can be more important than a strong anchoring to TiO_2 for the improvement of solar cell performance.

Table 4.1 shows the maximum absorption wavelength and the molar extinction coefficient, calculated in this work or previously measured in other works, of the homoleptic complexes in solution and compared to the state-of-the-art Ruthenium N719 dye. With the exception of $[Cu(L1)_2]^+$ and N719, which were measured in MeOH, the other complexes refer to an ACN solution. While the visible spectra are not significantly influenced by the use of a different solvent, the extinction coefficient value is slightly affected thus it is important to indicate it.[46]

Table 4.1: Maximum absorption wavelength and its relative molar extinction coefficient for the homoleptic complexes in solution in comparison with the state-of-the-art dye for DSCs, N719.

Complex	λ_{max} abs (nm)[d]	$\varepsilon_{\lambda,max}$ ($M^{-1}cm^{-1}$)
$[Cu(L1)_2]^+$	485[a,c]	15800[a,c]
$[Cu(L2)_2]^+$	455[b]	7200[b,d]
$[Cu(L4)_2]^+$	476[b]	13505[d]
$[Cu(L5)_2]^+$	445[b]	4710[b,d]
$[Cu(L6)_2]^+$	547[b,e]	3690[b,e]
$[Cu(L7)_2]^+$	432[b]	2394[d]
N719	535[a,c]	14800[a,c]

[a]In methanol solution; [b]In acetonitrile solution; [c]According to Biagini *et al.*[48]

[d]Calculated in this work; [e]According to Jahng *et al.*[63]

The extinction coefficient of the copper (I) complexes $[Cu(L7)_2]^+$, $[Cu(L6)_2]^+$, $[Cu(L2)_2]^+$ show really low values, while $[Cu(L4)_2]^+$ is comparable to N719 and $[Cu(L1)_2]^+$ according to the value calculated by Biagini and co-workers[48] is even greater than N719.

Since constrained to the TiO_2 film for the assembling of the heteroleptic complexes, a calculation of the extinction coefficient of these was not performed, since it would have been affected by many approximations.

No clear emission spectra were detected on the complexes absorbed on the TiO_2 probably due to quenching mechanisms which covered the peak of interest. Therefore, the HOMO-LUMO gaps in this work were calculated from the onset of the absorption spectrum. **Table 4.2** shows the maximum absorption and the lowest energy electronic transitions of the self-assembled complexes adsorbed on TiO_2. The HOMO-LUMO gap is important regarding the basic function of the dye, which indeed needs to have a lower energetic HOMO compared to the electrolyte redox couple and a higher energetic LUMO of the conduction band of the semiconductor, in this case, TiO_2.

Table 4.2: Maximum absorption wavelength and the HOMO-LUMO gap of the complexes adsorbed on TiO_2

Complex	λ_{max} abs (nm)	$E_{0\text{-}0}$ (eV)[c]
$[Cu(L1)_2]^+$	473[a]	2.16
$[Cu(L1)(L2)]^+$	459[a]	2.30
$[Cu(L1)(L4)]^+$	471[a]	2.23
$[Cu(L1)(L5)]^+$	460[a]	2.25
$[Cu(L1)(L6)]^+$	531[a]	1.96
$[Cu(L1)(L7)]^+$	439[b]	1.88

[a]On the surface of mesoporous films of anatase TiO_2, [b]Calculated using the fitting line in **Figure 4.8**,

[c]Calculated from the onset of the absorption spectrum.

4.4.2 Discussion

The maximum absorption wavelength of the complex $[Cu(L6)_2]^+$, because of the extended conjugation of the 2,2' biquinoline ligands, which are strong electron acceptors, is substantially red-shifted compared to the others. Its value perfectly matches the value previously reported in the literature.[63] Complex $[Cu(L1)_2]^+$ possesses bipyridine-based ligands with phenyl group connected through a single bond to the core, resulting in a partial interruption of the conjugation, which leads to a MLCT transition at higher energies. Similarly $[Cu(L4)_2]^+$ has phenyl groups connected via a single bond to the phenanthroline-based ligands. Since ligands L2 and L5 do not have any aromatic substituents on the phenanthroline core, their complexes resulted more blue-shifted compared to $[Cu(L4)_2]^+$. Finally, $[Cu(L7)_2]^+$ cannot be explained based on conjugation degree because of the broad shoulder typical of its anisyl substituents, and its λ_{max} is the most blue-shifted but its absorption takes place through the entire visible spectrum.

By plotting the maximum absorption wavelength of the heteroleptic self-assembled complexes with L1 on TiO_2 with their corresponding homoleptic in solution, the trend shown in **Figure 4.8** was observed. This trend is highly interesting since it can give a tool to predict unknown λ_{max} of heteroleptic complexes with the same anchoring ligand.

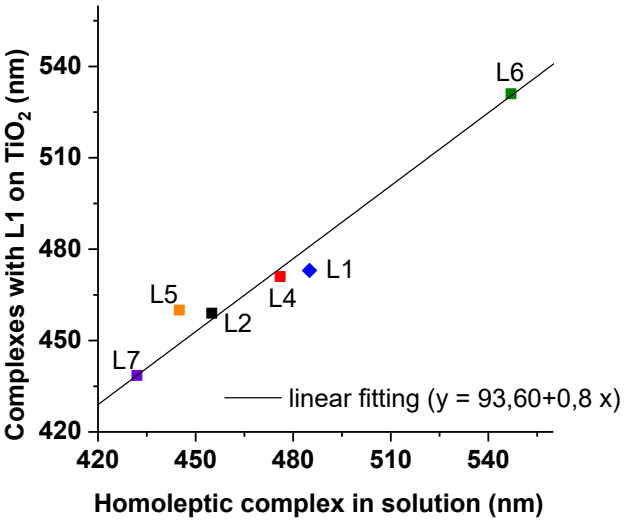

Figure 4.8: Maximum absorption wavelengths of the homoleptic complexes in acetonitrile solution (x-axis) and of the corresponding complexes formed on the surface of TiO_2 with L1 as the anchoring ligand (*y*-axes). The point related to the ligand L7 is a prediction based on the fitting line obtained from the data.

The trend follows a linear pattern described by the equation with slope 0,8 and intersection at 93,60. The trend consider both the influence of the assembling with L1 and the presence of TiO_2. To find the linear fitting only the points including ligands L2, L4, and L6 were used. Complexes $[Cu(L1)_2]^+$ and $[Cu(L5)_2]^+$/$[Cu(L1)(L5)]^+$ were not taken into account for the fitting since slightly outside the pattern, but their error from the linear fitting is fairly low. Furthermore, $[Cu(L1)_2]^+$ in solution was measured in a different solvent compared to the others, and even if this should not matter considerably, the value is anyways subjected to more approximations. From the absorption spectra of the complex $[Cu(L1)(L7)]^+$, it was not possible to detect a value of λ_{max}, and the presented model was thus used to predict its value, which should be located at approximately 439 nm.

For the molar extinction coefficients, since lacking the values of the heteroleptic complexes, a similar pattern could not be shown but it can be hypothesized.

4.5 Electrochemical characterization

4.5.1 Results

It is widely reported in the literature that the 2,9 substituents in the phenanthrolines give a shift towards the higher (more positive) potential of around 400 mV compared to phenanthrolines which lack these groups. Meyer and co-workers[46] in particular worked on complexes with 1, 10-phenantroline-ligands, $[Cu(phen)_2]^+$, and 2,9-dimethyl-1,10-phenanthroline, $[Cu(dmp)_2]^+$, the latter corresponding to $[Cu(L2)_2]^+$ in this work. They explained the shift through the steric effect, indeed these positions 2,9 do not allow to achieve a high degree of planarity, therefore making the oxidation more difficult.

Figure 4.9 shows the cyclic voltammetry of the homoleptic complexes, $[Cu(L_{ancillary})_2]^+$ measured in 0,1 M tetrabutylammonium hexafluorophosphate, $TBAPF_6$, in ACN; the potentials were measured *vs* $Ag/AgNO_3$ and then were reported *vs* ferrocene.

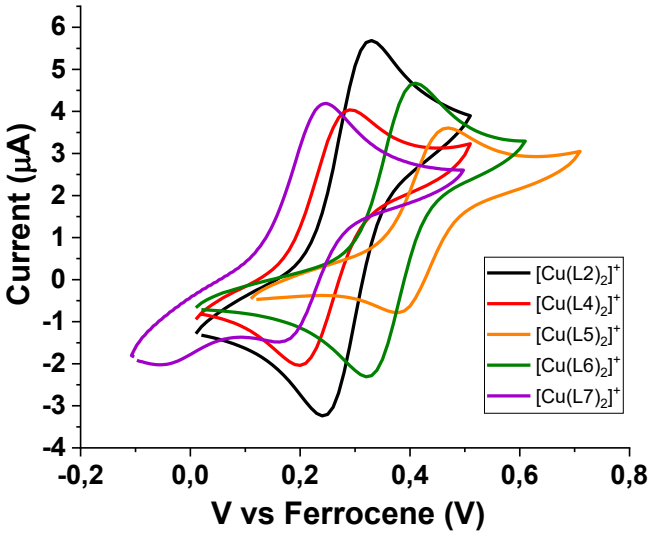

Figure 4.9: Cyclic voltammetry of the homoleptic complexes in ACN (0.1 M $TBAPF_6$). (only the 3rd cycles are shown)

All the homoleptic complexes measured in **Figure 4.9** exhibit one distinctive *quasi*-reversible redox process, related to the oxidation from Cu(I) to Cu(II). Within the CVs series, the trend, from the easiest to the hardest to oxidize, is the following: $[Cu(L7)_2]^+$, $[Cu(L4)_2]^+$, $[Cu(L2)_2]^+$, $[Cu(L6)_2]^+$ and $[Cu(L5)_2]^+$.

Table 4.3 summarizes the redox potentials, $E_{1/2}$, *versus* ferrocene (Fc^+/Fc) and *versus* normal hydrogen electrode (NHE) and the peak-to-peak separations, ΔE_p, measured for the homoleptic complexes shown in **Figure 4.9**.

Table 4.3: Redox potential and peak-to-peak separation of the homoleptic complexes.

Homoleptic complexes	$E_{1/2}$ *vs* Fc^+/Fc (V)	$E_{1/2}$ *vs* NHE[a] (V)	ΔE_p (mV)
$[Cu(L2)_2]^+$	0,285	0,915	90
$[Cu(L4)_2]^+$	0,245	0,875	90
$[Cu(L5)_2]^+$	0,425	1,055	90
$[Cu(L6)_2]^+$	0,365	0,995	90
$[Cu(L7)_2]^+$	0,205	0,845	85

[a]A conversion factor of Fc^+/Fc *vs* NHE of 0,63 mV was used.

The peak-to-peak separations were slightly higher than the 57 mV which delimits a fully reversible electrochemical reaction. However, the values resemble the ones known in the literature for this kind of coordination complexes.[46]

A particular study for $[Cu(L1)_2]^+$ was conducted due to its insolubility in ACN. Since L1 was given in limited amount only as a ligand, it was not possible to perform the synthesis and purification of the corresponding homoleptic Cu(I) complex. Therefore, a solution containing 1,5 mM of copper(I) hexafluorophosphate and 3 mM of L1 in DMSO with 0,1 M of $TBAPF_6$ as supporting electrolyte was prepared to measure the cyclic voltammetry. By doing so, different mechanisms that could highly influence the CV could also occurred, such as substitution of the solvent with the ligand leading to $[Cu(L1)(CH_3CN)_2]^+$ and suspected coordination of carboxylic acid with copper.[64] In order to compare its voltammetry with the only copper, **Figure 4.10** shows the CVs of tetrakis (acetonitrile) copper (I)

hexafluorophosphate copper, $[Cu(CH_3CN)_4]PF_6$, to the left and of the mix L1 + $Cu(PF_6)$ in DMSO to the right.

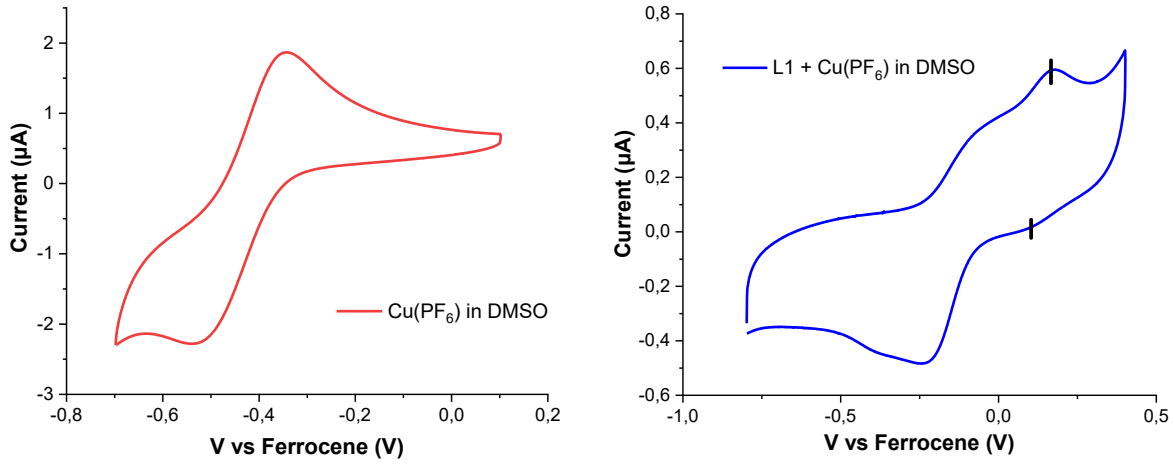

(a) (b)

Figure 4.10: Cyclic voltammetry of $[Cu(CH_3CN)_4]^+$ PF_6^- in DMSO (0.1 M $TBAPF_6$) (a) and mix L1 + $Cu(PF_6)$ in DMSO (0.1 M $TBAPF_6$) (b). (only the 3rd cycles are shown)

It is reasonable to think that the peaks pointed out in black in **Figure 4.10b** are the oxidation and the reduction of the desired complex $[Cu(L1)_2]^+$ and the redox potential, $E_{1/2}$, occurs at around 0,12 V *vs* Fc^+/Fc in DMSO. Experiments of increasing the concentration of copper starting from a solution of the only L1 were conducted to have a better understanding of this mechanism but increasing the copper (I) concentration only led to an increase almost equal of the different oxidation peaks. This behaviour was unexpected, and it should be subjected to a more thorough investigation in future works.

For the complexes self-assembled on the surface of TiO_2, the study of the cyclic voltammetry resulted more challenging due to the thick substrates used for the measurements and the low actual amount of the dye adsorbed. Even if some cyclic voltammetries were recorded, due to the difficulty in identifying the anodic and cathodic peaks, the use of differential pulse voltammetry (DPV) technique was preferred. Furthermore, due to the limited stability of these complexes, with CV measurements there was the possibility of influencing the result by losing some of the copper and the $L_{ancillary}$ in the solution of ACN and supporting electrolyte. **Figure 4.11** compares the DPV of the homoleptic complexes in solution with the self-assembled complexes on TiO_2 substrates. Once again, since $[Cu(L1)_2]^+$ in solution was measured in DMSO its curve is dash-dotted. On the other hand, when adsorbed on the TiO_2 surface, even if measured in acetonitrile solution like the other complexes, a significantly lower current was shown. In order to focus on the different shift in potential, the current intensity was then normalized.

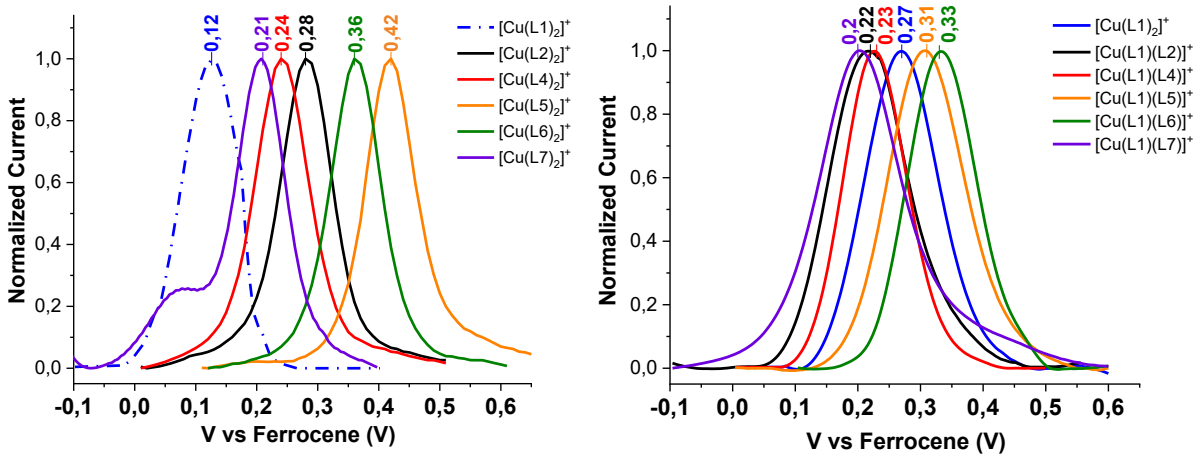

Figure 4.11: DPVs of the homoleptic complexes in solution, measured in ACN (0.1 M $TBAPF_6$), with the exception of $[Cu(L1)_2]^+$, dash-dotted line, which was measured in DMSO (0.1 M $TBAPF_6$) (a). DPVs of the self-assembled complexes on the surface of TiO_2 measured in ACN (0.1 M $TBAPF_6$) (b).

Meyer *et al.*[46] observed that the copper complexes redox chemistry is solvent dependent. Indeed, copper (I) complexes as a result of their ligand lability and changes in conformation from Cu(I) to Cu(II), are highly influenced by the solvent in which they are measured. In their work, the redox potential of the copper complex under investigation was shifting of 0,13 V towards more positive potentials, going from DMSO to ACN. They explained that this behaviour is caused by the addition of solvent to the complex while the oxidation of Cu(I) to Cu(II) at the electrode surface occurs. Solvent interaction raises the free energy of the electron transfer when highly coordinating solvents such as DMSO are involved and decreases when the adduct formation occur less in slightly weaker coordinating solvents.

Based on this observation, since to study complex $[Cu(L1)_2]^+$ in DMSO solution was used, to compare the oxidation peak with the other copper(I) complexes, the potential was positively shifted of approximately 0,13 V. Following this approximation, the complex $[Cu(L1)_2]^+$ has, therefore, a supposed oxidation potential *vs* Fc^+/Fc of 0,25 V in ACN, which is rather close to the value of the complex measured on TiO_2, 0,27 *vs* Fc^+/Fc .

Table 4.4 compares the oxidation potentials, E_{Ox}, taken from the DPV of all the complexes, in solution and on TiO_2, both *versus* Fc^+/Fc and NHE.

Table 4.4: Oxidation potentials measured by the DPV of the homoleptic complexes and the self-assembled complexes on TiO_2

Complexes in solution	E_{Ox} vs Fc^+/Fc (V)	E_{Ox} vs NHE (V)	Complexes on TiO_2	E_{Ox} vs Fc^+/Fc (V)	E_{Ox} vs NHE (V)
$[Cu(L1)_2]^+$	0,25	0,88	$[Cu(L1)_2]^+$	0,27	0,90
$[Cu(L2)_2]^+$	0,28	0,91	$[Cu(L1)(L2)]^+$	0,22	0,85
$[Cu(L4)_2]^+$	0,24	0,87	$[Cu(L1)(L4)]^+$	0,23	0,86
$[Cu(L5)_2]^+$	0,42	1,05	$[Cu(L1)(L5)]^+$	0,31	0,94
$[Cu(L6)_2]^+$	0,36	0,99	$[Cu(L1)(L6)]^+$	0,33	0,96
$[Cu(L7)_2]^+$	0,21	0,84	$[Cu(L1)(L7)]^+$	0,20	0,83

4.5.2 Discussion

The redox potential reflects two main aspects of the complexes: the effectiveness of the "blocking" positions, which gives values shifted towards higher potentials, and the electron donator effect of the ligands, which moves the potentials towards lower values.

Among the complexes in solution, $[Cu(L5)_2]^+$ was the hardest to oxidize due to the sec-butyl groups in position 2,9 of the phenanthroline, indeed since more sterically hindered compared to the others, it was harder for the complex to reach the flatten configuration of Cu(II) geometry. It was followed by $[Cu(L6)_2]^+$ which has sterically demanding phenyl group to prevent this distortion to occur. Complexes $[Cu(L7)_2]^+$ and $[Cu(L4)_2]^+$ were the easiest to oxidize. Indeed, the phenyl substituents connected to the main phenanthroline body have an electron donating effect, making the oxidation from Cu(I) to Cu(II) easier. Finally, complex $[Cu(L2)_2]^+$ highly resembled $[Cu(L4)_2]^+$ but lacked the phenyl groups in the 4,4' positions, thus, since deficient of the aforementioned donating effect, it had slightly higher oxidation potential. Including $[Cu(L1)_2]^+$ in the series of the complexes in ACN, by moving it of 0,13 V to the value measured in the DMSO, the same argument of complexes $[Cu(L4)_2]^+$and $[Cu(L7)_2]^+$ could be used to explain its behaviour.

From the peak-to-peak separation values of the homoleptic complexes, $[Cu(L_{ancillary})_2]^+$, in ACN (**Figure 4.9**), the system could be considered *quasi*-reversible, since the ΔE_p was slightly higher than the reversibility range 1-57 mV. The *quasi*-reversible electrochemical reaction it is due to reorganization energy influenced by the lability of the system in solution.

Figure 4.12 shows the correlation between the DPV of the homoleptic complexes in solution with their respective heteroleptic, self-assembled with L1 on the TiO_2 surface. By comparing the electrochemical data of the homoleptic complex $[Cu(L1)_2]^+$ in solution and absorbed on the surface of TiO_2, assuming the shift of 0,13 V taken from the literature[46], a small redox potential difference was observed.

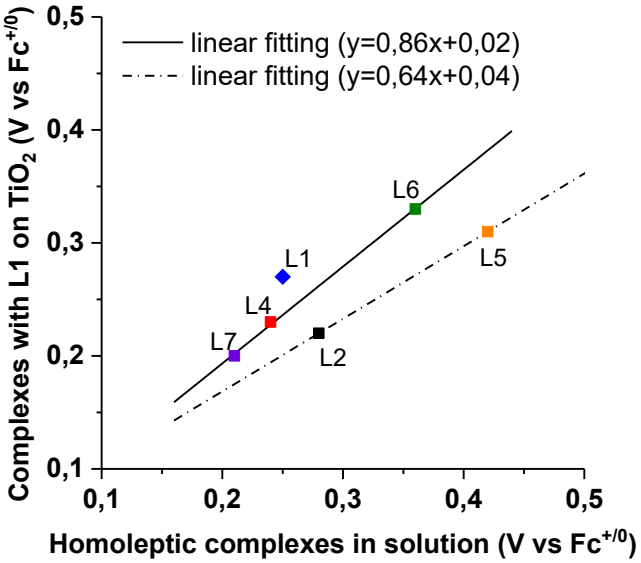

Figure 4.12: Redox potentials measured from the DPVs of the homoleptic complexes in acetonitrile solution (x-axis) and of the corresponding complexes formed on the surface of TiO_2 with L1 as the anchoring ligand (*y*-axes). The point related to L1 has been obtained considering a 0,13 V shift towards a more positive potential from the DPV in DMSO to acetonitrile.[46]

A good pattern as for the maximum absorption wavelength was not identified, but two main trends were suggested, as shown in **Figure 4.12** by the linear fittings. The homoleptic

$[Cu(L1)_2]^+$, as it is affected by the several assumptions made, was not included in the general patterns.

The "solid" fitting line covered the behaviour of the complexes possessing ligands L4, L6 and L7. These three ligands have in common the presence of donating phenyl groups connected to the phenanthroline core or a more electron donating biquinoline structure. These ligands, when heteroleptic with L1, had the greatest effect on the redox potential, which indeed highly resembled the value of their homoleptic with only tiny shift of around 10-30 mV.

The "dash-dotted" fitting line included ligands L2 and L5. These two ligands indeed do not possess any phenyl substituent on the phenanthroline core and present shifts toward lower potential of 60-110 mV. This could be interpreted considering as main effect on the shift the flattening of the structure which occur more easily when heteroleptic with L1 than homoleptic. Nevertheless, these hypothesized trends need to be further investigated by trying more ancillary ligands with different characteristics.

4.5.3 Energy Level Diagram

The energy level diagram indicates the differences in the HOMO-LUMO levels of the self-assembled copper (I) complexes (shown in **Figure 4.13**). The HOMO-LUMO gap was previously calculated by the absorption spectra while the HOMO level corresponds to the electrochemical oxidation potential *vs* NHE.

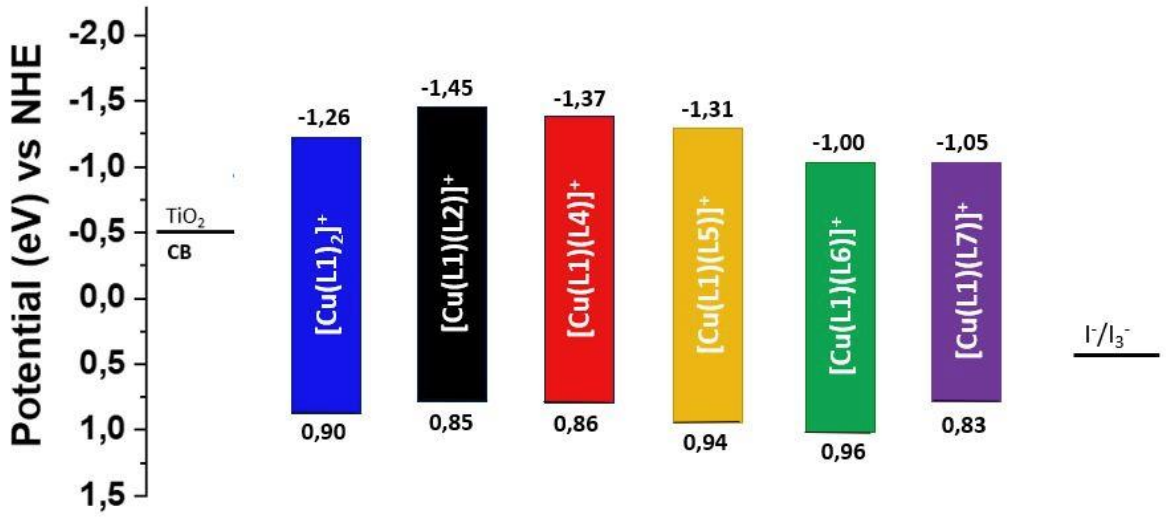

Figure 4.13: Energy level diagram of the self-assembled complex on TiO_2 surface.

Considering the potential of the conduction band of anatase TiO_2 at -0.50 V *vs* NHE[65] and the simplified I^-/I_3^- redox potential at around 0,40 V *vs* NHE,[66] all the dyes satisfied the requirement necessary for injection and regeneration. They all showed a more positive potential compared to the redox potential of iodide/triiodide, which means that they could efficiently be reduced and regenerated during the process. While the LUMO levels were located at more negative potential compared to the conduction band edge of TiO_2, with the possibility of effectively inject the electrons into the semiconductor.

5 Characterization of the photovoltaic devices

5.1 Current-voltage characteristic

The current-voltage characteristic (*I-V*) constitutes one of the most important characterization techniques for a solar cell and define its operation within an electrical circuit. It shows the relationship between the current flowing, generated by the light, through the electronic device and the applied voltage across its terminals. When light is applied, there is a shifting of the *I-V* curve into the fourth quadrant and the cell begins to generate power, which since it is generated, the convention is to invert the current axis[67] (see **Figure 5.1).**

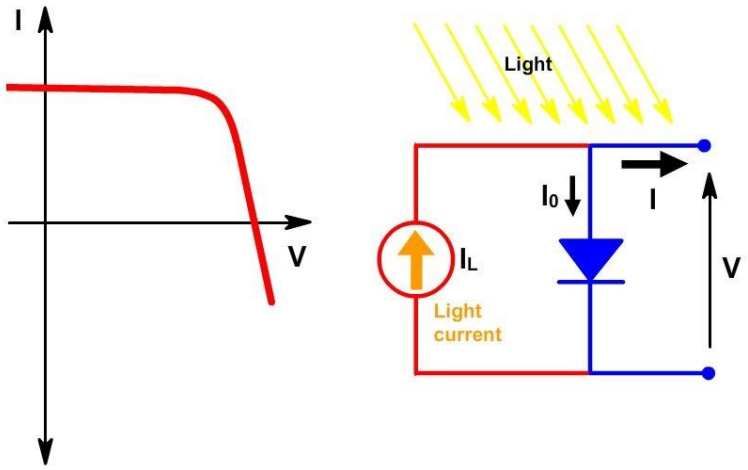

Figure 5.1: *I-V* characteristic when the light generates current.[67]

The basic solar cell structure is a diode with the donor component (anode) and acceptor component (cathode). Photons are absorbed in the donor component, electrons will move from the anode to the cathode and a reverse bias current also called photocurrent will occur. Without any external voltage applied, the photocurrent is referred to as short circuit photocurrent (I_{SC}). When starting to apply a voltage, a forward bias, it will compensate for the reverse photocurrent and, after reaching the threshold, it will reach the point where the current goes to zero. This point is referred to as the open circuit voltage (V_{OC}), since no current occur even if voltage is applied, as the circuit is open.[68]

The overall power conversion efficiency, η, is the most basic parameter used to compare the performance of solar cells. The efficiency is given by Equation 5.1.

$$\eta = \frac{I_{SC} \cdot V_{OC} \cdot FF}{P_{in}} \qquad 5.1$$

where I_{SC} is the short circuit current, V_{OC} is the open circuit voltage, FF is the fill factor and P_{in} is the intensity of the incident light.

I_{SC} is due to the generation and collection of the electrons excited by the light and efficiently injected into the system. Since it depends on the area is more common to refer to the short circuit current density, J_{SC} in mA/cm^2.

V_{OC} is the open circuit voltage obtained in the solar cell, it is a measure of the work that can be done by the generated photocurrent and it physically corresponds to the difference between E_F (*quasi*-Fermi level) of the semiconductor and the E_{redox} (redox potential) of the redox couple in the electrolyte.

The FF is the ratio of the area of the rectangle created by the product of current and voltage at the maximum power point (I_{MP}, V_{MP}) divided by the rectangle generated from the product $I_{SC} \cdot V_{OC}$ (see Equation 5.2) and it can be given in percentage, assuming values between 0 and less than 100%.

$$FF = \frac{I_{MP} \cdot V_{MP}}{I_{SC} \cdot V_{OC}} \qquad 5.2$$

As shown in **Figure 5.2**, it is a measure of the "squareness" of the *I-V* characteristic, where the maximum power point, P_{max}, is given when a forward bias is applied and the current in the opposite direction of the reverse photocurrent balance this last one. If the diode system was ideal, the FF would be 100% and the photocurrent would be flat until the V_{OC} and then straight up vertically.

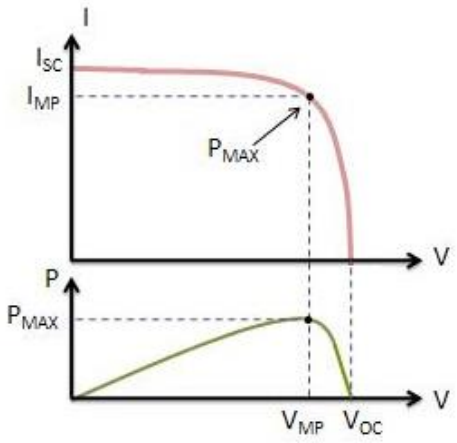

Figure 5.2: In red (top part), the *I-V* curve of the solar cell. In green (bottom part), the power curve obtained from the same solar cell.[69] The power curve shows that at a certain value of current and voltage, power is maximum at the P_{max} point.

The FF is an important factor to consider when studying recombination problems in the cell. Often the fill factor is around 40-60% and in the most efficient cases, it reaches up to 80-85%.[68]

When investigating the types of resistances occurring in a solar cell, a useful parameter is the characteristic resistance, R_{CH}, which is the resistance at the maximum power point of the solar cell and is described by the equation $R_{CH} = V_{mp}/I_{mp}$ (**Figure 5.3**).

For solar cells which exhibit a high value of FF, the characteristic resistance can be approximated as $R_{CH} \approx V_{OC}/I_{SC}$. Since the value depends on the area of the device, typically it is expressed as $R_{CH} \approx V_{OC}/J_{SC}$ $(\Omega \cdot cm^2)$.

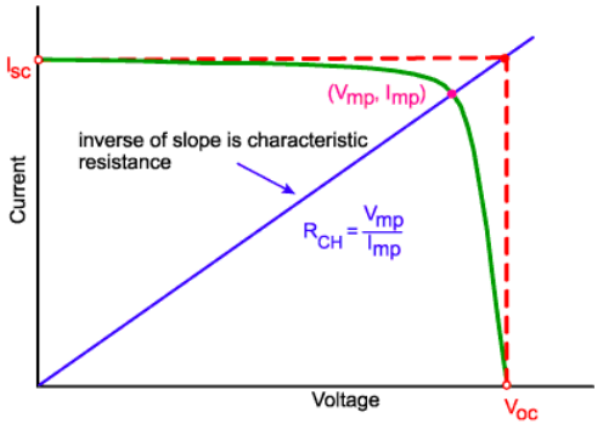

Figure 5.3: Characteristic resistance.[70]

Other types of resistances which highly influence the fill factor value and reduce the efficiency of the solar cell can be described in terms of series resistances and shunt resistances as shown in **Figure 5.4**.

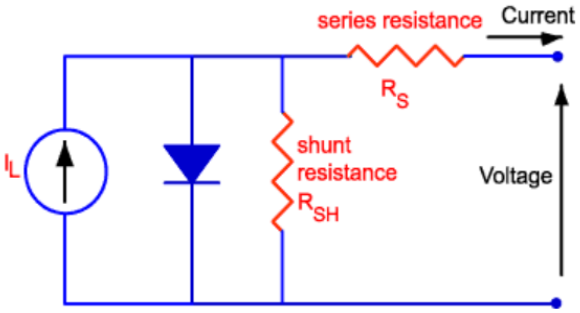

Figure 5.4: Series resistance and shunt resistance present in a solar cell circuit.[71]

Series resistances, R_S, do not affect the short circuit current until the resistance is extremely large. However, it strongly affects the *I-V* curve near the open-circuit voltage. They can be caused by obstacles to the movement of current through the device such as bulk substrates and due to some contact resistances, which leads to an additional voltage drop within the cell. An approximate method of estimating the series resistance from a solar cell is measuring the slope of the *J-V* curve near the V_{OC}, shown in **Figure 5.5a**.

Shunt resistances, R_{SH}, provide a different current path for the light-generated current. They are due to manufacturing defects more than intrinsic mechanism problems. At low light intensity, less light current is generated, and the effect of shunt resistances is greater. Also, when a lower voltage is produced, the impact of the parallel resistance is more effective. A rough estimation of R_{SH} value can be determined from the slope of the *J-V* curve near the J_{SC} point as shown in **Figure 5.5b.**

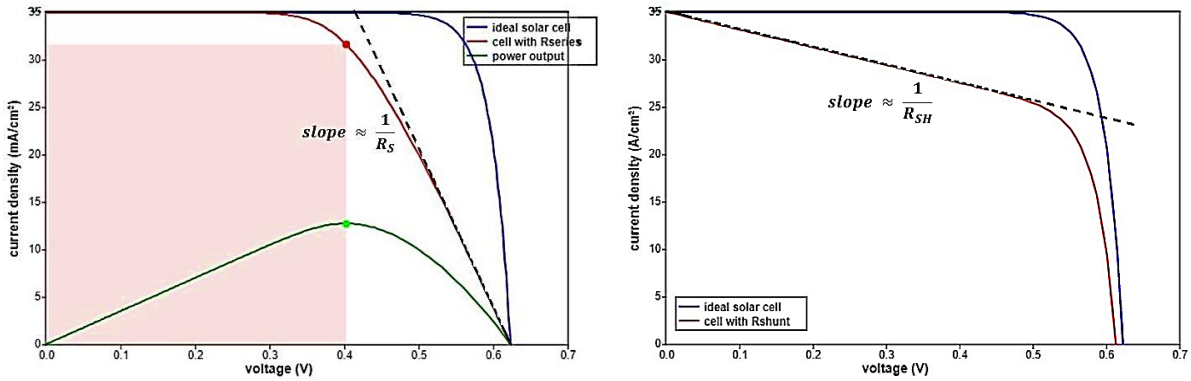

Figure 5.5: Effect on the *J-V* curve of series resistance (a) and shunt resistance (b).[71]

5.1.1 Effect of light intensity

The output parameters of the solar cells, such as V_{OC}, J_{SC}, FF and η, are affected by external environment factors such as the intensity of the light and the temperature.[72] The intensity of the radiation depends on the sky conditions, the position of the sun, and the orientation of the Earth. In order to be able to compare solar devices, some standard conditions have been defined, which include the spectrum distribution, the intensity and the temperature. For instance, spectral distribution depends from the filtration of the ozone layer and the intensities depends on the path through the atmosphere.

The standard spectra are prefixed with "AM" which stand for "Air Mass", followed by a number indicating the direct optical path length through the Earth's atmosphere in relation to the shortest length. The formula can be approximated by $AM = 1/\cos\theta$, where θ is the angle of elevation of the sun, the zenith angle.[73] *J-V* characteristics are performed in standardized conditions simulating air mass 1.5 global ("AM 1.5 G"): 1 sun illumination , zenith angle equal to 48° and the temperature of 25 °C.

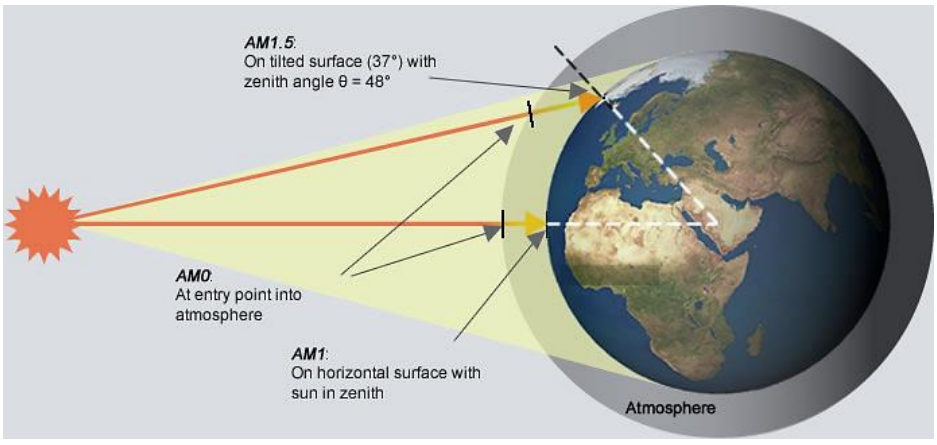

Figure 5.6: Different intensities of solar irradiation depending on the position of the sun and orientation of the Earth.[73]

Environment impact on the performance of solar cells have mostly been studied for silicon solar cells since DSCs are a combination of several concurrent mechanisms that make this system more complex. Tian *et al.*[74] stated that DSCs have better resistance and are less affected to changes in temperature and changes in incident light angle, thus their use could be more convenient for building integration and indoor application. In silicon cells, photocurrent

density is directly proportional to light intensity since they are both directly proportional to the flux of photons generated, while open circuit photovoltage increases logarithmically with light intensity.[75] In DSCs, the diffusion of the redox couple species within the electrolyte solution may have to be considered, but a similar pattern for the photocurrent and the photovoltage is expected.

Other effects resulting from working in low light intensities are due to the higher influence of the shunt resistance or the presence of trapped states, which become more important. Thus, under cloudy conditions, a solar cell highly effected by shunt resistance loses relatively more power than a cell which does not suffer from this problem and the presence of trapped state, state of recombination with lower energy than the conduction band, become more evident, leads to much more evident losses in efficiency.

5.1.2 Dark Current

The *I-V* characteristic measured in the dark is so-called dark current. Below a certain threshold, in reverse bias, the electrons go from the anode to the cathode. Since no oxidized dye molecules are present in the dark, no electrons are in the LUMO of the donor component and there will be hardly any current. In forward bias, above a certain threshold, an injection barrier to overcome, the electrons start flowing from the cathode to the anode and generate a very large current. The moment when the dark curve starts to gain slope corresponds to when, by applying forward bias, the current generated in the opposite direction of the reverse photocurrent balance this last one.

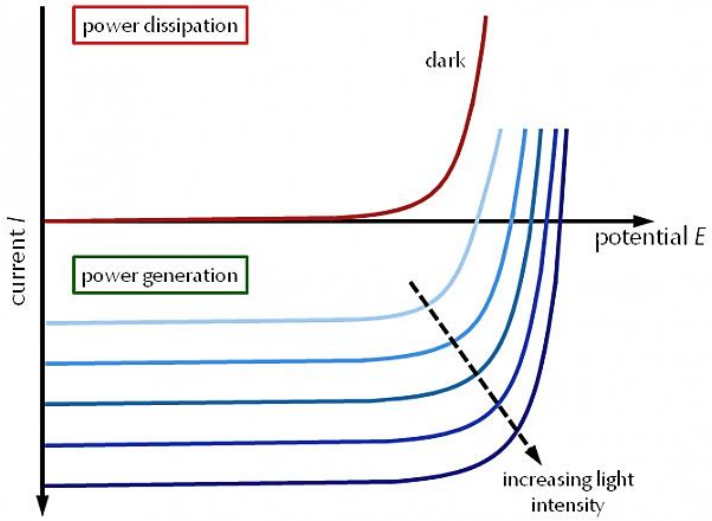

Figure 5.7: *I-V* curves in the dark and increasing light intensity.[76]

Dark current gives information about recombination of the electrons in the anode with the oxidized redox species. It also gives information about the bulkiness and the amount of dye covering the nanoparticles of TiO_2, since the dye works as a barrier to separate TiO_2 and the redox species.

5.2 Incident photon-to-current efficiency (IPCE)

The incident photon-to-current efficiency (IPCE), also referred to as external quantum efficiency (EQE), provides insights on how efficiently the incident light at a specific wavelength is converted into current. In other words, the IPCE gives information about the monochromatic quantum efficiencies of the solar cell and it is described by the ratio between the short circuit photocurrent density and the monochromatic photon flux, as described by Equation 5.3.[5]

$$\text{IPCE} = \frac{J_{sc}(\lambda)}{e \cdot \phi(\lambda)} = 1240 \frac{J_{sc}\,[A\,cm^{-2}]}{\lambda\,[nm] \cdot P_{in}(\lambda)\,[W\,cm^{-2}]} \qquad 5.3$$

where e is the elementary charge of an electron and $\phi(\lambda)$ is the photon flux that hit the cell.

The IPCE is useful to estimate the process that could limit the performance of the DSCs. It can be better described as the collection probability generated from a single wavelength, integrated over the device thickness and normalized to the incident number of photons. The differences between the integrated current based on the IPCE spectrum and the current obtained in the *J-V* characteristic is mostly due to the mask used on top of the cells during IPCE measurements, which limits the working area of the cell. Furthermore, IPCE is recorded under lower light intensities and the electrolyte diffusion limitation is not counted in *J-V* measurements.

A typical quantum efficiency curve is shown in **Figure 5.8**. An ideal quantum efficiency has a square shape, since the quantum efficiency for the photons below the band gap, at longer wavelengths, must be zero. In reality, overall reductions are present. At higher energy (lower wavelength) the response is mostly reduced due to front surface recombination since the light is absorbed very close to the semiconductor. Green-coloured light of the visible spectrum is absorbed mostly in the bulk of a solar cell. The lower energy response is reduced due to rear surface recombination at the dye level and due to generally reduced absorption at long wavelengths.[77]

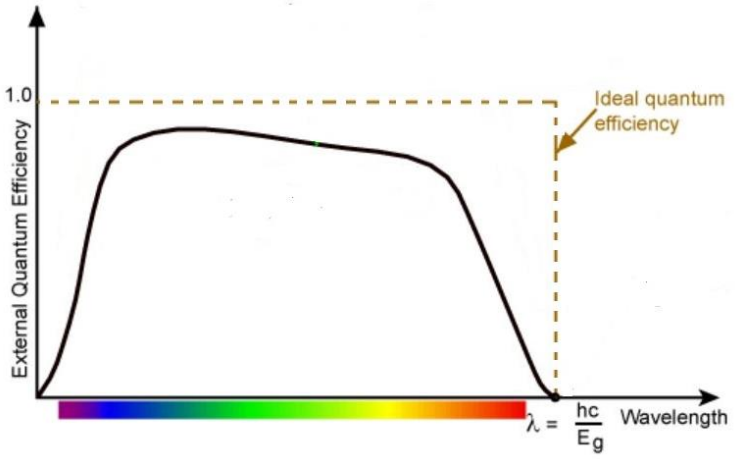

Figure 5.8: Typical external quantum efficiency spectrum (AM 1.5 G).[77]

The incident light of a given wavelength is supplied by a Xenon lamp and sent through a monochromator. The monochromatic light is absorbed by the solar cell and produces a current which is monitored. To calibrate the light intensity supplied by the instrument and to estimate the IPCE under one sun irradiation, (AM 1.5 G), a standard silicon solar cell is used.

IPCE, as described by Equation 5.4, combines the efficiencies occurring at the photoanode/electrolyte interface, the electron injection from the excited dye to the TiO_2 conduction band, the regeneration of the oxidizes dye by reduced species in the electrolyte and electron collection by the back contact before recombination with electron acceptors in the electrolyte.

$$\text{IPCE}(\lambda) = \text{LHE}(\lambda) \cdot \phi_{inj} \cdot \phi_{reg} \cdot \eta_{cc} \qquad 5.4$$

where LHE is the light harvesting efficiency, directly correlated to the absorption spectrum and the amount of dye attached to the semiconductor surface, ϕ_{inj} is the injection efficiency of the electron from the dye to the TiO_2 conduction band (CB), ϕ_{reg} is the regeneration efficiency of the oxidized dye and η_{cc} represents the charge collection efficiency.[5]

5.3 Electron Lifetime

The electron lifetime (τ_e) is a central quantity to determine the dynamics of charge recombination processes of the device.[78]

As mentioned, the operation of a solar cell is based on the competition of two main processes: desired processes such as photoexcitation, electron injection in TiO_2 conduction band and dye regeneration which create a flow of electrons and generate current, and undesired processes caused by carriers recombination (red arrows shown in **Figure 2.9**). One approach mentioned by Bisquert *et al.*[78] is to see the lifetime as chemical capacitance and recombination resistance. The electron lifetime is an indication of the time the electrons spend in the TiO_2 prior to recombine with the oxidized dye or the oxidized electrolyte couple. Lower lifetime values suggest more recombination processes; thus, a higher lifetime value is desired.

The system set-up to evaluate this cell parameter consists of a white light-emitting diode (LED) probe whose intensity can be modulated by changing the applied bias. Indeed, the electron lifetime is related to the electron density on the TiO_2 thus it is related to the bias of the illumination. The electron density has an exponential dependence on the voltage, leading to an exponential relation between lifetime and applied voltage, where an increase in voltage means more recombination and shorter lifetime.[5] The open circuit voltage response is measured and the corresponding rise and fall times are calculated with the aid of the Levenberg-Marquardt (LM) curve fitting algorithm (see **Figure 5.9**). By averaging the rise and fall times, lifetimes of the solar cells for different voltage values are then obtained.

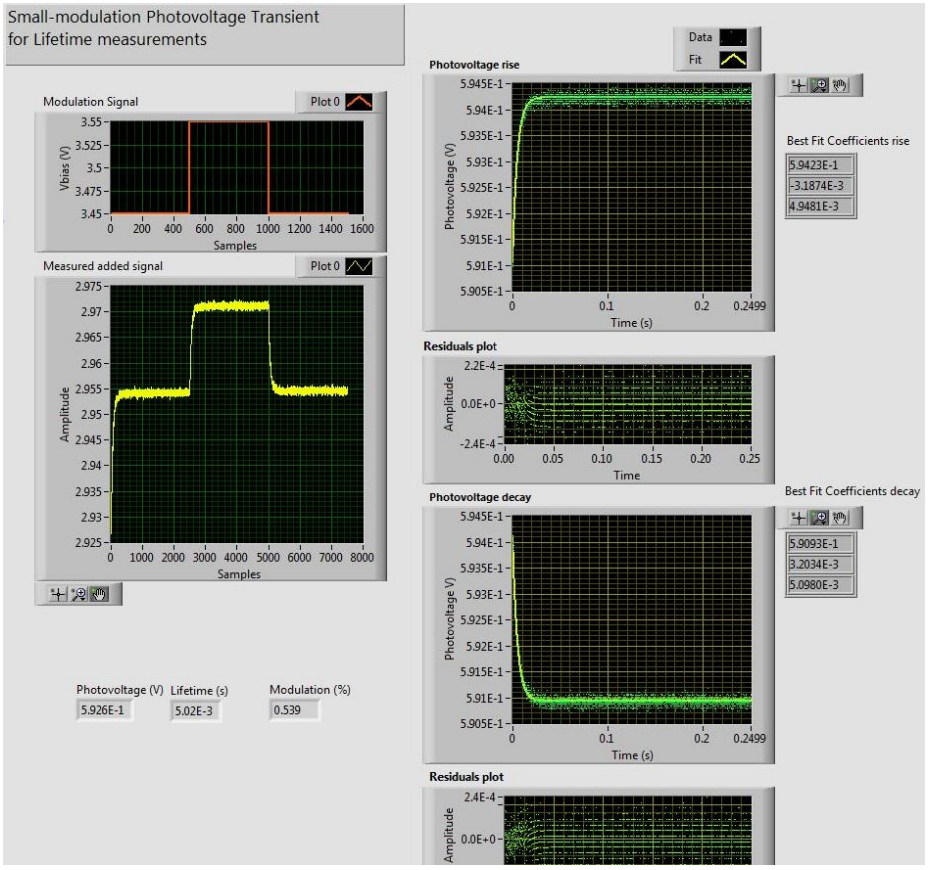

Figure 5.9: Modulation photovoltage transient for Lifetime measurements. To the left top, the applied square-wave photovoltage signal and left bottom the measured signal. To the right, the photovoltage response in the corresponding rise and fall times and their respective residuals plots.

The evaluation of electron lifetime gives an understanding and control on the degree of recombination and gives a hint for improving the performance of the solar cell.

5.4 Fabrication of DSCs

5.4.1 Working electrodes

The FTO glasses used as current collectors were first cleaned in a detergent solution using an ultrasonic bath for 30 min. Then they were rinsed with water and immersed in a second bath of acetone for another 30 min. To follow, they were rinsed with clean acetone and sonicated for 30 minutes in ethanol. The cleaned glasses were finally rinsed with ethanol and dried with compressed air. TiO_2 films are prepared by screen-printing technique, with an active area of 0,36 cm^2 (6 mm x 6 mm), using two different types of TiO_2 pastes. The paste resulting in a transparent layer of TiO_2 was purchased from GreatCell Solar (18NR-T), while the light-scattering, anti-reflecting layer was realized by using an opaque paste (GreatCell Solar, WER2-O). Between the different steps of the screen-printing process, the substrates are first left few minutes in an ethanol atmosphere and then dried at 125 °C for around 5-10 minutes.

After screen printing, a first sintering up to 450 °C was made. After that, the samples were immersed in a $TiCl_4$ solution (40 mM in water) at 70°C for 30 min. Subsequently, the substrates were rinsed first with water, then with ethanol and dried with compressed air. Then,

a final sintering step at 500 °C for 30 min was made. In the last sintering process the temperature increases gradually: 25 minutes to reach 325 °C where it stays for 15 min and 15 min to reach the desired temperature, 450 or 500°C for half an hour.

After cooling, the electrodes could be finally immersed in the first bath containing the anchoring ligand and left in solution overnight before the immersion in the ancillary ligand bath, where the self-assembly process previously described occurs and the desired heteroleptic copper (I) complex is attained.

5.4.2 Counter electrodes

To prepare the platinum counter electrodes, FTO glasses, with a predrilled one-hole of around 1 mm diameter, were employed. The same procedure to clean the working electrodes was followed, and in order to remove residuals of organic contaminants they had been heated in air for 30 min at 400°C. After cooling down to room temperature, a few µL of a 4,8 mM H_2PtCl_6 solution in ethanol was deposited on each counter electrode and heated again in air at 400 °C for 30 min. By heating, the reactions that occur on the surface of the counter electrode are the following:

$$H_2PtCl_6 \xrightarrow{\Delta} 2HCl_{(g)} + PtCl_4$$
$$2PtCl_4 \xrightarrow{\Delta} Pt_2Cl_6 + Cl_{2\,(g)}$$
$$Pt_2Cl_6 \xrightarrow{\Delta} 2\,PtCl_2 + Cl_{2\,(g)}$$
$$PtCl_2 \xrightarrow{\Delta} Pt + Cl_{2\,(g)}$$

5.4.3 Electrolyte

A suitable electrolyte solvent should possess a wide electrochemical window, high dielectric constant, low viscosity and low vapour pressure. Commonly used suitable solvents for liquid electrolyte-based DSCs are acetonitrile (ACN), valeronitrile, methoxyproprionitrile (MPN) and ionic liquids (ILs). Their properties are shown in **Table 5.1**.

Table 5.1: Physical properties at room temperature and 1 atm of commonly used solvents for DSCs

Properties (RT, 1atm)	**ACN**[79]	**Valeronitrile**[80]	**MPN**[81]	**ILs**
Vapor pressure	9,9 kPa	7 hPa	2,3 hPa	$\sim 10^{-10}$ Pa
Boiling point	81,6 °C	139 to 141 °C	164-165 °C	> 400 °C[82]
Viscosity	0,35 cP	0,779 cP	1,6 cP	21,8 cP[83]
Dielectric constant	37,5	17,7	40	9-35[84] depending on the anions

Constable *et al.*[9] in their work have mostly used LiI (0,1 M), I_2 (0,05 M), 1-methylbenzimidazole (0,5 M), 1-butyl-3-methylimidazolinium iodide (0,6 M) in 3-methoxypropionitrile in combination with Cu(I) complexes of the type present in this thesis. Their choice was dictated basically by the low volatility of the solvent. On the contrary, Biagini and co-workers[48] have demonstrated higher performances by using an electrolyte composition of LiI (0,04 M), I_2 (0,28 M), 1-butyl-3-methylimidazolinium iodide (0,65 M) and tert-butylpyridine (0,28 M) in 85/15 (v/v) acetonitrile/valeronitrile. In this work, both compositions were tested, but for the entire complex series characterization, the latter composition was

employed. For greater clarification, **Table 5.2** shows the electrolyte composition used for the characterization of the solar cells based on the whole series of the Cu(I) complexes explored in this work.

Table 5.2: Compositions of the electrolyte employed for the entire series characterization

Acetonitrile/valeronitrile (v/v)	85/15
1-butyl-3-methylimidazolinium iodide	0,65 M
LiI	0,025 M
I_2	0,04 M
Tert-butylpyridine	0,28 M

5.4.4 DSCs Assembly

The working electrode and Pt-counter electrode were sealed in a sandwich-type configuration (**Figure 5.10**) with a press (HeptaChroma SolarTech) by using a 25 µm thick thermoplastic surlyn frame (Solaronix Meltonix 1170-25). The frame had been created with a vinyl cutter (SummaCut) and made of the size of 7 mm x 8 mm (2 mm larger than the TiO_2 area and 1 mm wider). From the hole of the counter electrode, a drop of the electrolyte was introduced into the cell via "vacuum backfilling" technique, i.e. placing the cell in a vacuum chamber to remove first inside air, then reopening to ambient pressure, the electrolyte is driven into the cell. The hole was then sealed with another layer of surlyn film and an aluminium foil sheet. Finally, to have a good electrical contact for the connections of the measurement set-up, the edges of the FTO glasses of the cell were covered with silver paint.

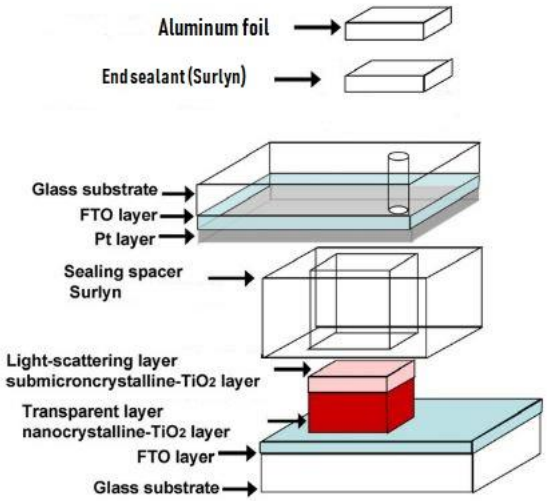

Figure 5.10: Assembly of a dye-sensitized solar cells.[85]

The cell thickness was measured with the profilometer, Veeco Dektak 150.

Current density-voltage (*J-V*) characteristics were measured using a Newport solar simulator (model 91160) and a Keithley 2400 source. The light was calibrated using a certified reference silicon solar cell (Fraunhofer ISE) to have the standard spectral distribution (AM 1.5 Global, $1000\ \mathrm{W \cdot m^{-2}}$).

IPCE spectra were recorded using a Xenon light source (Spectral Products ASB-XE-175).

For lifetime measurements a white LED lamp (Luxeon Star 1W) was used as a light source. It was calibrated with the same silicon solar cell reference to stabilize the distance where

the cells had to be measured in order to have the same light intensity of 1 sun at 3,5 V bias of the LED lamp.

All data shown are considered consistent and reproducible since a minimum number of five/six devices for each experiment were tested.

5.5 Optimization process

5.5.1 Results

Initial studies were focused on the optimization of the system based on complex $[Cu(L1)(L4)]^+$ shown in **Figure 5.11**, which was chosen for its intense red colour shown in the absorption spectra (**Figure 4.6**). Indeed, even if complex $[Cu(L1)_2]^+$ is already reported in the literature and would have been a good starting point for several comparisons, the presence of the carboxylic acid, suspected to have some interaction with the copper centre, made this complex more peculiar compared to the others.

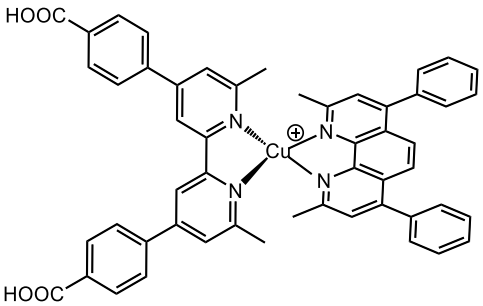

Figure 5.11: Copper complex $[Cu(L1)(L4)]^+$], used as photosensitizers in this initial studies of the optimization process.

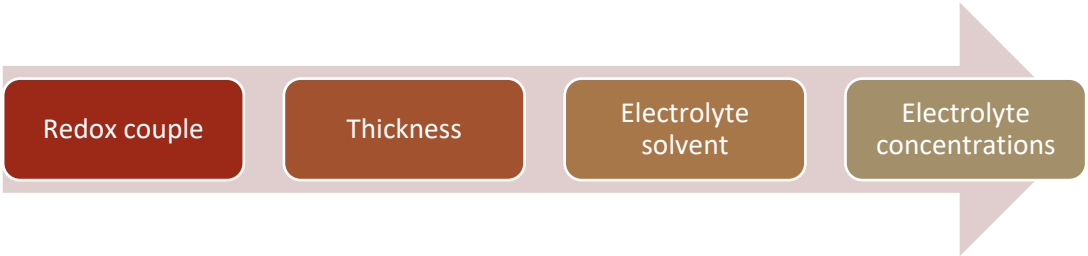

Initially, two different redox couples, cobalt complexes $[Co(bpy)]^{3+/2+}$ and iodide/triiodide (I_3^-/I^-), were first tried. Clear evidence showed better efficiency of the latter, where, in particular, the fill factor and the current density values benefited from this redox couple in the system in exam. Furthermore, the majority of the studies for copper (I) complexes as sensitizers present in the literature refer to iodide/triiodide redox couple.[12,48,86,87]

Once decided the redox couple, the thickness of the substrate was optimized. **Table 5.3** shows different efficiencies related to the different thickness of the semiconductor on the working electrode. The electrolyte employed in this experiment was the same as the one used for the entire series characterization and summarized in **Table 5.2**.

Table 5.3: Efficiencies of the cells with different TiO_2 thickness on the working electrode.

"Double layer of TiO_2" screen printed	**2 transparent 2 scattering**	**3 transparent 2 scattering**	**4 transparent 2 scattering**
Thickness (µm)	12-14	15-17	18-20
Efficiency[a]	1,86%	1,74%	1,45%

[a] measured right after the device assembly

The highest efficiency was reached with a thickness of 12-14 µm; thus, it was the thickness employed for the rest of the characterization.

The electrolyte composition of Biagini and co-workers[48] resulted more efficient of one percentage point compared to the one used by Constable *et al.*[9] in their work. The main electrolyte compositions exploited are listed in **Table 5.4**, while **Figure 5.12** shows the electrolyte aspect after the respective electrolyte injection. Since additives such as Li^+ and 4-tert-butylpyridine (TBP), in most cases, improve the performance of the cell[9], higher concentrations were tried first in ACN (Electrolyte 2) and afterwards in the same 85/15 ACN/valeronitrile mixture (Electrolyte 3). Nevertheless, this increase in concentration led to higher desorption of the dye from the surface of the TiO_2.

Table 5.4: Electrolyte compositions exploited in this work.

Electrolyte 1	
ACN/valeronitrile (v/v)	85/15
1-butyl-3-methylimidazolium iodide	0,65 M
LiI	0,025 M
I_2	0,04 M
TBP	0,28 M

Electrolyte 2	
ACN	
1-butyl-3-methylimidazolium iodide	1 M
LiI	0,1 M
I_2	0,05 M
TBP	0,5 M

Electrolyte 3	
ACN/valeronitrile (v/v)	85/15
1-butyl-3-methylimidazolium iodide	1 M
LiI	0,1 M
I_2	0,05 M
TBP	0,5 M

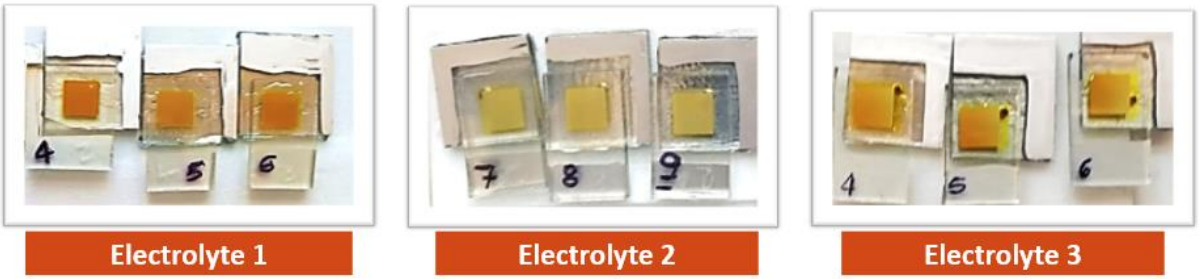

Figure 5.12: Electrodes aspect right after electrolyte injection.

Other electrolyte compositions were tried, increasing the volume amount of valeronitrile used as solvent up to 50/50 v/v, and increasing all the compositions as in Electrolyte 3 with the exception of TBP, which could be responsible for reacting with the copper centre as a ligand. Indeed pyridine based molecules such as TBP are known to form stable molecular complexes with copper.[88] Further efforts include the use of an extra blocking layer directly to the FTO glasses. This technique was proved to give better results with cobalt redox couple[89], but it did not bring any evident change in the system of interest in this work.

Since cells with Electrolyte 2 clearly produced less efficient devices compared to the use of the other two electrolyte composition, **Figure 5.13** shows the stability over time of cells made with Electrolyte 1 and Electrolyte 3.

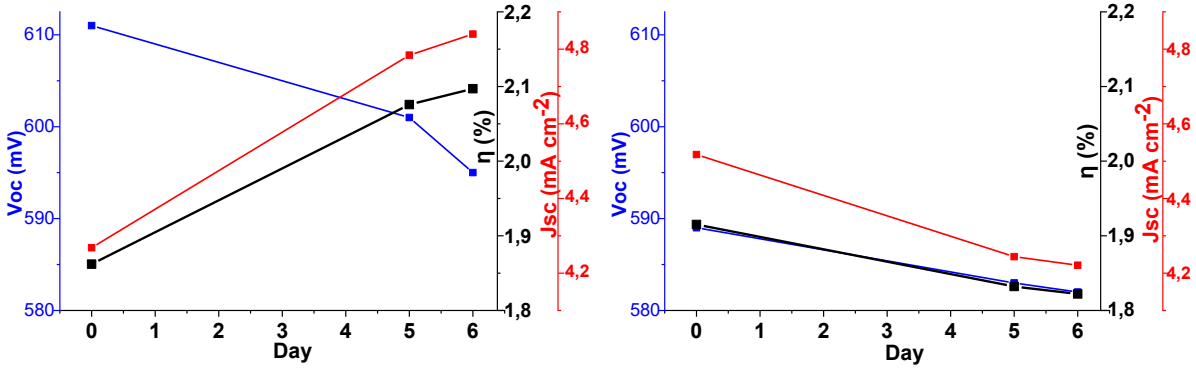

Figure 5.13: Stability test. Main solar cell parameter changing over time for cells with Electrolyte 1 (a). and for cells with Electrolyte 3 (b).

Measurements performed directly after electrolyte injection ("Day 0") showed slightly better performance with Electrolyte 3 compared to Electrolyte 1, respectively 1,92% against 1,86%. Nevertheless, studying changes to the system over time demonstrated that with Electrolyte 1 the device was more stable, and its performance increased of few decimal points in efficiency with concurrently a slight increase of the current density. On the contrary, the devices containing Electrolyte 3 were decreasing a little in efficiency and current density with time. In both cases, the open circuit voltage lost some mV units over time.

To study the different performances of the cell under different light intensity, the current density-voltage characteristics (shown in **Figure 5.14**) are measured in the dark, at 0,1 sun, 0,5 sun and 1 sun and the main parameters are listed in **Table 5.5**. The curves were obtained as an average of several cells with $[Cu(L1)(L4)]^+$ as photosensitizers and Electrolyte 1 as electrolyte composition.

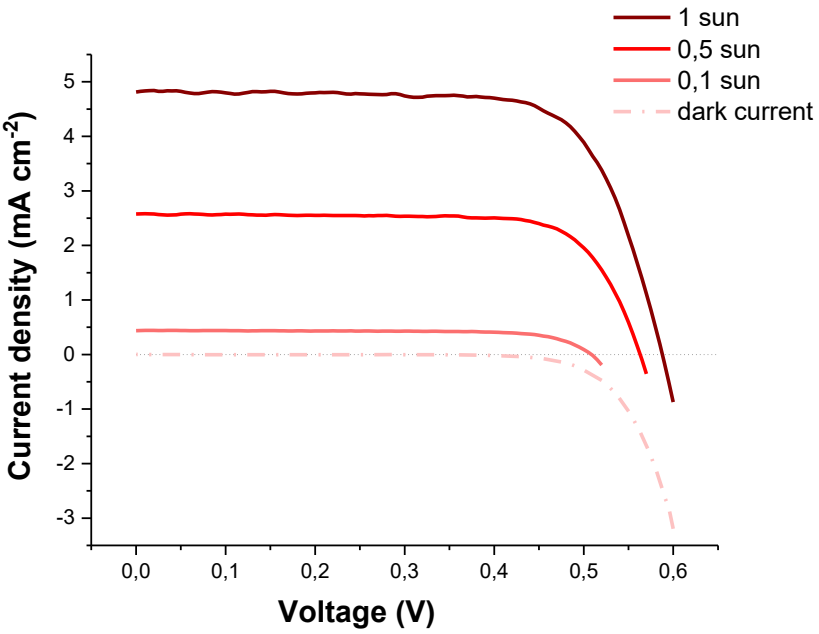

Figure 5.14: *J-V* characteristic measured on "Day 2".

Table 5.5: Photovoltaic parameters of optimized working conditions with $[Cu(L1)(L4)]^+$ as photosensitizer. All data were measured on "Day 2".

Dye	Light intensity	η (%)	V_{OC} (mV)	J_{SC} (mA cm-2)	FF (%)
$[Cu(L1)(L4)]^+$	1 sun	2,05	590	4,789	72,5
	0,5 sun	2,18	565	2,574	74,8
	0,1 sun	1,67	510	0,437	74,9

An improvement in efficiency is noticed when light intensity is half the standard illumination, with a respective increase in fill factor and current density values influenced quite linearly by light intensity.

5.5.2 Discussion

Optimization of the thickness of the semiconductor on the working electrode is of great importance for the device. Once decided the basic system (dye, redox couple and type of catalyst on the counter electrode), this optimization could be done. Thick TiO_2 substrates leads to more recombination process since the path of the electron to reach the FTO/glass is longer. On the other hand, having thinner TiO_2 layers means less amount of dye in the cell and fewer electrons excited by the solar light. The optimized thickness highly depends on the system in exam since it depends on the interactions between dye, TiO_2 and electrolyte redox couple. For the system of interest, the best compromise in thickness was found around 12-14 μm (2 transparent layers + 2 scattering layers) which resembles the one also used in similar work with copper(I) complexes.[9,48]

The optimization of the electrolyte, solvent and concentration, was also of great importance to reach the best-operating conditions. The electrolyte is the part of the device responsible for charge transport. The circuit, indeed, is closed through the movement of the redox mediator in the solvent from the counter electrode to the working electrode. The size of the redox mediator and the viscosity of the solvent are the main factors influencing this transport.

By changing the solvent from 3-methoxypropionitrile to acetonitrile/valeronitrile, an increase of almost 1-point percentage in the efficiency of the device was reached. While by using only ACN, a much higher degree of desorption was obtained as it was clearly visible in **Figure 5.12**. Also using the same solvent mixture with different concentration in the compositions led to some differences in desorption. The tert-butylpyridine component could be accused to be responsible of this occurrence. It is known in the literature that an interaction between TBP and the copper complex could occur, thus it is reasonable to suppose that an increase of TBP concentration in the electrolyte led to an increase of these interactions. The differences in desorption between the use of only ACN solvent or mixture of ACN and valeronitrile could be explained by a different equilibrium in the self-assembly mechanism in these two solvents. Acetonitrile was, indeed, the same solvent used in the second step of the "on surface self-assembly" and probably could interact more with the ancillary ligand compared to the mixture solvent. Once reached this first optimization, further attempts were made but they did not lead to any evident increase in performance, as if a plateau in efficiency values was reached. A value of 2,05% efficiency was measured on "Day 2" and it can be considered a good performance for the system in this study work. Indeed, other heteroleptic copper complexes mostly studied by Constable *et al.*[12] reached similar values with the advantage, in this study, of using as $L_{ancillary}$ a ligand commercially available.

Figure 5.13a shows an enhancement of efficiency over time. Such behaviour was already identified in previous works and it was explained as a time-dependent reorganization of the dye molecules on the nanoparticle of TiO_2. It had already been observed also for ruthenium (II)-based dyes other than many copper (I) complexes.[9] With "Electrolyte 3, this time enhancement did not occur indeed, **Figure 5.13b** shows a decreasing in efficiency over time. The higher interaction with the electrolyte probably is stronger than the reorganization process itself. For this reason, even if on "Day 0" a better efficiency was reached with Electrolyte 3, considering the importance of stability over time in potential indoor and outdoor applications, Electrolyte 1 is substantially a better choice.

From **Figure 5.14** and **Table 5.5** can be noted as about half of the current is reached when the illumination is half sun compared to the standard conditions and nearly one-tenth when 0,1 sun is applied. Thus, cells with $[Cu(L1)(L4)]^+$ as sensitizers, show a quite direct proportion between light intensity, photon generation, and photocurrent density; while photovoltage decreases logarithmically when lowering light intensity as expected.

Studies of parameters under different light intensity can suggest mass transport limitation due to electrolyte redox couple mobility or in general due to resistance-problems within the device. If the mobility of the redox couple is somehow also prevented, at 1 sun this mechanism is more pronounced: more dye will be in the excited-state and faster redox couple transport is necessary to reduce it. Because of the higher amount of oxidized dye that need to be regenerated at 1 sun, the efficiency is slightly lower compared to the value at 0,5 sun, but mass transport is not usually a problem when iodide/triiodide couple and a solvent not particular viscous, are employed. The lower efficiency showed at 0,1 sun can suggest the presence of electron trapped states in the semiconductor, states with lower energy than the CB which lead to recombination. Their presence and their effect become indeed more evident when very limited number of electrons are activated within the mechanism.

The cell system possesses an enviable fill factor of ~73%. Clearly from the curves at different intensities, the system in this work does not suffer from shunt resistances, meaning that does not contain short circuit path or manufacturing defects. Studies at lower intensities are able to emphasise this type of defects, but this system does not show any greater effect due to R_{SH} resistance at lower sun illumination. Series resistances are due to obstacles to the movement of current and contact resistances at different interface levels.

To define the characteristic resistance, R_{CH}, of the device with reasonable approximation, V_{OC} and J_{SC} at 1 sun can be used for the calculation, giving a result of 123 Ω cm^2. From the slope of the *J-V* curve at the V_{OC}, as shown in **Figure 5.15a**, the series resistance could also be evaluated. The value of the slope was 61,15 mA cm^2/V. While, from the inverse of the slope of the line at the J_{SC}, shown in **Figure 5.15b**, the value of the shunt resistance was measured.

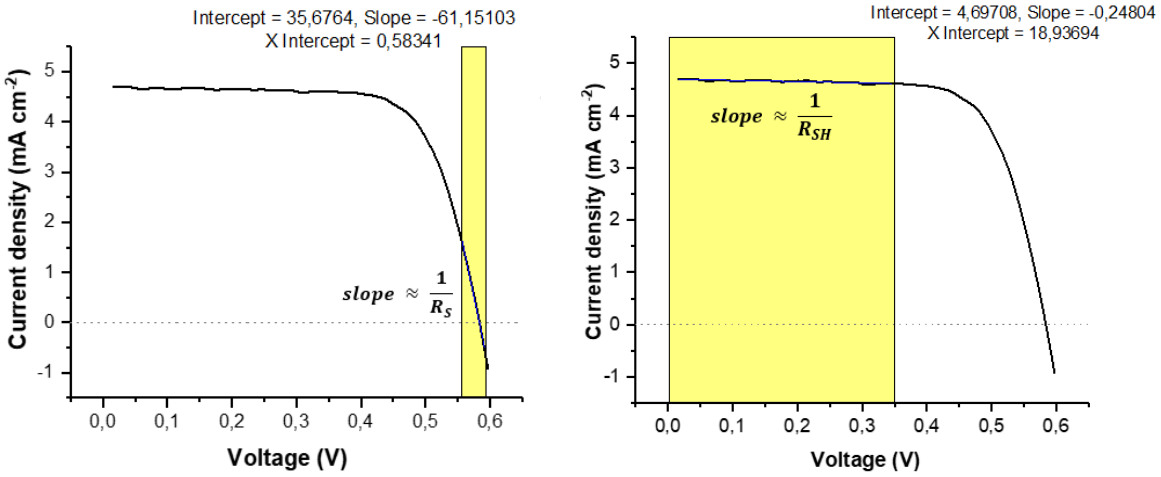

(a) (b)

Figure 5.15: Series resistance estimated from the slope at V_{OC} extracted by the fitting of the line within the yellow area (a). Shunt resistance estimated from the inverse of the slope at the J_{SC} extracted by the fitting of the line within the yellow area (b).

The series resistance for complex $[Cu(L1)(L4)]^+$ amounted to 16,35 Ω · cm^2, while the shunt resistance was 4,03 · 10^3 Ω · cm^2. Such a high value of shunt resistance is an indicator of the good design of the cell. The series resistances dominate the fill factor value of the DSC device but their values are in good agreement with the values shown in the literature by other devices in the DSC field.[90] Good fill factors, as the ones obtained, generally mean low recombination problems between the excited electron with either the oxidized dye or the oxidized electrolyte couple.

The dark current reflects the mechanism of charge-recombination. In the dark no dye is oxidized and, above a certain voltage all the current comes from the electrons flowing from the cathode to the anode and, recombination of the electrons in the anode with the redox couple occur. If high resistance to recombination exists, the dark current occurs at a higher voltage threshold value. High resistance to recombination is given by great degree of coverage and bulky dyes, which efficiently make this process harder. The system of interest has a dark current raising up to a relatively low value of voltage hence it seems to exhibit lower resistance to recombination, probably due to the low amount of dye coverage of TiO_2.

5.6 DSCs characterization with different copper (I) complexes

5.6.1 Results

The current density-voltage characteristics of the DSCs sensitized with copper (I) complexes self-assembled on the surface of TiO_2 are shown in **Figure 5.16**, under full illumination and in the dark. Since enhancement of the main parameters was previously observed during the optimization process with $[Cu(L1)(L4)]^+$, the *J-V* curves refer to measurements on "Day 2".

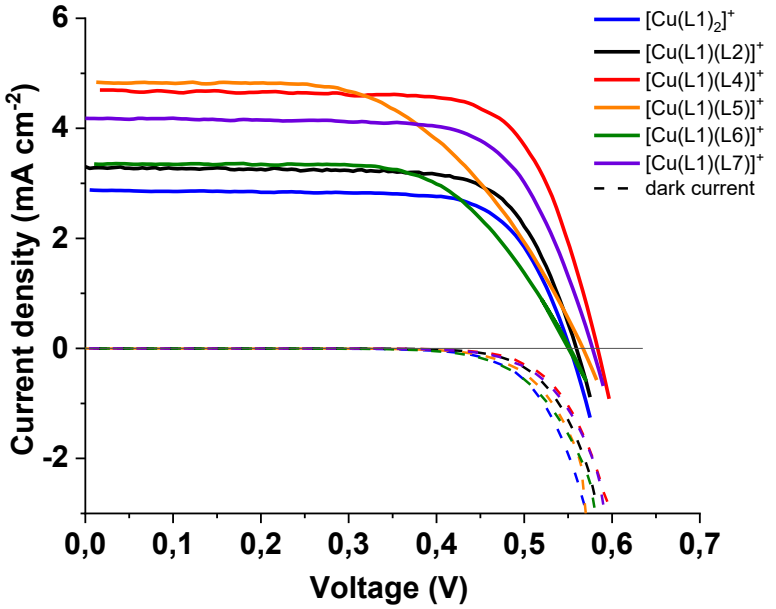

Figure 5.16: Current density *vs* applied potential, measured under "AM 1.5 G" illumination. The results refer to an average of the several cells all measured on "Day 2" after their assembling.

At 1 sun illumination, the best performance was given by complex $[Cu(L1)(L4)]^+$ which, on "Day 2", reached up to 2,05% of efficiency, followed by $[Cu(L1)(L7)]^+$, with 1,73%, $[Cu(L1)(L5)]^+$ with 1,71%, $[Cu(L1)(L2)]^+$, $[Cu(L1)(L6)]^+$ and $[Cu(L1)_2]^+$ with 1,43%, 1,23% and 1,17% respectively. From the *J-V* characteristics at 1 sun, it is evident that $[Cu(L1)(L5)]^+$ and $[Cu(L1)(L6)]^+$ were the complexes suffering of the worse fill factor and higher recombination compared to the other complexes.

To compare the series of the copper (I) complexes with the state-of-the-art and benchmark dye, ruthenium (II) complex N719, similar measurements were made. The working electrodes were immersed in a solution of 0,5 mM of N719 in ethanol solution overnight, as described in the literature,[91] and the working and counter electrodes were assembled in cells with the same electrolyte composition. The experimental current density-voltage characteristic is shown in **Figure 5.17**, measured as well on "Day 2".

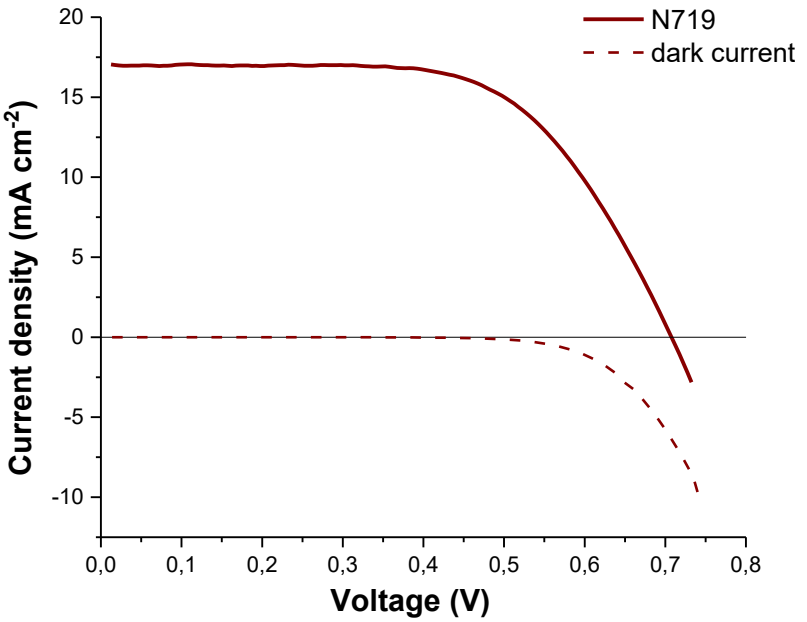

Figure 5.17: Current density vs applied potential, "AM 1.5 G", on "Day 2".

In **Table 5.6**, the most important parameters at 1 sun on "Day 2" are listed for all the cells based on copper (I) complexes in comparison with N719.

Table 5.6: Photovoltaic parameters with all the heteroleptic complexes at 1 sun. Data measured at "Day 2".

Dye	η (%)	V_{OC} (mV)	J_{SC} (mA cm-2)	FF (%)
$[Cu(L1)_2]^+$	1,17	550	2,870	74,2
$[Cu(L1)(L2)]^+$	1,43	565	3,409	73,9
$[Cu(L1)(L4)]^+$	2,05	590	4,789	72,5
$[Cu(L1)(L5)]^+$	1,71	563	4,782	63,6
$[Cu(L1)(L6)]^+$	1,23	553	3,351	66,6
$[Cu(L1)(L7)]^+$	1,73	580	4,161	71,6
N719	7,57	700	17,81	60,9

Solar cells sensitized with N719 had performances which were more than triple compared to the copper (I) complexes. The main outstanding difference by comparing the two type of dyes was the J_{SC} parameter, much higher for N719. The V_{OC} of the latter is a proof that a higher *quasi*-Fermi level is reached when N719 is employed, which means that the dye absorbed more light and injected more electrons in the CB. But, overall, better fill factors were achieved with the copper (I) complexes.

From a visual observation of the substrates in **Figure 5.18**, it is evident how the colours of the copper (I) complexes were much less intense compared to the Ruthenium N719. Light harvesting is the first mechanism that takes place to activate the DSC devices and limited presence of dye on the surface of TiO_2 diminishes the electron flow through the cell. It also resulted evident, from direct optical observation of the sample, the difference in colour that occurs right after the electrolyte injection.

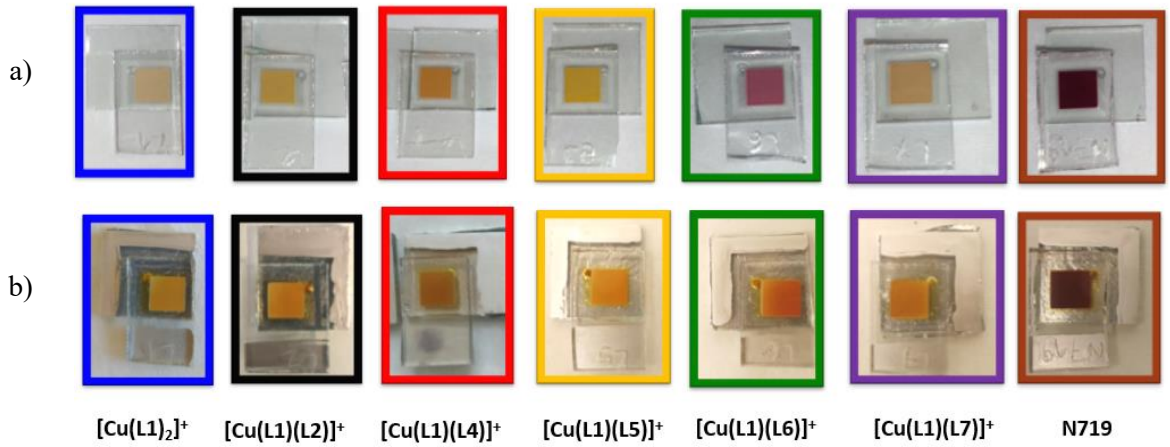

Figure 5.18: Substrates with different sensitizers. Before (a) and after electrolyte injection (b).

Figure 5.19 shows the behaviour of the most important parameters at different light intensities.

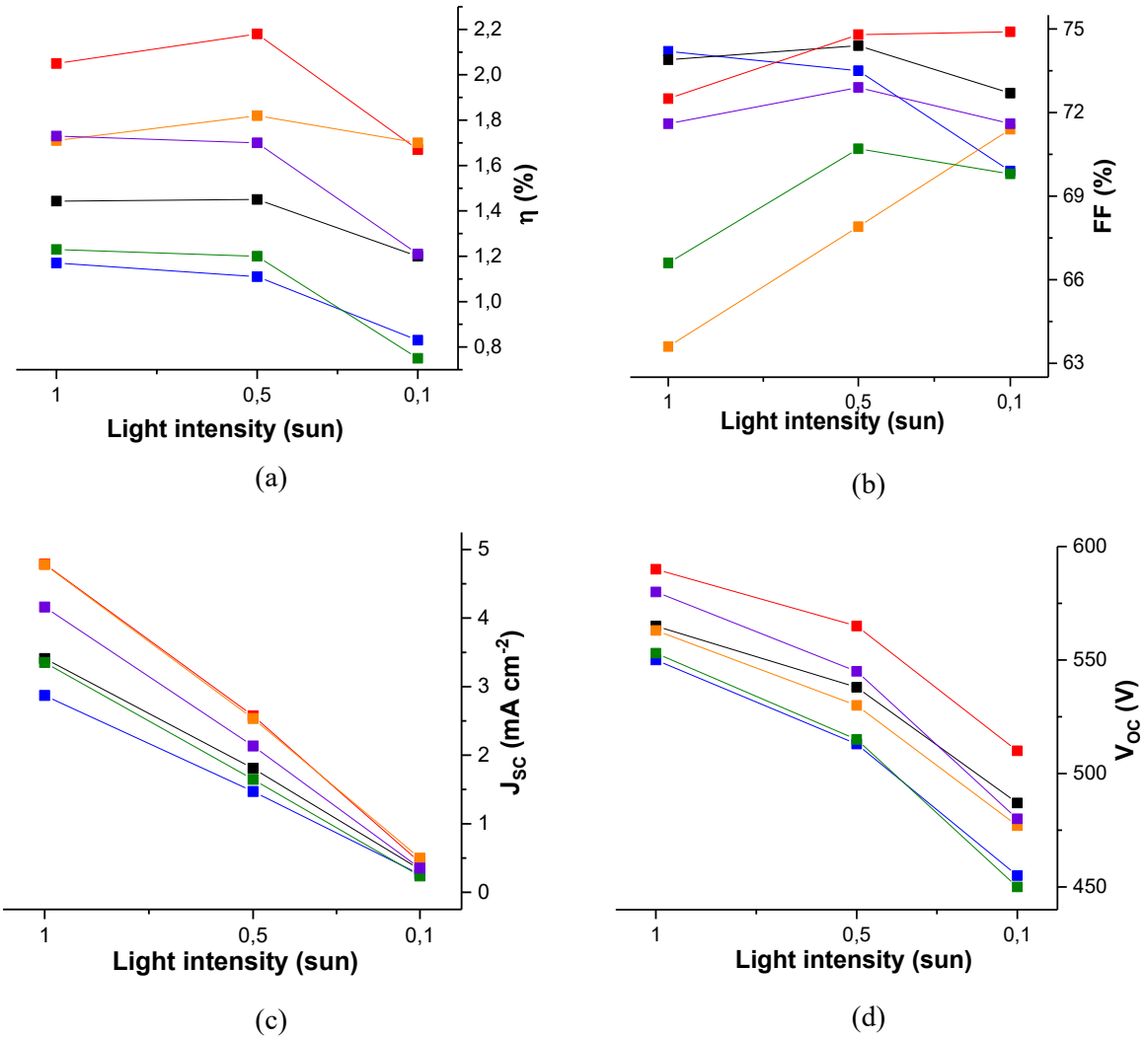

Figure 5.19: Photovoltaic parameters of the DSCs sensitized with copper (I) complexes at different light intensities, measured on "Day 2". Efficiency (a), fill factor (b), current density (c), and open circuit voltage (d) *vs* sun illumination. The colours refer to the complexes as in **Figure 5.16**.

General patterns can be observed among the different copper (I) complexes. Typically, a constant or a slight improvement in efficiency is noticed when light intensity is at 0,5 sun. Fill factor values tend to become better at lower illumination and current density follows a quite linear trend with light intensity while the open circuit voltage follows a logarithmic trend.

The incident photon-to-current efficiency, IPCE spectra, of the devices sensitized with the heteroleptic copper (I) complexes, the homoleptic $[Cu(L1)_2]^+$, and the benchmark N719, are shown in **Figure 5.20**. To be consistence with the *J-V* curves shown also the IPCE spectra shown were measured on "Day 2".

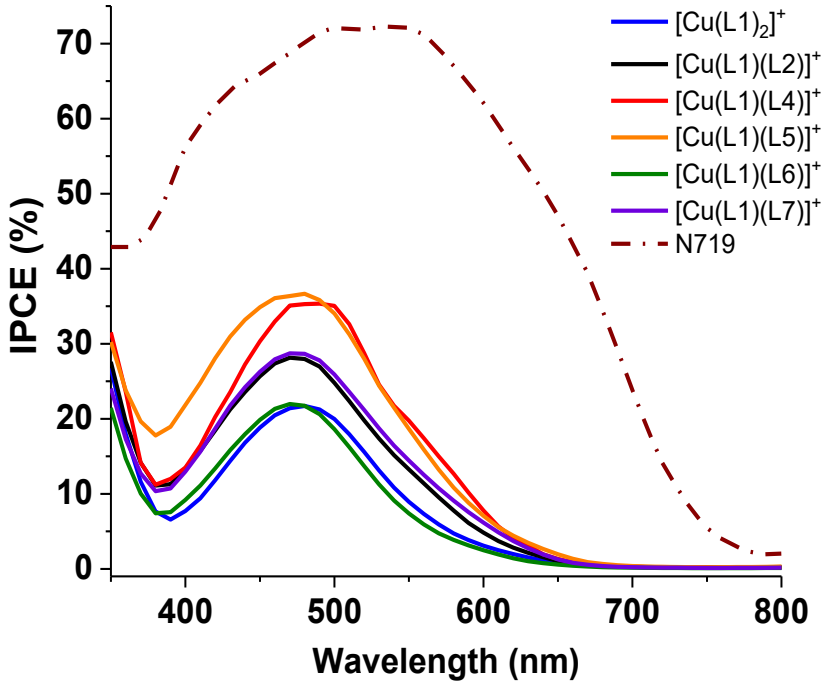

Figure 5.20: IPCE spectra of the DSCs sensitized by the complexes of interest and N719. The results refer to an average of the several cells all measured on "Day 2".

All the different copper (I) complexes possess a wavelength at maximum IPCE value, $\lambda_{IPCEmax}$ (or at maximum external quantum efficiency, EQE_{max}), falling in the same range 470-490 nm, and generally much lower intensity and smaller range compared to the benchmark N719. The data are in accordance with other works published by Constable *et al.*[9] and Biagini *et al.*[48], with similar copper (I) complexes used as sensitizers.

Within the series, from the highest to the lowest $IPCE_{max}$, $[Cu(L1)(L5)]^+$ soon followed by $[Cu(L1)(L4)]^+$, $[Cu(L1)(L7)]^+$, $[Cu(L1)(L2)]^+$ and lastly $[Cu(L1)(L6)]^+$ and $[Cu(L1)_2]^+$. As expected, this trend resembles in good approximation, the value of current density obtained for the respective devices.

Table 5.7 shows the current density recorded with the *J-V* characteristic and the integrated current based on the IPCE spectrum. For the *J-V* characteristic, this time, a black mask with an aperture slightly smaller than the active area of the cell, was applied on top of the cell (0,5 x 0,5 cm^2). When measuring with the mask, the efficiency is lower since the contribution from light hitting the cell outside its active area is reduced. Therefore, these values are considered more reliable in order to not overestimate the performance of the device.

Table 5.7: Photocurrent data resulting from the *J-V* characteristics and from the IPCE integrated curves.

Dyes	Jsc (mA cm^{-2}) I-V curve, when mask is applied	Jsc (mA cm^{-2}) IPCE curve
$[Cu(L1)_2]^+$	2,261	1,838
$[Cu(L1)(L2)]^+$	3,004	2,423
$[Cu(L1)(L4)]^+$	4,096	3,190
$[Cu(L1)(L5)]^+$	3,762	3,385
$[Cu(L1)(L6)]^+$	2,408	1,679
$[Cu(L1)(L7)]^+$	3,192	2,547
N719	14,00	12,40

The little difference displayed is due to a different shading mask used on top of the cell in these two measurements and different light source used which led to slightly different intensities. Nevertheless, counting the loss in the IPCE values, the results are mostly in agreement with the ones measured from the *J-V* curves.

For lifetime assessment, the reported measurements were recorded on "Day 4" of the life of the cell. Enhancement of electron lifetime corresponds to increased performance. By decreasing the voltage, the recombination rate decreases, and the lifetime is consequently expected to increase. In **Figure 5.21** the lifetimes for the only copper(I) complexes cells are plotted semi-logarithmic against the photovoltage.

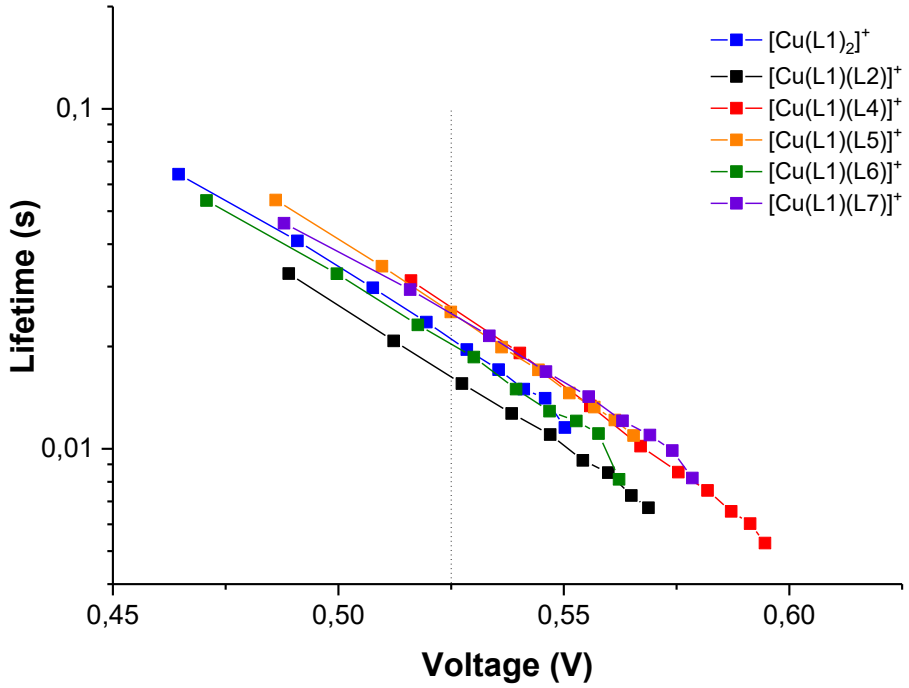

Figure 5.21: Electron lifetime of the copper(I)-based devices, measured on "Day 4". The dotted line represents a fixed value of potential in order to compare the lifetimes of the complexes within the series.

As expected, in a semi-logarithmic plot, all the lifetimes showed a quite linear decrease with an increase of the photovoltage, since electron density has an exponential dependence on the voltage. To compare the electron lifetime between different complexes, a fixed value of potential was taken (the dotted line in **Figure 5.21**). By doing so, a fixed voltage is considered. Supposing similar coverage and amount of charge for all the complexes on the semiconductor,

a fair comparison can be made. In **Table 5.8**, the lifetimes of the copper (I) complexes at 0,525 V are listed.

Table 5.8: Electron lifetime of the copper (I) complexes at the same photovoltage equal to 0,525 V.

Complex	Electron lifetime (s)
$[Cu(L1)_2]^+$	$2{,}11 \cdot 10^{-2}$
$[Cu(L1)(L2)]^+$	$1{,}61 \cdot 10^{-2}$
$[Cu(L1)(L4)]^+$	$2{,}63 \cdot 10^{-2}$
$[Cu(L1)(L5)]^+$	$2{,}54 \cdot 10^{-2}$
$[Cu(L1)(L6)]^+$	$2{,}01 \cdot 10^{-2}$
$[Cu(L1)(L7)]^+$	$2{,}47 \cdot 10^{-2}$

The differences between the lifetimes of the complexes are quite small, their order partially resemble the degree of the performance of the device, where $[Cu(L1)(L4)]^+$ that showed the highest efficiency showed the highest electron lifetime value.

Figure 5.22 shows the stability over time in terms of efficiency and fill factor of the complexes of interest.

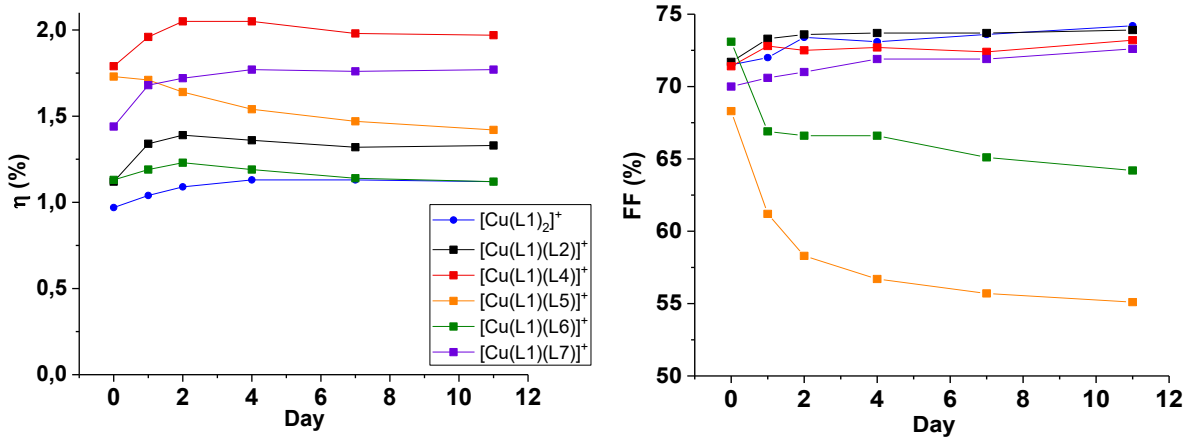

(a) (b)

Figure 5.22: Stability over time of the DSCs of interest, in terms of efficiency (a) and fill factor (b).

All the cells during the very first days of their life showed a similar enhancement trend, growing of some decimal percentage point in efficiency. Nevertheless, while complexes $[Cu(L1)(L4)]^+$, $[Cu(L1)(L7)]^+$, $[Cu(L1)(L2)]^+$ and $[Cu(L1)_2]^+$ showed a really similar behaviour reaching the stability after a couple of days, $[Cu(L1)(L5)]^+$ and $[Cu(L1)(L6)]^+$ showed a different tendency and decreased in time. This pattern is reinforced by the trends of the fill factors, which visibly decreases for the latter complexes, while remains quite constant for all the others. The trends in J_{SC} values are not showed since highly resemble the trend of the efficiencies. The values for the V_{OC} vary little over time, with the exception of $[Cu(L1)(L5)]^+$. Right after electrolyte injection, the V_{OC} of $[Cu(L1)(L5)]^+$ reached values of 630 mV but after one day it stabilized to 570, which is similar to the values shown by the other complexes.

An important test about the stability over long time was performed with $[Cu(L1)(L4)]^+$. Its parameters were also calculated about two months after sealing, on "Day 58", obtaining a value of 1,89% efficiency (92% of the efficiency recorded on "Day 2"), a V_{OC} of 590 mV, J_{SC} equal to 4,426 mA cm^{-2} and a FF of 72%.

5.6.2 Discussion

In general terms, it can be concluded that all the heteroleptic copper(I) complexes have very similar behaviours in their operation within the DSC device. The main conclusions, drawn for complex $[Cu(L1)(L4)]^+$, thus can be generalized for all the complexes.

From the *J-V* characteristics (**Figure 5.16**), it is evident that with these dyes in liquid DSCs no shunt resistance effect is shown. Complexes $[Cu(L1)(L5)]^+$ and $[Cu(L1)(L6)]^+$ showed a bit higher series resistance compared to the others, and consequently lower values of fill factor. A rough estimation of the characteristic resistance, series resistance and shunt resistance are shown in **Table 5.9** also to compare the differences within the copper (I) complexes and with N719. The *J-V* curves in **Figure 5.16** were taken for the calculations.

Table 5.9: Characteristic resistance, series resistance and shunt resistances of the copper (I) series and N719.

Dye	R_{CH} (Ω cm^2)	R_S (Ω cm^2)	R_{SH} (Ω cm^2)
$[Cu(L1)_2]^+$	191,64	29,85	$7{,}69 \cdot 10^3$
$[Cu(L1)(L2)]^+$	165,74	26,41	$6{,}85 \cdot 10^3$
$[Cu(L1)(L4)]^+$	123,20	17,50	$4{,}03 \cdot 10^3$
$[Cu(L1)(L5)]^+$	117,73	38,17	$33{,}3 \cdot 10^3$
$[Cu(L1)(L6)]^+$	165,03	36,69	$67{,}5 \cdot 10^3$
$[Cu(L1)(L7)]^+$	139,40	23,25	$5{,}23 \cdot 10^3$
N719	39,304	1,007	$10{,}5 \cdot 10^3$

All the copper (I) complexes showed characteristic resistances of about three times higher than the R_{CH} of the state-of-the-art reference dye N719 measured in this work in the same operating system. In comparison, commercial silicon solar cells instead have usually a low resistance and typically possess a high current and low voltage giving a characteristic resistance of around 16 Ω cm^2. As expected, the shunt resistances values are really high, thus their effect can be considered negligible, and the influence of the series resistances dominate the fill factors.

Complexes $[Cu(L1)(L6)]^+$ and $[Cu(L1)(L5)]^+$, showed the greatest series resistances and worse fill factors, as well as less stability over time. Their performances within the cell need further investigation and more tests in order to draw a certain conclusion. Nevertheless, their behaviour, in the optical and electrochemical characterization, was showing distinct properties compared to the other complexes. Their oxidation potentials were higher compared to $[Cu(L1)_2]^+$, taken as a reference point since present in all the heteroleptic complexes. Despite lower fill factor and less stability over time, complex $[Cu(L1)(L5)]^+$, showed quite good performance and one of the highest current density within the series. Complex $[Cu(L1)(L6)]^+$, was expected to have lower performance in according with Constable *et al.*[9] since the phenyl group in the "blocking position" probably leads to a higher degree of ligand exchange in presence of the electrolyte.

Concerning the values of the molar extinction coefficients, based on the statement of Biagini and co-workers,[48] they are also an important factor to consider, directly connected to the lower performance of the device.

Nevertheless, complex $[Cu(L7)_2]^+$ has the lowest ε_λ and its performance as a dye, self-assembled with L1, was one of the most successful after $[Cu(L1)(L4)]^+$. This could be explained since broader sun light absorption takes place even if the IPCE shows an injection efficiency of almost the same order of $[Cu(L1)(L2)]^+$.

$[Cu(L1)(L4)]^+$ showed the highest performance accomplished with copper (I) complexes in this work. It showed the best efficiency and highest stability over time. However, it should

be pointed out and considered, that the system was first studied and optimized for this complex, thus this result is not totally surprising. In general, complexes $[Cu(L1)_2]^+$, $[Cu(L1)(L2)]^+$, and $[Cu(L1)(L7)]^+$ showed similar behaviour compared to $[Cu(L1)(L4)]^+$ with differences mainly in the current density intensity, which resulted in different efficiencies.

The photovoltaic performance of complex $[Cu(L1)_2]^+$ is much lower than expected from the literature,[48] even considering the good-match of a high extinction coefficient and absorption wavelength. Its behaviour though, can be affected by some degree of uncertainty since its bath was, as previously mentioned, prepared by a solution 1mM : 0,5mM of L1 and $Cu(PF_6)$ respectively in MeOH. While it does not seem to be a problem for the other complexes, L1 behaviour is peculiar for the presence of the carboxylic acid that could be responsible of some interaction with the copper centre.

IPCE is a useful tool for evaluating the operating properties of the devices. IPCE data give information mainly about light harvesting efficiency and charge collection. The spectra revealed poor conversion of the incident photon into electrical current compared to N719. By the shape of the spectra, the main problem could be adduced to low light harvesting efficiency due to limited coverage of TiO_2. Moreover, it is hypothesized that some interaction between copper (I), the iodide and the tert-butylpyridine (TBP) of the electrolyte have occurred. Evidence that these interactions seem to occur is shown in **Figure 5.18**. Clearly, after electrolyte injection all the substrates assumed a similar aspect. From the literature, it is known that copper (I) interacts with TBP since pyridine-based and with iodide for the formation of cubane-type clusters.[92] **Table 5.10** shows the wavelength of maximum absorption and maximum quantum efficiency in comparison, in order to evidence the shift between them.

Table 5.10: Comparison between λ_{max} of the absorption spectra and $\lambda_{IPCEmax}$ from the IPCE curves.

Dye	λ_{max} (nm)	$\lambda_{IPCEmax}$(nm)
$[Cu(L1)_2]^+$	473	480
$[Cu(L1)(L2)]^+$	459	475
$[Cu(L1)(L4)]^+$	471	488
$[Cu(L1)(L5)]^+$	460	472
$[Cu(L1)(L6)]^+$	531	472
$[Cu(L1)(L7)]^+$	439	473

The shapes of the IPCE spectra resemble the shapes of an absorption spectra but all $\lambda_{IPCEmax}$ values are all in the same range independently from the λ_{max} of the complex at the beginning . This is even more evident for $[Cu(L1)(L6)]^+$, whose $\lambda_{IPCEmax}$ was blue-shifted of around 60 nm. This evidence made the hypothesis about the interactions between copper (I) and the electrolyte more grounded.

6 Conclusions

The properties of new heteroleptic copper (I) complexes were successfully investigated through UV-Vis spectroscopy, cyclic voltammetry (CV), and differential pulse voltammetry (DPV), which gave exhaustive information about their optical and electrochemical behaviours. By these measurements, the energy levels of the complexes were found and their suitability as photosensitizers was ensured. Most importantly, it was interesting to discover a linear trend in the distribution of the maximum absorption wavelengths between the heteroleptic complexes formed on the surface of TiO_2 with the same anchoring ligand ("L1") and their corresponding homoleptic complexes in acetonitrile solution. This pattern indeed allows future prediction of hypothetical heteroleptic complexes with the same anchoring ligand with fair precision. In the presence of other anchoring ligands, it is reasonable to suppose that similar patterns can be found. Regarding the redox potentials measured from the DPVs, correlations between the heteroleptic and the homoleptic complexes in solution were also searched. This time, a less certain result was obtained, but two patterns were suggested. One trend was less influenced by the presence of "L1" and was followed by ligands with higher donating effect: "L4", "L7" that have more phenyl groups connected to the phenanthroline core and "L6" which contains a more aromatic structure (biquinoline). The second trend includes "L2" and "L5" which resulted much more shifted towards lower potentials when in combinations with "L1", probably due to higher degree of flattening when heteroleptic. Nevertheless, these hypothetical trends need to be further verified by trying more ancillary ligands with different characteristics.

The performances of the complexes as photosensitizers within the DSC devices were then investigated by measuring the current density-voltage (*J-V*) characteristics at different light intensities and in the dark. These measurements gave a series of information about the mechanism within the cell, like charge-recombination, charge transfer, amount of the dye on the surface and resistances occurring (characteristic, series and shunt). The incident photon-to-current efficiency (IPCE) was measured to have more information about charge collection and light harvesting efficiency (LHE). Combining the latter results with the information given by the *J-V* curves, and considering the high fill factor values obtained, it was reasonable to suggest a problem of incomplete dye coverage of TiO_2. This assumption was also supported by the low absorption values coming from the complexes adsorbed on the TiO_2 during the "first set" of experiments, which were in the range of 0,2 – 0,4. By direct optical comparison of the devices, it could have been further said that a lower dye coverage was reached compared to the much more intense red colour coming from the substrate of TiO_2 that had adsorbed the benchmark dye, ruthenium (II) complex, N719.

Overall, all the copper (I) complexes showed similar behaviour. Some small differences were observed with $[Cu(L1)(L5)]^+$ and $[Cu(L1)(L6)]^+$ which showed a slightly higher series resistance, and consequently lower values of fill factor, and lower stability over time. Both the complexes with ligand "L5" and "L6" had redox potentials higher than the only anchoring ligand complex and this behaviour could have influenced negatively the cell, leading to more recombination. However, more devices with these two ligands should be investigated in order to avoid any hasty conclusion and to further understand the intrinsic mechanism occurring. Adding other ancillary ligands to the study would also help to generalize any conclusion drawn and to consolidate a real pattern. The best device, $[Cu(L1)(L4)]^+$, which was also the complex first used to optimize the process of electrolyte composition and thickness of the photoanode semiconductor, gave a power conversion efficiency up to 2,05%. Very good performance was

also shown by $[Cu(L1)(L7)]^+$ with 1,73%, soon followed by $[Cu(L1)(L5)]^+$ with 1,71%. Those dyes possessed a decent efficiency of around 20-25% compared to the DSCs based on N719. Lower results were given from $[Cu(L1)(L2)]^+$ with 1,43%, and $[Cu(L1)(L6)]^+$, which showed an efficiency of 1,23%. The electron lifetimes within the series where compared at the same voltage. They were quite close with each other and partially resembled the performing efficiency of the devices, for instance $[Cu(L1)(L4)]^+$ showed the best performance and the highest electron lifetime. What also captured the attention was the shape of the IPCE curves, which highly resembled the shape of the UV-Vis absorption spectra. Furthermore, regardless of the starting maximum absorption wavelength of the complexes, the wavelengths of the IPCE maximum values were all falling in the same range between 470-490 nm. Speculating about this distinctive result, some interaction between the copper dyes and the iodide/triiodide electrolyte redox mediator and the co-additive tert-butylpyridine could be hypothesized.

The case of $[Cu(L1)_2]^+$, either in solution or adsorbed on TiO_2, was often dealt slightly differently. Due to its insolubility in acetonitrile, it had to be studied in methanol or dimethyl sulfoxide in several cases. Furthermore, the carboxylic acid moieties, necessary for binding the surface of TiO_2, could interact with copper while tempting to form the homoleptic, resulting in a different complex and a smaller amount of the desired one. Nevertheless, its characterization was of fundamental importance as internal benchmark in the "first set" of the experiments in order to finalise the patterns found. In the "second set", this complex also played the important role of internal benchmark since it was the only one already known in the literature in its application within the cell. However, in this work, just above one-third of the efficiency reported was reached by the devices with $[Cu(L1)_2]^+$. This result needs to account the lack of the pure complex in solution which, as mentioned, probably led to very little coverage of the intended complex on the surface of TiO_2.

Heteroleptic copper (I) complexes are an interesting system which alone leads to high curiosity and even more in their application in such intriguing system as the DSCs. Despite the expected lower performances compared to the standard dye N719, the simplicity of the system in exam still makes it a promising technology inspired by a greener future. In general, the DSCs technology has competitive features in the market for the variety of design, colours, applicability on glass or on flexible plastic, short energy payback time, and enhanced performances under diffuse light. The use of copper (I) complexes as alternative dyes, makes this technology even more affordable by everybody in the every-day life, for building integration in the windows of the houses or only as a panel to charge electronic devices. Low-cost and largely available dyes can make the DSC technology completely fulfil the economic market demand in terms of low prices and solution for energy supply.

7 Future Outlook

Such a mutually interactive system, like the one of the DSCs, always raises interesting questions which need to be further investigated with a much greater extent. This research work in particular and the resulting analysis led to some question marks which need to be deeper explored to lead the way to this innovative system based on copper.

About the interesting matter of the predictability of the optical and electrochemical properties of the complexes with the same anchoring ligand on TiO_2 once known the characteristics of the starting homoleptic complexes in solution, more ancillary ligands could be tested to further validate the pattern already found. Despite more measurements needed, a scientific manuscript about these findings is currently being written. Such prediction capability gives indeed a valuable and effective tool for further researches.

Another captivating curiosity that needs closer investigation is the influence of the carboxylic acid moieties present in the anchor ligand and their suspected interaction with the copper centre.

Regarding the application of the heteroleptic copper (I) complexes in DSC devices, an interesting first characterization has been studied in this work, since few studies ahead about these complexes were previously done. The main advantage of this technology for their application on an industrial scale is the simplicity and the low-cost of the entire system. The system could be revolutionized if a way to push the equilibrium towards the formation of the complexes on TiO_2 could be found. To do so, a closer exploration of the mechanism of the self-assembling needs to be made. A further step towards this field is already on-going. Through X-ray photoelectron spectroscopy (XPS), a closer look at the actual amount of the anchor ligand attached to the surface of TiO_2 is being explored. To follow, a measure of the amount of the ancillary ligand on top of TiO_2 after the self-assembling mechanism should give a glance of the effectiveness of the "on-surface self-assembly" system and answer the question with certainty about the limiting problem in the cells. A closer look should be also given on the interaction occurring between copper-based dyes, iodide/triiodide couple and tert-butylpyridine.

Even though the DSC system might have reached almost a plateau in the efficiency of around 12% regardless the dye, it is still a promising photovoltaic technology for future applications with much more potential than other competitors in the market. Thus, much more studies and efforts should also focus to improve its integration in indoor and outdoor applications.

Since a practical disadvantage of liquid DSCs is the volatile nature of the electrolyte solvent, some future work could also focus on the use of these complexes as photosensitizers in solid state dye-sensitized solar cells (SS-DSCs).

Bibliography

[1] Renewable Energy Policy Network for the 21st Century, REN21. Renewables 2018 Global Status Report. Available at: http://www.ren21.net/gsr-2018/. (Accessed: 17th February 2019)

[2] Graetzel, M., 2001, Photoelectrochemical cells. *Nature*, **414**, 338–344.

[3] Green, M. A., Hishikawa, Y., Dunlop, E. D., Levi, D. H., Hohl-Ebinger, J. and Ho-Baillie, A. W. Y., 2018, Solar cell efficiency tables (version 52). *Progress in Photovoltaics: Research and Applications*, **26**, 427–436.

[4] Fraunhofer Institute for Solar Energy Systems, ISE. Photovoltaics Report, updated: 27 August 2018. Available at: www.ise.fraunhofer.de. (Accessed: 14th February 2019)

[5] Hagfeldt, A., Boschloo, G., Sun, L., Kloo, L. and Pettersson, H., 2010, Dye-sensitized Solar Cells. *Chemical Reviews*, **110**, 6595–6663.

[6] O'Regan, B. and Grätzel, M., 1991, A low-cost, high-efficiency solar cell based on dye-sensitized colloidal TiO2 films. *Nature*, **353**, 737–740.

[7] Mathew, S., Yella, A., Gao, P., Humphry-Baker, R., Curchod, B. F. E., Ashari-Astani, N., Tavernelli, I., Rothlisberger, U., Nazeeruddin, M. K. and Grätzel, M., 2014, Dye-sensitized solar cells with 13% efficiency achieved through the molecular engineering of porphyrin sensitizers. *Nature Chemistry*, **6**, 242–247.

[8] Abbotto, A., Sauvage, F., Barolo, C., De Angelis, F., Fantacci, S., Graetzel, M., Manfredi, N., Marinzi, C. and Nazeeruddin, M. K., 2011, Panchromatic ruthenium sensitizer based on electron-rich heteroarylvinylene π-conjugated quaterpyridine for dye-sensitized solar cells. *Dalton Transactions*, **40**, 234–242.

[9] Housecroft, C. E. and Constable, E. C., 2015, The emergence of copper(I)-based dye sensitized solar cells. *Chemical Society Reviews*, **44**, 8386–8398.

[10] Bozic-Weber, B., Constable, E. C. and Housecroft, C. E., 2013, Light harvesting with Earth abundant d-block metals: Development of sensitizers in dye-sensitized solar cells (DSCs). *Coordination Chemistry Reviews*, **257**, 3089–3106.

[11] Mara, M. W., Fransted, K. A. and Chen, L. X., 2015, Interplays of excited state structures and dynamics in copper(I) diimine complexes: Implications and perspectives. *Coordination Chemistry Reviews*, **282**–**283**, 2–18.

[12] Brauchli, S. Y., Malzner, F. J., Constable, E. C. and Housecroft, C. E., 2015, Copper(i)-based dye-sensitized solar cells with sterically demanding anchoring ligands: Bigger is not always better. *Royal Society of Chemistry Advances*, **5**, 48516–48525.

[13] BP Statistical Review of World Energy, 67th edition, June 2018. Available at: https://www.bp.com/content/dam/bp/business-sites/en/global/corporate/pdfs/energy-economics/statistical-review/bp-stats-review-2018-full-report.pdf. (Accessed: 10th February 2019)

[14] United nations, Department of Economic and Social Affairs. World population projected to reach 9.7 billion by 2050. Available at: http://www.un.org/en/development/desa/news/population/2015-report.html. (Accessed: 20th February 2019)

[15] Research Institute for Climate Impact., 2012, *Renewable Energy Sources and Climate Change Mitigation*. Cambridge University Press, New York, USA. [ISBN:9781107607101]

[16] Environmental Justice Atlas, Banqiao dam failure in 1975, Henan, China. Available at: https://ejatlas.org/conflict/baquio-dam-failure-henan-china. (Accessed: 16th February 2019)

[17] Lewis, N. S. and Nocera, D. G., 2006, Powering the planet: Chemical challenges in solar utilization. *Proceedings of the National Academy of Sciences of the United States of America*, **103**, 15729–15735.

[18] Morton, O. and Dennis, C., 2006, Silicon Valley sunrise. *Nature publishing group*, **443**, 18–19.

[19] The International Energy Agency, IEA. Technology Roadmap: Solar Photovoltaic Energy. Available at: https://www.iea.org/publications/freepublications/publication/TechnologyRoadmapSolarPhotovoltaicEnergy_2014edition.pdf. (Accessed: 10th February 2019)

[20] Wikipedia. Growth of Photovoltaics. Available at: https://en.wikipedia.org/wiki/Growth_of_photovoltaics. (Accessed: 17th February 2019)

[21] Ibn-Mohammed, T., Koh, S. C. L., Reaney, I. M., Acquaye, A., Schileo, G., Mustapha, K. B. and Greenough, R., 2017, Perovskite solar cells: An integrated hybrid lifecycle assessment and review in comparison with other photovoltaic technologies. *Renewable and Sustainable Energy Reviews*, **80**, 1321–1344.

[22] Wikipedia. Czochralski Process. Available at: https://en.wikipedia.org/wiki/Czochralski_process. (Accessed: 15th February 2019)

[23] Louwen, A., Van Sark, W., Schropp, R. and Faaij, A., 2016, A cost roadmap for silicon heterojunction solar cells. *Solar Energy Materials and Solar Cells*, **147**, 295–314.

[24] Frischknecht, R., Itten, R., Wyss, F., Blanc, I., Heath, G., Raugei, M., Sinha, P. and Wade, A., 2015, *Life Cycle Assessment of Future Photovoltaic Electricity Production from Residential - scale Systems Operated in Europe Life Cycle Assessment of Future Photovoltaic*. [ISBN:9783906042305]

[25] Centre of molecular materia materials for photonics and electronics, CMMPE, University of Cambridge. Dye-sensitized solar cells using liquid crystal charge transport layers. Available at: http://www-g.eng.cam.ac.uk/CMMPE/lcddss.html. (Accessed: 26th December 2018)

[26] Wikipedia. Shockley-Queisser limit. Available at: https://en.wikipedia.org/wiki/Shockley–Queisser_limit. (Accessed: 23rd December 2018)

[27] Green, M. A., 2001, Third generation photovoltaics: Ultra-high conversion efficiency at low cost. *Progress in Photovoltaics: Research and Applications*, **9**, 123–135.

[28] Fraunhofer Institute for Solar Energy Systems, ISE. New world record for solar cell efficiency at 46% – French-German cooperation confirms competitive advantage of European photovoltaic industry. Available at: https://www.ise.fraunhofer.de/en/press-media/press-releases/2014/new-world-record-for-solar-cell-efficiency-at-46-percent.html. (Accessed: 9th January 2019)

[29] National Renewable Energy Laboratory, NREL. PV Research Cell Record Efficiency Chart. Available at: https://www.nrel.gov/pv/assets/pdfs/pv-efficiency-chart.20190103.pdf. (Accessed: 16th February 2019)

[30] El-Khouly, M. E., El-Mohsnawy, E. and Fukuzumi, S., 2017, Solar energy conversion: From natural to artificial photosynthesis. *Journal of Photochemistry and Photobiology C: Photochemistry Reviews*, **31**, 36–83.

[31] Urbaniak, A., Photovoltaics, Organic Thin Film Solar Cells. Available at: http://urbaniak.fizyka.pw.edu.pl/Strona/Photovoltaics/Lecture 7.pdf. (Accessed: 10th February 2019)

[32] Boschloo, G., Hagfeldt, A. and Spectus, C. O. N., 2009, Characteristics of the Iodide / Triiodide Redox Mediator in Dye-Sensitized Solar Cells. *Accounts of Chemical Research*, **42**, 1819–1826.

[33] Kusters, J., Feldt, S. M., Gibson, E. a., Gabrielsson, E., Sun, L., Boschloo, G., Hagfeldt, A. and Kusters, J., 2007, Design of Organic Dyes and Cobalt Polypyridine Redox Mediators for High Efficiency Dye-Sensitized Solar Cells. *Journal of the American Chemical Society*, **1**, 2–7.

[34] Stergiopoulos, T., Rozi, E., Karagianni, C.-S. and Falaras, P., 2011, Influence of electrolyte co-additives on the performance of dye-sensitized solar cells. *Nanoscale Research Letters*, **6**, 307.

[35] Feldt, S. M., Gibson, E. A., Wang, G., Fabregat, G., Boschloo, G. and Hagfeldt, A., 2014, Carbon counter electrodes efficient catalysts for the reduction of Co(III) in cobalt mediated dye-sensitized solar cells. *Polyhedron*, **82**, 154–157.

[36] Lazorski, M. S. and Castellano, F. N., 2014, Advances in the light conversion properties of Cu(I)-based photosensitizers. *Polyhedron*, **82**, 57–70.

[37] Yoon, S., Tak, S., Kim, J., Jun, Y., Kang, K. and Park, J., 2011, Application of transparent dye-sensitized solar cells to building integrated photovoltaic systems. *Building and Environment*, **46**, 1899–1904.

[38] Syafinar, R., Gomesh, N., Irwanto, M., Fareq, M. and Irwan, Y. M., 2015, Chlorophyll Pigments as Nature Based Dye for Dye-Sensitized Solar Cell (DSSC). *Energy Procedia*, **79**, 896–902.

[39] Mariani, P., Vesce, L. and Di Carlo, A., 2015, The role of printing techniques for large-area dye sensitized solar cells. *Semiconductor Science and Technology*, **30**, 1–16.

[40] Wu, C., Chen, B., Zheng, X. and Priya, S., 2016, Scaling of the flexible dye sensitized solar cell module. *Solar Energy Materials and Solar Cells*, **157**, 438–446.

[41] Solar Novus Today, Learning from Nature: Dye-sensitized solar cells. Available at: https://www.solarnovus.com/learning-from-nature-dye-sensitized-solar-cells_N1598.html. (Accessed: 25th February 2019)

[42] AISIN SEIKI Co., Ltd and TOYOTA Central R&D Labs., Inc. (Japan). Available at: http://kuroppe.tagen.tohoku.ac.jp/~dsc/modules/company.htm. (Accessed: 25th February 2019)

[43] Alonso Vante, N., Ern, V. and Chartier, P., 1983, Spectral Sensitizationof Semiconductors by Copper(I) Complexes in Photoelectrochemical Systems. *Nouveau Journal de Chimie*, **7**, 3–5.

[44] InfoMine. Copper Price. Available at: http://www.infomine.com/investment/metal-prices/copper/. (Accessed: 22nd February 2019)

[45] InfoMine. Ruthenium Price. Available at: http://www.infomine.com/investment/metal-prices/ruthenium/. (Accessed: 22nd February 2019)

[46] Scaltrito, D. V., Thompson, D. W., O'Callaghan, J. A. and Meyer, G. J., 2000, MLCT Excited States of Cuprous Bis-phenanthroline Coordination Compounds. *Coordination Chemistry Reviews*, **208**, 243–266.

[47] Royal Society of Chemistry, RSC. Advancing the Chemical Sciences. Ultraviolet - Visible Spectroscopy (UV). Available at: http://www.rsc.org/learn-chemistry/content/UV-Vis_Spectroscopy.pdf. (Accessed: 28th December 2018)

[48] Colombo, A., Dragonetti, C., Roberto, D., Valore, A., Biagini, P. and Melchiorre, F., 2013, A simple copper(I) complex and its application in efficient dye sensitized solar cells. *Inorganica Chimica Acta*, **407**, 204–209.

[49] McCusker, C. E. and Castellano, F. N., 2013, Design of a long-lifetime, earth-abundant, aqueous compatible Cu(I) photosensitizer using cooperative steric effects. *Inorganic Chemistry*, **52**, 8114–8120.

[50] Blaskie, M. W. and Mcmillin, D. R., 1980, Photostudies of Copper(I) Systems. 6. Room-Temperature Emission and Quenching Studies of [Cu(dmp)2]+. *Inorganic Chemistry*, **19**, 3519–3522.

[51] Ashbrook, L. N. and Elliott, C. M., 2013, Dye-sensitized solar cell studies of a donor-appended bis(2,9-dimethyl-1, 10-phenanthroline) Cu(I) dye paired with a cobalt-based mediator. *Journal of Physical Chemistry C*, **117**, 3853–3864.

[52] Kaeser, A., Delavaux-Nicot, B., Duhayon, C., Coppel, Y. and Nierengarten, J. F., 2013, Heteroleptic Copper(I) complexes prepared from phenanthroline and bis-phosphine ligands. *Inorganic Chemistry*, **52**, 14343–14354.

[53] Lexys Pruett. Potential Cyclic Voltammetry. Available at: https://slideplayer.com/slide/4214725/14/images/16/Potential+Sweep+Gives%3A+Why.jpg. (Accessed: 10th February 2019)

[54] Zhou, Y., He, Q., Yang, Y., Zhong, H., He, C., Sang, G., Liu, W., Yang, C., Bai, F. and Li, Y., 2008, Binaphthyl containing green and red emitting molecules for solution processable organic light-emitting diodes. *Advanced Functional Materials*, **18**, 3299–3306.

[55] Research gate. Band gap. Available at: https://www.researchgate.net/post/How_can_I_calculate_the_band_gap_for_conjugated_polymers_from_UV-Vis_absorption_spectra. (Accessed: 9th January 2019)

[56] Elgrishi, N., Rountree, K. J., McCarthy, B. D., Rountree, E. S., Eisenhart, T. T. and Dempsey, J. L., 2018, A Practical Beginner's Guide to Cyclic Voltammetry. *Journal of Chemical Education*, **95**, 197–206.

[57] Bagotsky, V., 2005, Fundamentals of Electrochemistry. *Peptide Synthesis and Applications*, **298**, 3–24.

[58] Wikipedia. Differential pulse voltammetry. Available at: https://en.wikipedia.org/wiki/Differential_pulse_voltammetry. (Accessed: 10th January 2019)

[59] Gagné, R. R., Koval, C. A. and Lisensky, G. C., 1980, Ferrocene as an Internal Standard for Electrochemical Measurements. *American Chemical Society*, **19**, 2855–2857.

[60] Hewat, T. E., Yellowlees, L. J. and Robertson, N., 2014, Neutral copper(i) dipyrrin complexes and their use as sensitizers in dye-sensitized solar cells. *Dalton Transactions*, **43**, 4127–4136.

[61] Brauchli, S. Y., Malzner, F. J., Constable, E. C. and Housecroft, C. E., 2014, Influence of a co-adsorbent on the performance of bis(diimine) copper(I)-based dye-sensitized solar cells. *Royal Society of Chemistry Advances*, **4**, 62728–62736.

[62] Miller, M. and Karpishin, T., 1999, Phenylethynyl Substituent Effects on the Photophysics and Electrochemistry of [Cu(dpp)2] (dpp=2,9-Diphenyl-1, 10-phenanthroline). *Inorganic Chemistry*, **38**, 5246–5249.

[63] Jahng, Y., Hazelrigg, J., Kimball, D., Riesgo, E., Wu, F. and Thummel, R. P., 1997, Copper (I) Complexes of 3,3 ′ Bridged 2,2′-Biquinoline: Synthesis, Properties, and Structure. *Inorganic Chemistry*, **36**, 5390–5395.

[64] Provó Kluit, H. A. J., Spek, A. L., Agterberg, F. P. W., Oevering, H., Driessen, W. L., Reedijk, J., Buijs, W. and Lakin, M. T., 1997, Dinuclear Paddle-Wheel Copper(II) Carboxylates in the Catalytic Oxidation of Carboxylic Acids. *Inorganic Chemistry*, **36**, 4321–4328.

[65] Leandri, V., Zhang, J., Mijangos, E., Boschloo, G. and Ott, S., 2016, Incorporation of a fluorophenylene spacer into a highly efficient organic dye for solid-state dye-sensitized solar cells. *Journal of Photochemistry and Photobiology A: Chemistry*, **328**, 59–65.

[66] Wang, M., Grätzel, C., Zakeeruddin, S. M. and Grätzel, M., 2012, Recent developments in redox electrolytes for dye-sensitized solar cells. *Energy and Environmental Science*, **5**, 9394–9405.

[67] PVEducation. IV Curve. Available at: http://pveducation.org/iv-curve. (Accessed: 20th December 2018)

[68] SpringerBriefs in Applied Sciences and Technology. Physics of solar cells. Available at: http://depts.washington.edu/cmditr/modules/opv/physics_of_solar_cells.html. (Accessed: 26th January 2019)

[69] Samlex Solar. Power Panels Characteristics. Available at: http://www.samlexsolar.com/learning-center/solar-panels-characteristics.aspx. (Accessed: 16th January 2019)

[70] PVEducation. Characteristic Resistance. Available at: https://www.pveducation.org/pvcdrom/solar-cell-operation/characteristic-resistance. (Accessed: 12th February 2019)

[71] PVEducation. Effect of parasitic resistances. Available at: https://www.pveducation.org/pvcdrom/solar-cell-operation/effect-of-parasitic-resistances. (Accessed: 11th February 2019)

[72] Tobnaghi, D. M., Madatov, R. and Farhadi, P., 2013, Investigation of light intensity and temperature dependency of solar cells electric parameters. *Electric Power Engineering & Control Systems*, **55**, 90–83.

[73] Green Rhino Energy. Defining standard spectra for solar panels. Available at: http://www.greenrhinoenergy.com/solar/radiation/spectra.php. (Accessed: 8th February 2019)

[74] Tian, H., Yu, X., Zhang, J., Duan, W., Tian, F. and Yu, T., 2012, The Influence of Environmental Factors on DSSCs for BIPV. *Internation Journal of Electrochemical Science*, **7**, 4686–4691.

[75] Cuce, E., Mert, P. and Bali, T., 2013, An experimental analysis of illumination intensity and temperature dependency of photovoltaic cell parameters. *Applied Energy*, **111**, 374–382.

[76] Gamry Instruments. DSSC: Dye Sensitized Solar Cells. Available at: https://www.gamry.com/application-notes/physechem/dssc-dye-sensitized-solar-cells/. (Accessed: 12th February 2019)

[77] PVEducation. Quantum efficiency. Available at: https://www.pveducation.org/pvcdrom/solar-cell-operation/quantum-efficiency. (Accessed: 13th January 2019)

[78] Bisquert, J., Fabregat-Santiago, F., Mora-Serò, I., Garcia-Belmonte, G. and Giménez, S., 2009, Electron Lifetime in Dye-Sensitized Solar Cells: Theory and Interpretation of Measurements. *Journal of Physical Chemistry C*, **113**, 17278–17290.

[79] PubChem. Acetonitrile, CH3CN. Available at: https://pubchem.ncbi.nlm.nih.gov/compound/acetonitrile. (Accessed: 4th February 2019)

[80] PubChem. 3-Methoxypropionitrile, C4H7NO. Available at: https://pubchem.ncbi.nlm.nih.gov/compound/3-Methoxypropionitrile#section=Top. (Accessed: 4th February 2019)

[81] Hao, F., Jiao, X., Li, J. and Lin, H., 2013, Solvent dipole modulation of conduction band edge shift and charge recombination in robust dye-sensitized solar cells. *The Royal Society of Chemistry, Nanoscale*, **5**, 726–733.

[82] Rebelo, L. P. N., Lopes, J. N. C., Esperança, J. M. S. S. and Filipe, E., 2005, On the critical temperature, normal boiling point, and vapor pressure of ionic liquids. *Journal of Physical Chemistry B*, **109**, 6040–6043.

[83] Koller, T., Rausch, M. H., Schulz, P. S., Berger, M., Wasserscheid, P., Economou, I. G., Leipertz, A. and Fröba, A. P., 2012, Viscosity, interfacial tension, self-diffusion coefficient, density, and refractive index of the ionic liquid 1-ethyl-3-methylimidazolium tetracyanoborate as a function of temperature at atmospheric pressure. *Journal of Chemical and Engineering Data*, **57**, 828–835.

[84] Huang, M. M., Jiang, Y., Sasisanker, P., Driver, G. W. and Weingärtner, H., 2011, Static relative dielectric permittivities of ionic liquids at 25 °C. *Journal of Chemical and Engineering Data*, **56**, 1494–1499.

[85] Ito, S., Murakami, T. N., Comte, P., Liska, P., Grätzel, C., Nazeeruddin, M. K. and Grätzel, M., 2008, Fabrication of thin film dye sensitized solar cells with solar to electric power conversion efficiency over 10%. *Thin Solid Films*, **516**, 4613–4619.

[86] Dragonetti, C., Magni, M., Colombo, A., Melchiorre, F., Biagini, P. and Roberto, D., 2018, Coupling of a copper dye with a copper electrolyte: A fascinating springboard for sustainable dye-Sensitized solar cells. *ACS Applied Materials and Interfaces*, **1**, 751–756.

[87] Bozic-Weber, B., Brauchli, S. Y., Constable, E. C., Fürer, S. O., Housecroft, C. E., Malzner, F. J., Wright, I. a and Zampese, J. a., 2013, Improving the Photoresponse of Copper(I) Dyes in Dye-Sensitized Solar Cells by Tuning Ancillary and Anchoring Ligand Modules. *Dalton transactions (Cambridge, England : 2003)*, **42**, 12293–308.

[88] Boschloo, G., Häggman, L. and Hagfeldt, A., 2006, Quantification of the effect of 4-tert-butylpyridine addition to I -/I3- redox electrolytes in dye-sensitized nanostructured TiO2 solar cells. *Journal of Physical Chemistry B*, **110**, 13144–13150.

[89] Cameron, P. J., Peter, L. M., Zakeeruddin, S. M. and Grätzel, M., 2004, Electrochemical studies of the Co(III)/Co(II)(dbbip)2redox couple as a mediator for dye-sensitized nanocrystalline solar cells. *Coordination Chemistry Reviews*, **248**, 1447–1453.

[90] Dai, S., Xiao, S., Hu, L., Chen, S., Zhang, C., Huang, Y. and Sui, Y., 2009, Theoretical modeling of the series resistance effect on dye-sensitized solar cell performance. *Applied Physics Letters*, **95**, 243503.

[91] Li, J., Zhao, L., Wang, S., Hu, J., Dong, B., Lu, H., Wan, L. and Wang, P., 2013, Great improvement of photoelectric property from co-sensitization of TiO 2 electrodes with CdS quantum dots and dye N719 in dye-sensitized solar cells. *Materials Research Bulletin*, **48**, 2566–2570.

[92] Kim, S., Siewe, A. D., Lee, E., Ju, H., Park, I. H., Park, K. M., Ikeda, M., Habata, Y. and Lee, S. S., 2016, Ligand-Induced Formation of Copper(I) Iodide Clusters: Exocyclic Coordination Polymers with Bis-dithiamacrocycle Isomers. *Inorganic Chemistry*, **55**, 2018–2022.

List of Figures

List of Tables

Acknowledgement

This thesis has been realized as part of the Double Degree programme through agreements between Politecnico di Torino and KTH, Royal Institute of Technology in Stockholm.

I am very grateful to have had the opportunity to participate to this programme which helped my growth enormously and gave me the chance to appreciate two parallel educations from these two valuable universities.

As for any student, the thesis represents the end of a journey which opens the door to new adventures. This might be the toughest part of this writing, since I am afraid not to spend the right words to show all my gratefulness to the people that helped me to become who I am now.

First of all, I would like to express my heartfelt gratitude to the persons that guided me through the entire investigation of this work: my examiner James Gardner and my supervisor Valentina Leandri. They gave me the opportunity to be part of the group, followed me in each step of the research, patiently teaching me everything and never leaving me with unanswered question marks. Furthermore, I would like to thank my supervisor in PoliTo, Marco Vanni, for his willingness to accept this task and being a reference point in Italy through these six months.

Great thanks to the entire research group, in particular, Wei, Tamara, Hans, Ute, Erik, Yan, Lars, Sawsan, Annika and Ghada. Thank to them, I have felt always part of the group and surrounded by a pleasant environment alterning moment of relax with stimulating talks. A particular thank to Valentina, who has been more than a supervisor, and in the past six months she has been an important inspiration in what I want to do in my future.

My first special thank goes to my parents, they raised me with unconditional love and gave me amazing experience to live, and gigantic opportunities for my future.

Lots of thanks go to my friends in Stockholm who without them I would have not survived the winter twice and enjoyed the summer that much, in particular my corridor mates, Arun, Toni and Laura, all the Björkies and la Clica.

Eternal thanks to my friends in Rome, which I will always consider home, no matter where I will be. Thanks for being always supportive and extremely close to me even if most of the time I am not there. Special thanks to Beba, Leo, Anna Rita, Giuls, Nick, Gianlu and Ale.

Thousands of thanks to my friends in Turin, which I could consider my second home, and here a special thank goes to the best flat mates ever, Elisa, Laura and Marta.

It might sound silly, I know, but finally I would like to thank all the people I met in my path since they all have contributed to my growth and to my awareness of my being and my capacities and I feel ready to start a new journey.

"The important thing is not to stop questioning. Curiosity has its own reason for existing"

Albert Einstein, 1955